# AN AREAL SURFACE ENERGY BALANCE MODEL



HONG WANG

# AN AREAL SURFACE ENERGY BALANCE MODEL

BY

© Hong Wang

A thesis submitted to the School of Graduate

Studies in partial fulfilment of the

requirements for the degree of

Master of Science

Department of Geography

Memorial University of Newfoundland

May 1993

St. John's Newfoundland

ISBN 0-315-86640-3

# *ABSTRACT*

A methodology is presented in this thesis to estimate the spatial variations of the surface energy budget based on measurements from reference stations, topographical information and surface properties derived from remotely sensed imagery. According to this methodology, a physically-based areal surface energy balance model (ASEBM) is established to carry out the areal extrapolation of the surface energy flux terms. As an application, the ASEBM has been applied to an ice cap marginal area in the central Baffin Island for selected days from August, 1991. In order to have a general idea of the climate in the study area, a brief summary of the surface climate and energy balance during the spring and summer season has been presented. Although limitations in the observational data required that some assumptions be made in this application, the results are quite encouraging.

# *ACKNOWLEDGEMENTS*

This thesis was undertaken under the supervision of Dr. John D. Jacobs and I am grateful for his introducing me to an interesting area of climatology and much valuable advice on this thesis. I hope that this thesis meets his expectations.

I am indebted to Dr. Jacobs and his colleagues at the Canadian Climate Centre, who were responsible for the installation of the climatic autostations on Baffin Island and retrieval of data. Financial support for my graduate studies came from a School of Graduate Studies Fellowship, and employment as a research assistant under a grant to Dr. Jacobs from the Natural Sciences and Engineering Research Council of Canada. I am also thankful to Ms. Joan Luther, staff scientist, for her help with the use of the GEOIDAL facilities and the LANDSAT MSS imagery.

I am grateful to the faculty and staff members of the Department of Geography who have offered encouragement and help until the completion of my thesis, especially, Dr. Colin Banfield, Mrs. Carole-Anne Coffey and Mrs. Linda Corbett. I also appreciate the acquaintances of fellow graduate students.

Last, but certainly not least, I wish to thank for my wife, my mother and sister for giving me encouragement and loving support throughout my writing of the thesis. I wish to dedicate this thesis to them as well as to my newborn baby.

# *TABLE OF CONTENTS*

# *LIST OF TABLES*

# *LIST OF FIGURES*

# *Chapter 1 INTRODUCTION*

## 1.1 Surface Energy Balance

The surface energy balance model has been widely used in various studies. It can be expressed as:

$$Q^* = Q_H + Q_E + Q_G \quad \text{.....(1.1)}$$

Where $Q^*$ is the net radiation flux at the surface (taken positive if directed to the surface), and $Q_H$, $Q_E$ and $Q_G$ are the fluxes of sensible, latent and subsurface heat, respectively (taken positive if directed away from the surface). Over bare ground, $Q_G$ is referred to as soil heat flux. Over snow or ice-covered ground, $Q_G$ is equal to the total change of sensible and latent energy storage within the snow or ice pack. When snow cover exceeds a certain depth, it is possible to assume no soil heat flux at the base of the snowpack. If there is only a thin snow cover, the heat flux at the snow-soil interface should be included in equation 1.1. The exact partitioning of the net radiation among the three components ( $Q_H$, $Q_E$, $Q_G$ ) is governed by the nature of the surface and the ability

of the soil and atmosphere to transport energy. "The exact partitioning arrived at by a surface is probably the most important determinant of its microclimate" (Oke, 1987).

In Arctic areas, the surface energy balance has been investigated since the 1950's (Ohmura, 1982a). Most of the work had been done on tundra and glacier terrains during spring and summer seasons when the surfaces experience great change due to increased solar radiation (Ohmura et al., 1976; Weller et al., 1972; Weller et al., 1974; Rouse and Stewart, 1972; Stewart and Rouse, 1976; Weick and Rouse, 1991a; Weick and Rouse, 1991b; Rott et al., 1992; Andrews, 1964; Havens, 1964;). As to the tundra surface, snowmelt happens during this period, resulting in dramatic changes in the surface energy balance and hence, its climate (Ohmura, 1982b). The main features of the energy balance on Arctic tundra have been summarized and moreover, the differences of energy budget have been described among various arctic surfaces: interior tundra, coastal tundra, ablation and accumulation areas of glaciers (Ohmura, 1982b). The previous studies on the surface energy regime proved a useful approach to acquiring knowledge for the causes of surface climates over various terrains in the Arctic.

Most studies on the surface energy regime are based on single point microclimate measurements which lack areal representativeness in terms of the solution to the surface energy balance. Although some work has shown the spatial variations of surface energy budget on different plots within an area (Price et al., 1976; Munro, 1990), no systematic attempt has been made to estimate the spatial variation of surface energy balance terms. Based on the ever-increasing remotely sensed information on terrain, automated

meteorological measurements, and the fruits of previous studies on this regime, it is possible to estimate the spatial variation of surface energy balance induced by varied terrain, surface properties and atmospheric conditions.

The purpose of this paper is to present a methodology to estimate the spatial variations of the surface energy budget. As an application, an areal surface energy balance model (ASEBM) has been established to extrapolate spatially the surface energy budget terms for an ice cap marginal area in central Baffin Island, N.W.T. Based on the meteorological measurements from two reference automated stations (autostations), the ASEBM carries out the physically-based areal extrapolation with reference to the spatial variations induced by terrain and surface properties. The ASEBM features the integration of the field measurements, digital elevation model (DEM) and LANDSAT imagery into a geographical information system. The model has been applied to selected days from August, 1991. The results demonstrate that the methodology underlying the model is useful in studies concerning the spatial patterns of the surface energy balance. The ASEBM itself, which is originally designed for the ice cap marginal area, is flexible and can be applied elsewhere where the information required by the model is available.

## 1.2 Study Area and Autostations

Baffin Island, with an area of nearly 500,000 km$^2$, is the largest island in the Canadian Arctic Archipelago. It currently has permanent climatological stations at 16 sites, all but one a coastal location (Fig. 1.1). To improve the situation of inadequate stations in the interior, climatic autostations were installed, starting in 1987, with support from the Canadian Climate Centre (Jacobs et al., 1993). As an effort towards the mesoscale mapping technique of surface climates, the ASEBM is applied to an interior area in the central Baffin Island (Fig. 1.2). The study area is an ice cap marginal area of about 150 km$^2$. It features recently deglaciated terrain in the west and the Barnes Ice Cap in the east. Over the tundra, less than 2% of the area is covered by water, and the rest of the terrain is sparsely vegetated. This area was the subject of intensive interdisciplinary investigations by scientists in the 1960's (Jacobs, 1991). Recently, based on a comparison of a 1988 satellite image with 1961 aerial photography, Jacobs et al. (in review) found an average retreat of the Lewis Glacier and adjacent parts of the northwest Barnes Ice Cap margin of about 30 m per year. This area is climatologically interesting for its distinctive characteristics of varied terrain (tundra[1] and glacier) and complex topography.

---

[1] "Tundra" usually refers to well-vegetated terrain, but in this study it simply means those areas that are not covered by the glacier.

Measurements from two of the autostations are used by the ASEBM in this study: one is the Blockade Bend autostation in the study area, and the other is the Barnes Ice Cap autostation about 35 km southeast of the study area (Fig. 1.1.). The Blockade Bend station (70°24'N, 74°57'W, 420 m.a.s.l.) was established during the 1989 summer, six kilometres from the northwest margin of the Barnes Ice Cap. The autostation measures air temperature and humidity at 2 m, wind speed and direction at 3.5 m, atmospheric pressure, precipitation, global solar radiation, and soil temperatures at 0 m, 0.10 m and 0.20 m depth. The Barnes Ice Cap station (70°14'N, 74°01'W, 1085 m.a.s.l.) was installed in the summer of 1991 near the summit of the ice cap. It monitors air temperature and humidity at 2.2 m, differential temperature between 4.0 and 2.2 m, wind speed and direction at 4.6 m, snowdepth and englacial temperatures. The sampling interval is three hours for both stations (Jacobs et al., 1993).

The surface energy balance at the Blockade Bend station site (main station) is estimated in Chapter 2 to provide the ASEBM with a baseline for areal extrapolation. The meteorological measurements from both autostations are used in the model to estimate the atmospheric conditions over the tundra and glacier.

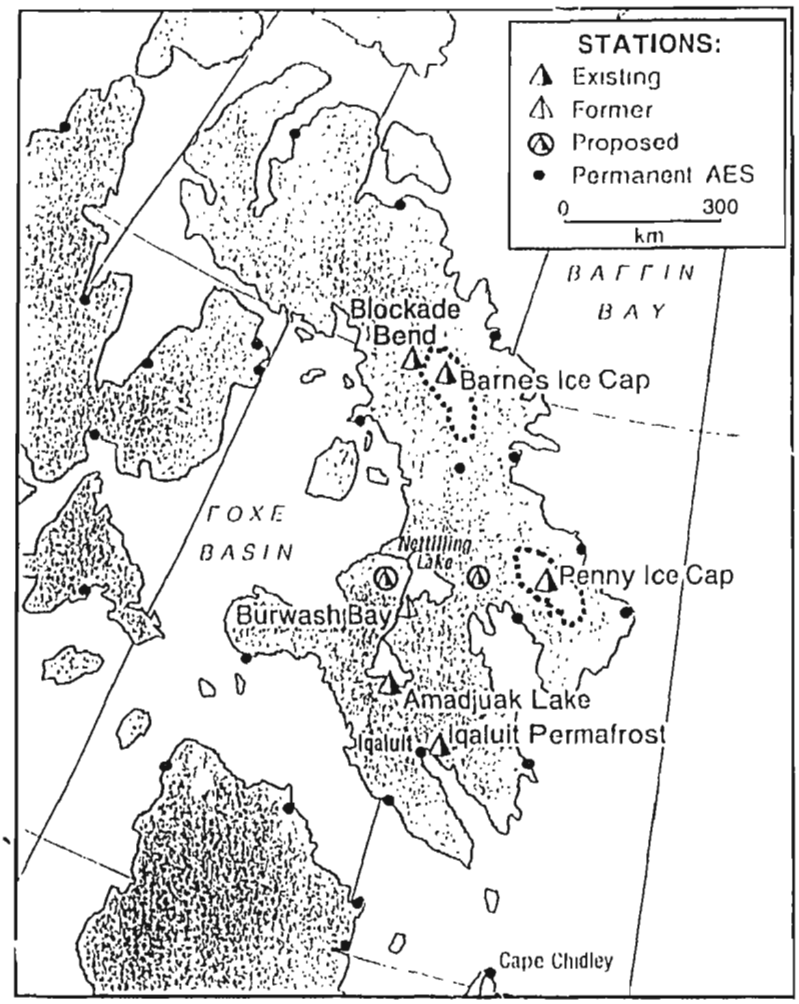


Figure 1.1. Baffin Island region showing climate station locations (source: Jacobs et al., 1993)

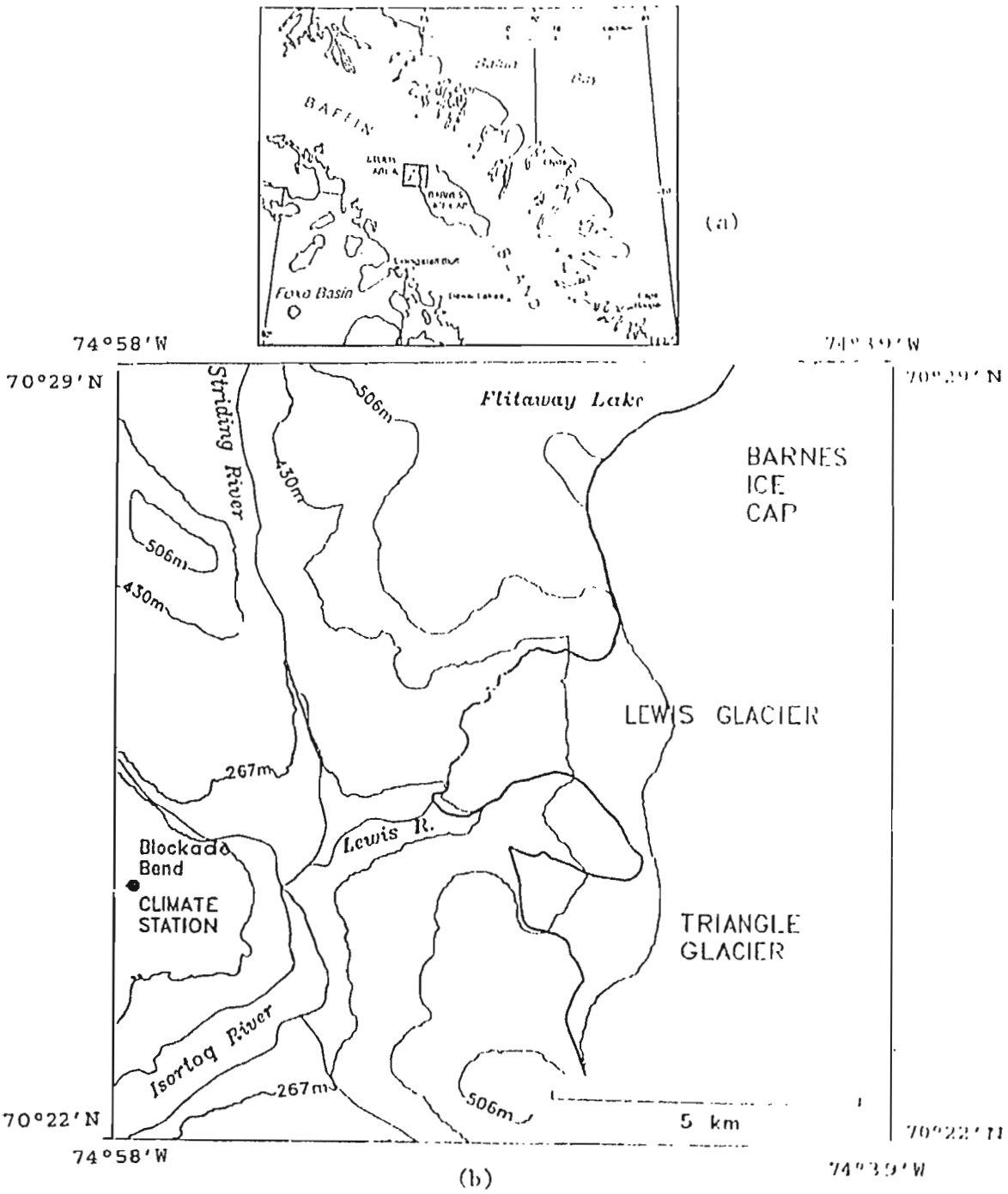


Figure 1.2. Study area. (a) Location of the study area, (b) base map of the study area.

# *Chapter 2*

# *GENERAL CLIMATE AND SURFACE ENERGY BALANCE AT THE REFERENCE STATION*

The reference stations are important to the ASEBM in terms of providing the atmospheric conditions and a baseline of the surface energy balance for the areal extrapolation. The Blockade Bend station (main station) has a relatively long record, from July 1989 through 1992, while the record from the Barnes Ice Cap is only available for August of 1991. Therefore the application of the ASEBM will only be carried out for selected days from August, 1991, when the record from both stations overlaps. However, in order to have a general idea of the surface climate and the surface energy balance at the main station site during the spring and summer, the surface energy budget calculation has been carried out for both the melting and post-melting periods.

## 2.1 Climatic Conditions

### 2.1.1 Climatic Background of the Region

There is only one permanent meteorological station in the interior of central Baffin Island, Dewar Lakes (68°39'N, 71°14'W, 518 m.a.s.l), which is located about 100 km south of the Barnes Ice Cap (Fig. 1.2.). The average daily temperature in summer (JJA) is about 2.5°C, and in winter (DJF), -26.4°C. The average annual precipitation is about 252 mm. Based on the record from Dewar Lakes and the others in the region, Maxwell (1980) described an interior upland subregion with average July temperatures of about 5°C, and annual precipitation of 200 to 300 mm.

### 2.1.2 Spring and Summer Climatic Conditions at the Blockade Bend Station

As shown in Table 2.1(a), air temperature was recorded below-freezing in May, above freezing in June, reached the highest in July and then, dropped back in August. The July temperatures in 1990 and 1991 were much higher than the 5°C average July temperature estimated for the interior upland subregion by Maxwell (1980). Figure 2.1 shows the daily air temperature from May through June for each of the three years. The daily air temperature exceeded 0°C from 19 June in 1990, 31 May in 1991, and 21 June

in 1992. In terms of daily average, 1991 had the warmest season among the three. Table 2.1(b) shows the total precipitation during the period, most of which occurred in July and August. The lower values of precipitation in May of 1991, May and June of 1992 are suspect. Although it largely depended on weather conditions, the global solar radiation (Table 2.1(c)) was relatively high in May and June. Less radiation was received in July and August, and this was attributed to both seasonal decline of the extraterrestrial radiation and the higher occurrences of cloud-cover, as evidenced by precipitation in this period. The prevailing wind directions during the study period are SSW and NW. The average wind speed and prevailing wind for each month are listed in Table 2.2.

## 2.2 Surface Energy Budget

The period from May to August can usually be divided into 3 phases: 1) pre-melting, 2) melting and, 3) post-melting periods. The surface energy balance during both melting and post-melting periods is presented here.

**Table 2.1.**
**Climatic conditions**
**in spring and summer at Blockade Bend**

(a) Mean air temperature (°C)

| Month | 1990 | 1991 | 1992 | Average |
|---|---|---|---|---|
| May | -7.9 | -8.5 | -11.5 | -9.3 |
| June | 3.4 | 4.2 | 1.6 | 3.1 |
| July | 9.1 | 10.0 | - | 9.6 |
| August | 5.0 | 4.5 | - | 4.8 |

(b) Total precipitation (mm)

| Year | 1990 | 1991 | 1992 |
|---|---|---|---|
| May | 68.1 | 1.6 | 5.1 |
| June | 10.4 | 21.1 | 2.2 |
| July | 76.9 | 50.8 | - |
| August | 56.3 | 87.9 | - |
| Total | 211.7 | 161.4 | - |

(c) Global Solar Radiation ($MJm^{-2}day^{-1}$)

| Year | 1990 | 1991 | 1992 | Average |
|---|---|---|---|---|
| May | 22.7 | 26.1 | 26.2 | 25.0 |
| June | 25.2 | 20.8 | 26.7 | 24.2 |
| July | 14.3 | 19.4 | - | 16.9 |
| August | 10.7 | 10.8 | - | 10.8 |

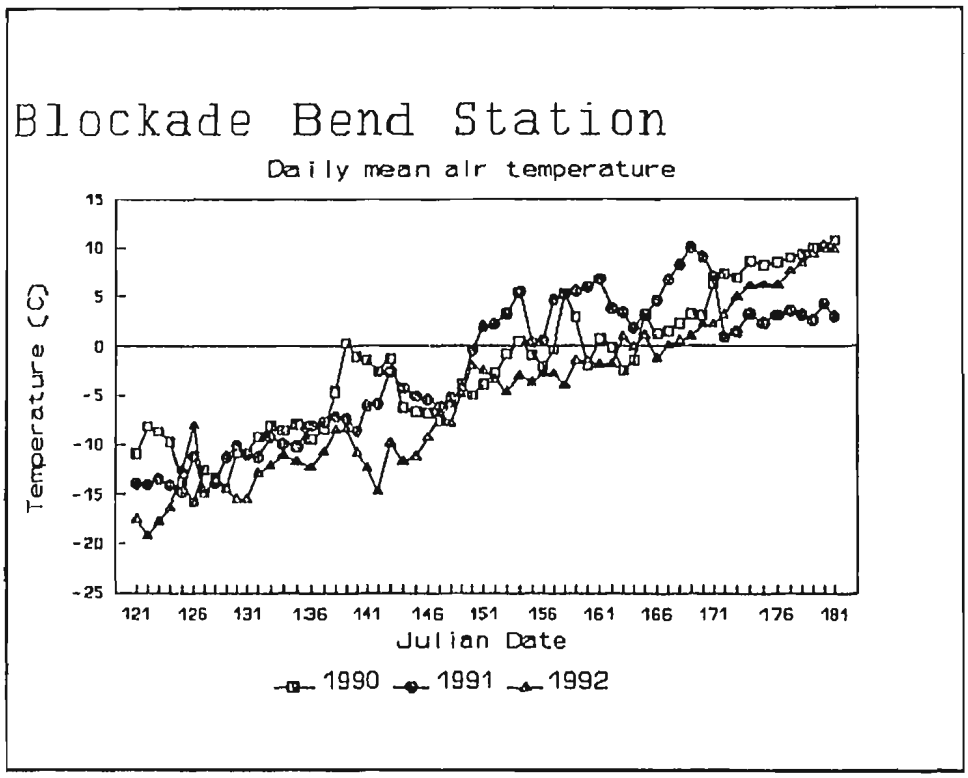


**Figure 2.1. Daily air temperature in May and June of 1990, 1991 and 1992**

**Table 2.2 Wind speed and wind direction during the study period**

| Month | Mean wind speed ($m\ s^{-1}$) | Prevailing wind direction |
|---|---|---|
| 1990 | | |
| May | 6.8 | NW |
| June | 5.8 | NW |
| July | 4.4 | SSW |
| August | 4.5 | SSW |
| 1991 | | |
| May | 4.8 | NW |
| June | 5.2 | SSW |
| July | 4.6 | NE |
| August | 5.3 | SSW |
| 1992 | | |
| May | 4.1 | NW |
| June | 4.6 | NW |

### 2.2.1 Melting Period

Since there is no measurement for snow depth, the exact dates of the beginning and ending of the snowmelt can not be determined. Nevertheless, approximate dates of the onset and end of the snowmelt can be inferred from the time series of the air temperatures. According to the records for the three years, snowmelt began at the Blockade Bend site from late May to early June, and lasted less than a week. Figures 2.2 and 2.4 show the three-hourly air temperature ($T_a$) series from late May to July from 1990 through 1992. It is known that the active snowmelt begins when the daily maximum air temperature consistently exceeds the freezing point, and, based on this criterion, the snowmelt began on days 159, 151 and 164 in 1990,1991 and 1992, respectively. The end of the snowmelt is inferred from the change in the amplitudes of diurnal variation of $T_a$ . From day 165 of 1990, 152 of 1991, and 168 of 1992, the amplitudes of $T_a$ became relatively large and consistent, implying the disappearance of snow cover.

The above estimations are certainly crude. Accurate dates of beginning and ending of the snowmelt can be determined if the snow depth is measured at the autostation, as is the case at some other locations (Jacobs, et al., 1993).

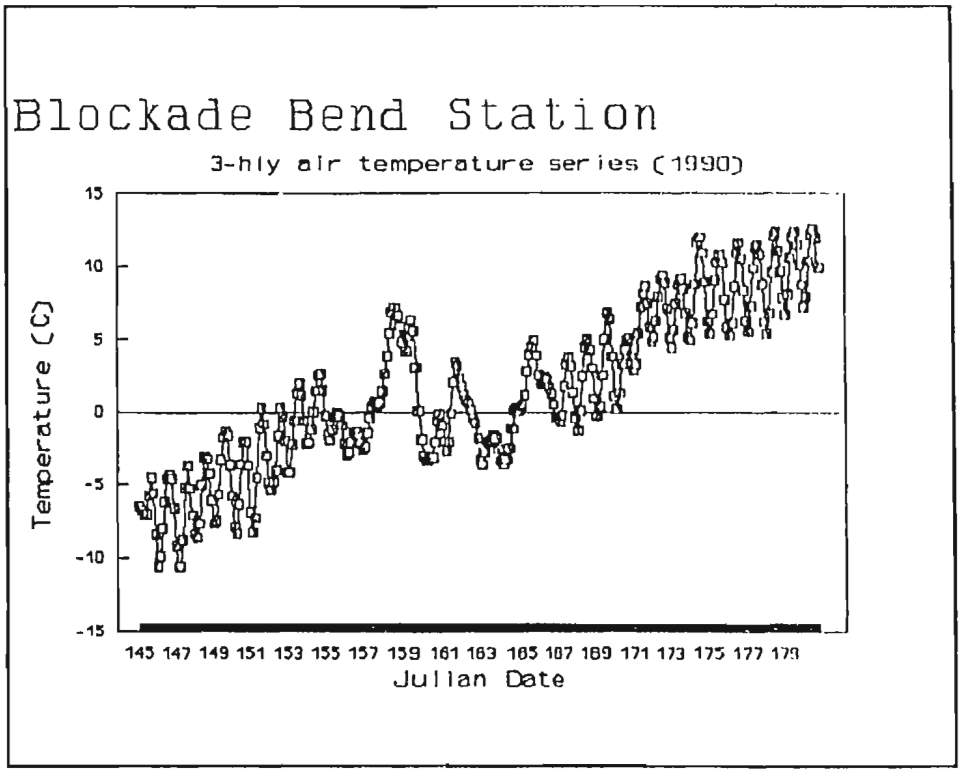


**Figure 2.2. Three-hourly series of air temperature as an indicator of the onset and end of the snowmelt of 1990.**

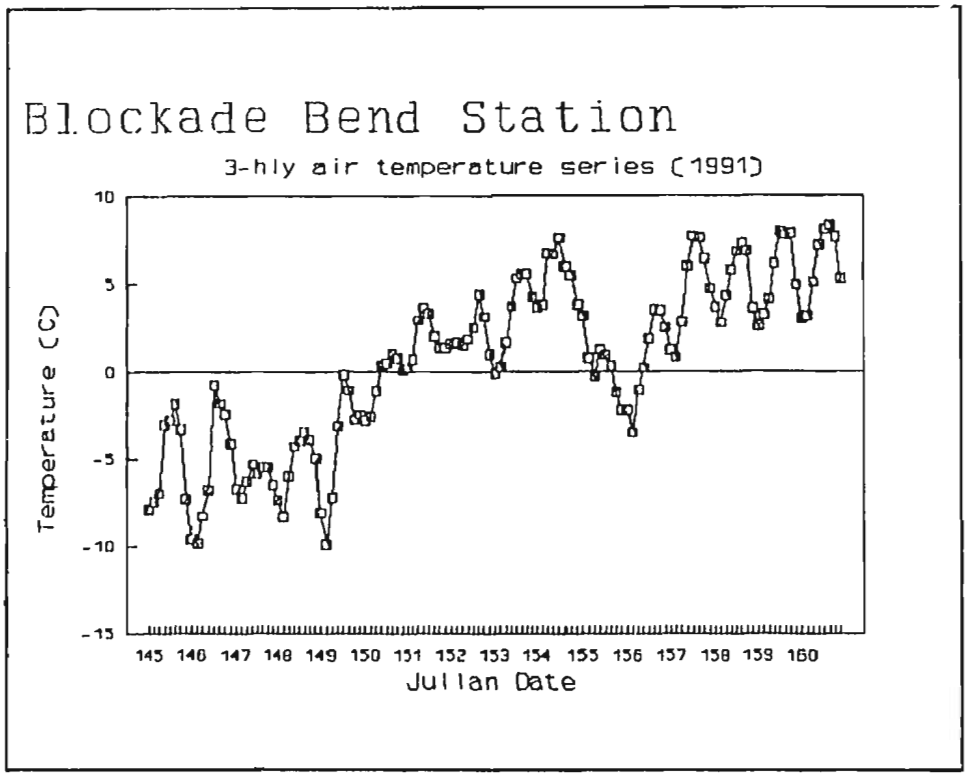


**Figure 2.3. Three-hourly series of air temperature as an indicator of the onset and end of the snowmelt of 1991.**

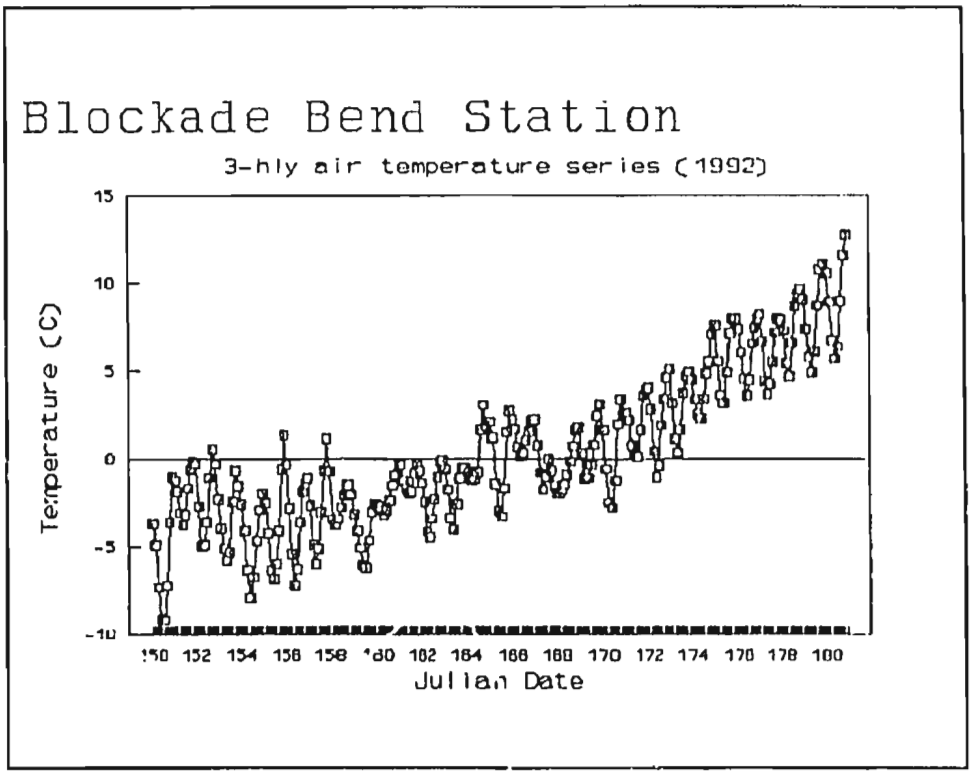


**Figure 2.4. Three-hourly series of air temperature as an indicator of the onset and end of the snowmelt of 1992.**

2.2.1.1 Assumptions

During the melting period, one can assume no soil heat flux at the base of the snowpack and a snowpack surface temperature of 0°C; therefore, the surface temperature and vapour pressure are fixed at the freezing point and 6.11 mb, respectively. It is assumed that there is no sensible heat storage within the snowpack. Therefore, the only change within the snowpack is the phase change, depending on whether there is a positive or negative surface energy balance. Equation 1.1 can be rewritten as:

$$Q^* = Q_H + Q_E + Q_M \quad \text{.....(2.1)}$$

where $Q_M$ is the latent heat storage for phase change within the snowpack.

2.2.1.2 Net Radiation

Net all-wave radiation is expressed as:

$$Q^* = K\downarrow(1-\alpha) + L^* \quad \text{.....(2.2)}$$

where $K\downarrow$ is the global solar radiation (taken positive if directed to the surface), $\alpha$ is the surface albedo, and $L^*$ is the balance of incoming ($L\downarrow$) and outgoing ($L\uparrow$) long-wave

radiation. The long-wave incoming, or downward radiation, is taken positive if directed to the surface, and the outgoing, or upward radiation, is positive away from it.

$Q^*$ can be determined by any of three methods:

(1) Direct measurements with a radiometer.

(2) If only the global solar radiation is measured, $L^*$ can be calculated as an empirical function of air humidity, surface and air temperature, and sky conditions (Oke, 1987). Based on measured or estimated value of surface albedo, $Q^*$ can be obtained by equation 2.2.

(3) Estimating $Q^*$ directly from measured global solar radiation by an empirical relation (Petzold, 1974).

Since net radiation is not a measured variable at Blockade Bend, but the global solar radiation is, the second and third methods can be used. However, an attempt to calculate $Q^*$ by method (2) proved to be unsuccessful (Price, 1976), probably due to difficulties in allowing for cloud-covered conditions. Having the same problem in terms of lacking information on sky conditions at the Blockade Bend site, we choose method (3) instead of (2) in this study.

According to the studies by Petzold (1974), for an open melting snow surface over tundra, a relationship existed between net radiation and global radiation of the form:

$$Q^* = a + b\bar{K}\downarrow \ldots\ldots KJ/m^2 day \ldots\ldots\ldots\ldots (2.3)$$

where a and b are constants determined from linear regression using observed values of $Q^*$ and $K\downarrow$. For Resolute, N.W.T. (74°43'N, 94°27'W), the constants are found to be -171.62 and 0.136, respectively, in June. A similar regression was carried out on daily values of $Q^*$ and $K\downarrow$ (June, 1973) observed at Broughton Island by Jacobs (1974), with the result that

$$a = -194.82 \text{ and } b = 0.179$$

which shows the similarity in this approach across the region for the same season and similar surface conditions. The daily relationship derived from Resolute has been converted into three-hourly relationship ( a = -21.45 and b= 0.136), and serves as a means of estimating $Q^*$ from $K\downarrow$ at Blockade Bend.

2.2.1.3. Sensible and Latent Heat Fluxes

The sensible and latent heat fluxes are both calculated by the aerodynamic method (Oke, 1987). The equations governing these fluxes in neutral conditions are:

$$Q_H = \rho C_p K_m (T_a - T_s) \quad \text{.....(2.4)}$$

and

$$Q_E = L_v K_m (q_a - q_s) \quad \text{.....(2.5)}$$

where $C_p$ and $L_v$ are the specific heat of air at constant pressure and the latent heat of evaporation, respectively, $T_s$ is the snow surface temperature, $q_s$ is the snow surface absolute humidity, and $T_a$ and $q_a$ are the air temperature and humidity at the measurement level ($q_a$ is determined from $T_a$ and relative humidity). The turbulent transfer coefficient $K_m$ is derived from neutral conditions, so that

$$K_m = k^2 U_a \rho / [\ln(z_a/z_0)]^2 \quad \text{.....(2.6)}$$

where k is the von Karman constant (=0.4), $\varrho$ is air density, $U_a$ is the wind speed at the level of measurement $z_a$, and $z_0$ is the surface roughness length.

To allow for the effects of atmospheric stability on the transfer coefficient, a simple correction using the gradient form of the Richardson Number is employed (Price, 1976). In stable conditions

$$K = K_m / (1 + \sigma R_i) \quad \text{.....(2.7)}$$

while in unstable conditions

$$K = K_m (1 - \sigma R_i) \quad \text{.....(2.8)}$$

where K is the transfer coefficient in stable or unstable conditions, the constant $\sigma$ has a

value of 10, and $R_i$ is the Richardson Number,

$$R_i=(gz\Delta T)/[TU_a^2]\text{.....(2.9)}$$

where g is gravitational acceleration, $\Delta T$ is the temperature difference between the surface and the height $Z_a$, and T is the mean absolute temperature over the measured layer.

With the assumptions of the isothermal condition made at the snow surface in 2.2.1.1., and the meteorological variables observed at the measured level, $Q_H$ and $Q_E$ can be determined from equations 2.4 through 2.9.

2.2.1.4 Snowmelt

As described in 2.2.1.2 and 2.2.1.3, four surface energy flux terms in equation 2.2 are determined except $Q_M$, the total energy available for melting snow, which can be obtained as a remainder term to equation 2.1 on a three-hour or daily basis. If $Q_M$ is positive, a certain amount of snow is melted, otherwise, it is assumed that the surface melted water refroze.

2.2.1.5 Results and Discussion

Table 2.3 shows the surface energy balance components on melting days ($Q_M > 0$) during the melting period of 1990, 1991 and 1992. During the 1990 melting period, the net radiation contributed 87% of the melt energy, which is much higher than results reported elsewhere (Munro, 1990; Oke, 1987). This indicates that the convective fluxes together supplied a small amount of heat. In fact, the sensible heat flux acted as source, while the latent heat fluxes acted as a sink.

During the 1991 melting period, $T_a$ had been consistently above freezing since the end of May. The air was warm and humid during the melting period. This made both the sensible and latent heat act as the significant sources for snowmelt. On average, the net radiation accounted for about 48% of the total melt energy and the convective fluxes for about 52%. The Bowen ratio is high, indicating that the sensible heat flux $Q_H$ provided as much as 8 times more melt energy than $Q_E$. The average ranking of heat sources agrees with the results by Munro (1990) during the melting period.

During the melting period in 1992, the net radiation acted as the only important heat source. Although $Q_H$ was a small source, the combined effect of convective fluxes was as a heat sink. Snowmelt used about 74% of the net radiation, which is higher than the results reported by Ohmura (1982b).

In all, the net radiation is always the most important energy component during the melting period. It can act as an only source for snowmelt or a source along with

**Table 2.3**
**Daily totals of energy balance components during the snowmelt period**

| Date | K↓ | $Q^*$ | $Q_H$ | $Q_E$ | $Q_M$ | ß | $Q^*/Q_M$ |
|---|---|---|---|---|---|---|---|
| | ----------$MJm^{-2}day^{-1}$---------- | | | | | | |
| 1990 | | | | | | | |
| 159 | 21.9 | 5.37 | -2.48 | 1.04 | 6.82 | -2.39 | 0.79 |
| 161 | 27.7 | 6.85 | -0.51 | 3.22 | 4.14 | -0.16 | 1.65 |
| 162 | 8.9 | 2.09 | -0.35 | 1.60 | 0.85 | -0.22 | 2.47 |
| 165 | 19.5 | 4.78 | -7.39 | 2.13 | 10.03 | -3.46 | 0.48 |
| Avg. | 19.5 | 4.77 | -2.68 | 1.20 | 5.46 | -2.23 | 0.87 |
| 1991 | | | | | | | |
| 151 | 16.2 | 3.92 | -4.28 | 0.55 | 7.66 | -7.84 | 0.51 |
| 152 | 11.2 | 2.67 | -2.03 | -1.38 | 6.08 | 1.47 | 0.44 |
| Avg. | 13.7 | 3.30 | -3.16 | -0.42 | 6.87 | 7.52 | 0.48 |
| 1992 | | | | | | | |
| 164 | 29.1 | 7.21 | -0.48 | 1.64 | 6.05 | -0.29 | 1.19 |
| 165 | 26.3 | 6.49 | 0.58 | 2.15 | 3.77 | 0.27 | 1.72 |
| 166 | 16.8 | 4.10 | -0.91 | 0.31 | 4.69 | -2.89 | 0.87 |
| 168 | 16.0 | 3.88 | 0.32 | 2.09 | 1.47 | 0.15 | 2.64 |
| Avg. | 22.1 | 5.42 | -0.12 | 1.55 | 4.00 | -0.07 | 1.36 |

convective fluxes. The sensible heat flux was always a heat source during the snowmelt, while the latent heat could either be an sink or source, depending on the air humidity. It should be noted that the exact ranking of the energy flux terms here may not be very accurate due to the limited measured variables at the reference station, however, it at least suggests that the relative importance of flux terms varies from year to year, depending strongly on weather conditions. There was no significant precipitation during the melting periods for all the three years. This indicates that the contribution of precipitation to the snowmelt was negligible. The air temperature varied from year to year. The highest air temperature during the snowmelt in 1991 explained the greatest contribution of the sensible heat flux to the snowmelt among the three years, while the relatively low air temperature in 1992 attributed to a relatively low ranking of the sensible heat flux during the melting period. It is interesting to find that, for each year, the amount of melted water derived from the calculated melt energy during the melting period agrees with the snow amount estimated from monthly total precipitation (Table 2.4).

**Table 2.4.**

**Melted snow[a] and observed snow amount[b]**

| | Melted snow (mm) | observed snow (mm) |
|---|---|---|
| 1990 | 227 | 232 |
| 1991 | 143 | 158 |
| 1992 | 166 | M[c] |

[a]melted snow is derived from the calculated melt energy using a snow density of 288 $Kgm^{-3}$ (Oke, 1987).

[b]observed snow amount is estimated by summing the monthly total precipitation from September (previous year) to May (present year);

[c]the total precipitation for April and May of 1992 is missing.

### 2.2.2 Post-melting Period

The surface is snow-free during the post-melting period. The determination of the surface energy budget over a snow-free surface is usually a process of finding an equilibrium surface temperature ($T_g$) to balance equation 1.1 ($T_g$ and $L^*$ are implicit in equation 1.1), since the only unknown in this equation is $T_g$ (Outcalt, 1972). Under clear sky conditions, net long-wave radiation $L^*$ can be well parameterized as a function of surface temperature, screen temperature and air humidity (Oke, 1987). However, under cloudy sky conditions, $L^*$ is hard to calculate, and this results in two unknowns in equation 1.1, $L^*$ and $T_g$. It should be noted here that the ground temperature measured at 0 cm ($T_0$) is not always the same as the equilibrium surface temperature because of possible direct heating of the sensor by solar radiation. However, under very cloudy skies, the differences should be negligible. Therefore, under very cloudy conditions, we assume that $T_0$ is equal to $T_g$, and hence the only unknown in equation 1.1 is $L^*$. An index of sky clearness (CI) is introduced to separate clear or partially cloudy from very cloudy skies. It is defined as the ratio of the measured global solar radiation to the extraterrestrial solar radiation. When CI exceeds a value of 0.3, the sky is assumed to be clear or partly cloudy, otherwise the sky is considered to be fully covered by cloud (Iqbal, 1983).

2.2.2.1 Clear Sky Conditions

In clear or partly cloudy conditions (CI > 0.3), $Q^*$ can be obtained by method (2) in 2.2.1.2. The long-wave radiation emitted by a cloudless atmosphere is used to approximate this condition, and it can be written in the form of the Stefan-Boltzman equation:

$$L\downarrow = \epsilon_a \sigma T_a^4 \text{.....(2.10)}$$

where $\epsilon_a$ is the atmospheric emissivity. The empirical formula for $\epsilon_a$ by Idso (Oke, 1987) is used:

$$\epsilon_a = 0.70 + 5.95x10^{-5} e_a \exp(1500/T_a) \text{.....(2.11)}$$

Where $e_a$ is the vapour pressure at the level of measurement, $T_a$ is the air temperature. Meanwhile, the outgoing long-wave radiation from the surface ($L\uparrow$) can be approximated by that from a full radiator at equilibrium surface temperature. Therefore, the net long-wave radiation can be expressed as:

$$L^* = \epsilon_a \sigma T_a^4 - \sigma T_g^4 \text{.....(2.12)}$$

$Q^*$ is then formulated as a sum of net short-wave and long-wave radiation, such that:

$$Q^* = K\downarrow(1-\alpha) + L^* \quad \text{.....(2.13)}$$

where $\alpha$ is the surface albedo.

The sensible and latent heat fluxes are formulated in the same way as in 2.2.1.3 except that the surface temperature and humidity are now unknown. The surface absolute humidity can be formulated as the product of saturated humidity at surface temperature and surface relative humidity (Myrup, 1969), such that:

$$q_0 = r \cdot q_{s0} \quad \text{.....(2.14)}$$

where, r is the surface relative humidity, which varies with surface wetness, and $q_{s0}(T_g)$ is the saturated humidity when the surface equilibrium temperature is $T_g$. The saturated humidity can be expressed as (Stull, 1988):

$$q_{s0} = (3.80/P) \cdot \exp[17.67(T_g - 273.16)/(T_g - 29.66)] \quad \text{.....(2.15)}$$

where, P is the air pressure (mb).

The soil heat flux is expressed as:

$$Q_G = k_s(T_g - T_{10})/Z_s \quad \text{.....(2.16)}$$

where $k_s$ is the thermal conductivity and $Z_s$ (= 0.1 m) is the measurement depth of soil

temperature $T_{10}$ .

By substituting equations 2.4 through 2.16 into equation 1.1, we have:

$$K\downarrow(1-\alpha)-\sigma T_g^4+\epsilon_a\sigma T_a^4=\rho K(T_g-T_a)+L_vK(q_g-q_a)+k_s(T_g-T_{10})/Z_s....(2.17)$$

The only unknown in equation 2.17 is the surface equilibrium temperature $T_g$. An algorithm for a numerical iterative process is used to solve $T_g$ in equation 2.17. The flux terms in equation 1.1 can be retained at the end of the iteration.

2.2.2.2 Cloudy Sky Conditions

When the clearness index CI is lower than 0.3, the sky is assumed to be very cloudy or dark at night. Under these conditions, $T_0$ is assumed to be equal to $T_g$. Therefore, $L\downarrow$ is now the only unknown in equation 1.1 and can be solved as the remainder of the equation.

2.2.2.3 Results and Analysis

The exact partitioning among the energy components during the post-melting period depends on both the net radiation and the surface moisture availability. Table 2.5 shows the daily energy components of four days from 1991. On day 158, the net radiation

**Table 2.5**

**Daily totals of energy balance components**

**during the post-melting period**

| Date | $Q^*$ | $Q_H$ | $Q_E$ | $Q_G$ | ß | $Q_G/Q^*$ |
|---|---|---|---|---|---|---|
| 1991 | ----------$MJm^{-2}day^{-1}$--------- | | | | | |
| 158 | 17.52 | 5.30 | 10.92 | 1.30 | 0.49 | 0.07 |
| 191 | 12.60 | 4.83 | 6.37 | 1.40 | 0.76 | 0.11 |
| 218 | 8.29 | 2.15 | 6.40 | -0.27 | 0.34 | -- |
| 223 | 5.45 | 0.82 | 7.39 | -2.78 | 0.11 | -- |

was high, and the large latent heat flux is attributed to the evaporation of the melted water. The convective heat fluxes together consumed about 93% of the net radiation. The soil heat flux $Q_G$ acted as a very small energy sink. Owing to a period of desiccation of the soil crust before day 191, as evidenced by no precipitation, the surface was drier than that after the snowmelt, the latent heat of evaporation was largely limited compared to day 158. The Bowen ratio rose to 0.76, and the ratio between the soil heat flux and the net radiation became 11%. From early August (218), the surface became very wet again because of the large amount of precipitation. On day 218, due to the precipitation of previous days, the latent heat flux is much larger than the sensible heat flux, resulting in a low value of Bowen ratio (0.34). The latent heat flux became much larger on day 223 after rainfall (29.4 mm) on the previous day. It is noted that the soil heat fluxes acted as a small energy source for both days. This can be explained by the substantial decrease of ground surface temperature in August (Ohmura, 1982).

It is evident that the net radiation is the only significant energy source during the post-melting period, with values much larger than those for the melting period. The latent heat flux was always more effective than the sensible heat flux in removing heat from the tundra surface, especially when the ground surface is wet due to either precipitation or melted water. However, if the soil crust was dessicated to a certain degree, a higher Bowen ratio can be found. The soil heat flux is generally a energy sink before August, but it can be an energy source when the ground surface temperature decreases to a certain extent.

Since the autostation was not designed to provide complete surface energy balance data, the results from the surface energy balance calculation based on the limited meteorological variables are only approximate. More detailed and accurate computation can be made if the complete measurements for surface energy data are available at the reference station. For example, the addition of a net radiometer removes the uncertainties in estimating $Q^*$ from $K\downarrow$. However, net radiometers require special attention and are not suited to unattended autostations.

# *Chapter 3 AREAL SURFACE ENERGY BALANCE MODEL (ASEBM)*

The areal surface energy balance model (ASEBM) is a two-dimensional model aimed at estimating the spatial variability of the surface energy balance induced by the varied topography, surface properties and atmospheric conditions. Although initially designed for the Baffin Island study area, the methodology and the procedures of the model can be applied elsewhere. This chapter will deal with the acquisition of the information required by the ASEBM as well as how the model works based on the given information.

## 3.1 Digital Elevation Model (DEM)

The local topography has a strong influence on the surface energy budget. In an area with complex terrain, the solar radiation varies spatially due to different slope and aspect angles of the surfaces. Furthermore, the surface wind can be modified significantly by the complex terrain. Both the solar radiation loading and surface wind are important for regulating the surface energy budget. In order to integrate the topographical information into the ASEBM, a digital elevation model (DEM) is required by the ASEBM to estimate the topographically-induced variations in surface energy budget. Based on the DEM, maps of slope and aspect can be derived under a geographical information system (GIS).

maps of slope and aspect can be derived under a geographical information system (GIS). In this study, the IDRISI system is used (Eastman, 1990).

The contours of the study area have been digitized into a DEM with a resolution of 100 m x 100 m for use within a GIS (Figure 3.1). The main features of the topography are the nearly parallel north-to-south hills and valleys in the tundra terrain and a nearly flat surface over the glacier. The elevation is relatively low in the southwest (around 200 m.a.s.l.), and much higher over the glacier, rising above 600 m.a.s.l. in the study area. The Blockade Bend autostation is located on a small ridge near the western margin of the area. Figure 3.2 shows the slope and aspect maps generated by GIS and mapped by a software package called SURFER (the origin of the coordinates has been shifted to the centre of the study area). The area is generally flat with the maximum slope angle less than 13 degrees. Most of the flatter terrain is over the glacier and the valley in the southwest. The aspect of slopes in the study area ranges from 90 to 280 degrees, which are in favourable directions in terms of receiving the solar radiation. The spatial patterns of the aspect clearly reflect the distribution of the topographical features within the study area.

These three maps are the base maps of topographical information for the study area required by the ASEBM to estimate the topographically-induced spatial variation in the surface energy budget. In practice, the resolution may be different from that of the base maps; therefore, the resolution of those base maps should be changed accordingly. This can be achieved by using the averaging or interpolation modules in the GIS software.

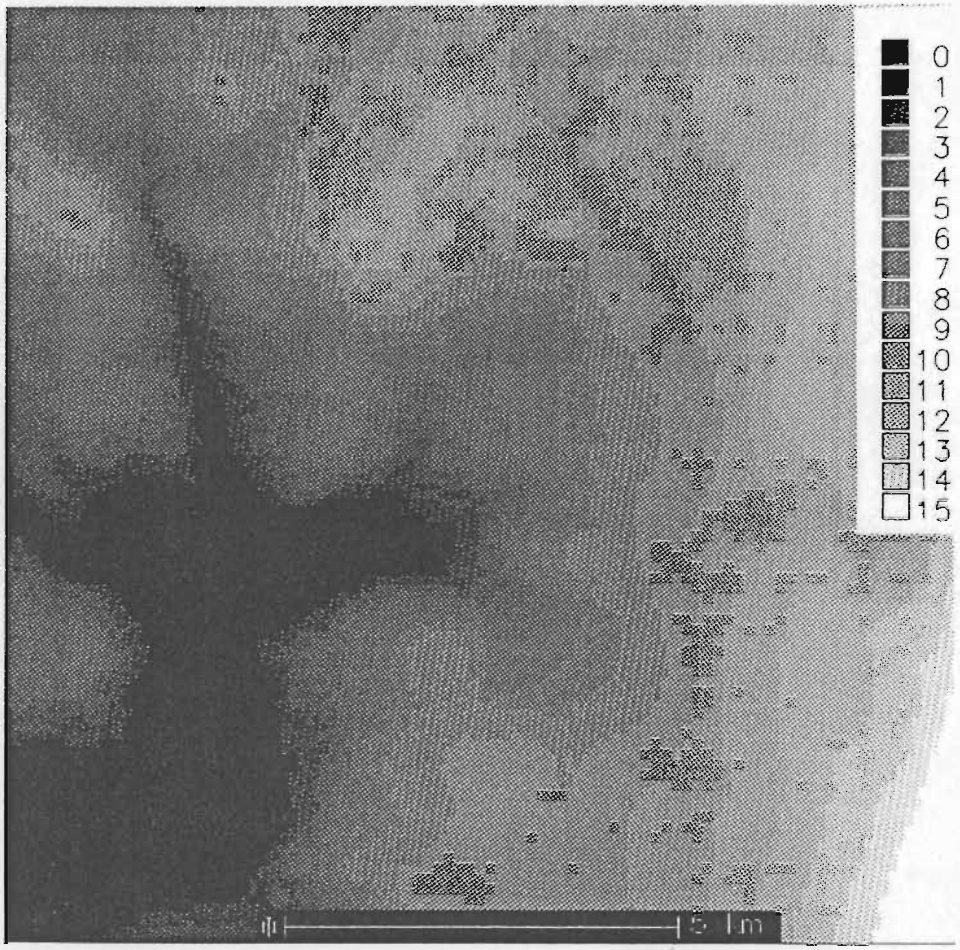


**Figure 3.1 Digital elevation model of study area shown in Fig.1.2b. Elevation classes are in 30 m intervals above a base at 200 m.a.s.l.**

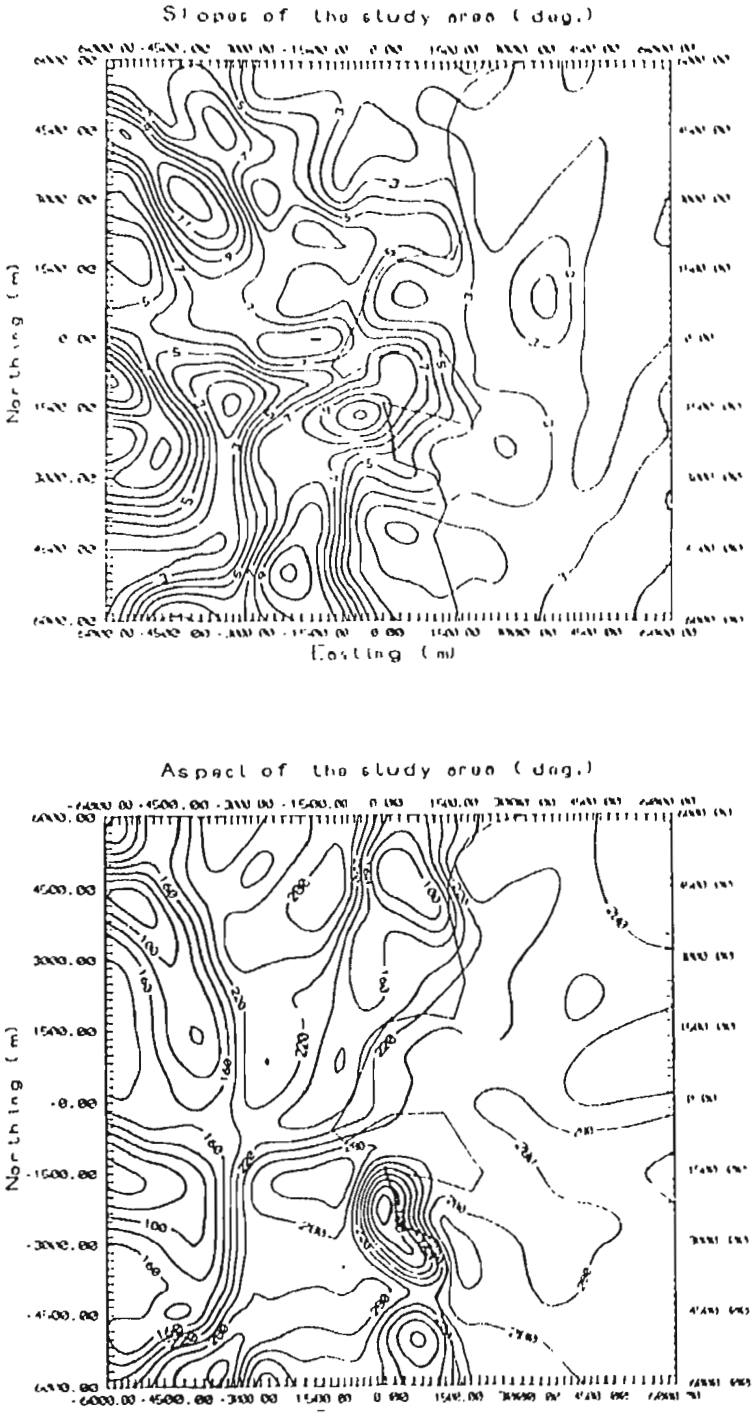


**Figure 3.2. Slope and aspect of the study area. (a) map of slope; (b) map of aspect.**

## 3.2 Maps of Surface Properties

The surface properties are important for determining the spatial variations of the surface energy budget. They include the surface albedo, roughness, relative humidity and thermal conductivity. The ASEBM allows for the effects of surface albedo, roughness and relative humidity on the spatial variability of the surface energy budget. The surface information can be obtained from field surveys and remotely sensed data. Surface albedo and relative humidity can be derived from LANDSAT MSS or TM imagery, and surface roughness is usually obtained from field work.

The methods of surface albedo determination from LANDSAT imagery have been widely used (Otterman and Fraser, 1976; Musick, 1986; Brest and Goward, 1987, Duguay et al., 1991). Computation of surface albedo from selected bands of LANDSAT imagery requires knowledge of spectral reflectivity of the surface, spectral distribution of solar radiation and atmospheric conditions (Brest and Goward, 1987).

The surface relative humidity depends not only on the surface types, but also on the surface moisture content. According to the definition of surface relative humidity proposed by Myrup (1969), which is the "fraction of area in water or freely transpiring vegetation," the surface relative humidity can be derived from a map with major vegetation types (bare ground, vegetation, water) classified from the LANDSAT data.

For this study, a LANDSAT MSS image of the study area (19 August 1988) is used to estimate the surface albedo. One of the visible bands of the image (Band 4) is shown

in Figure 3.3. It is evident that the relative spatial variation of the surface albedo is more important in this study than the absolute values. A simple approach, instead of detailed computation, is used here to calculate the surface albedo based on this visible band and the estimated values of albedo from several target grids. A linear relation is assumed between the digital counts, or brightness levels, of the visible band and the surface albedo, such that:

$$\alpha_i = a + b \cdot D_i \quad \text{.....(3.1)}$$

where $\alpha_i$ is the surface albedo of ith grid area, and $D_i$ is the digital counts of the corresponding grid in the visible band imagery. The constants a and b are -0.02 and 0.003, respectively. Based on equation 3.1, a map of surface albedo is generated from the LANDSAT imagery (not shown). The highest values (0.69) of the albedo exist over the glacier, and the values over the tundra are relatively low ( 0.1 - 0.18) compared to the measurements on tundra elsewhere (Oerlemans, 1993). This may result from the recent rainfall over the study area and/or the atmospheric degradation of the image on the day when the image was taken.

The other two surface properties are treated in a simple way for this study. As for the surface relative humidity, a value of 1 is assigned to the glacier surfaces. Over the tundra, knowing that the surfaces were wet and homogeneous in August of 1991, as evidenced by large amount of precipitation, the value used for the Blockade Bend site

(varying from day to day) is assumed to be representative for the whole tundra area. The surface roughness is treated in the same way. A typical value of 0.1 cm is assigned to the tundra terrain, and 0.001 cm to the glacier (Oke, 1987). Based on these assignments, a grid-based map is created by invoking a GIS routine.

It is evident that the simple treatment of surface properties in this application is not a limitation of the ASEBM, since a more detailed classification can be easily accommodated by the model when detailed surface information is available from either remotely sensed data or field survey.

## 3.3 Spatial Variation of Wind

The surface wind is an important factor for determining the convective fluxes. Therefore, the modification of surface wind by the complex terrain will have an effect on the spatial variations of the surface convective fluxes, and hence, the surface energy budget.

The flow over hills has been studied by many investigators (Taylor, 1977; Jackson and Hunt, 1975). In the near neutral conditions that exist when mechanical mixing is the dominant process, the surface wind flow over a complex terrain can be estimated from a single reference measurement using the MS3DJH model of Walmsley et al. (1986). This model is designed to compute the surface wind modified by varied topography and surface roughness. A microcomputer version of that model, MS-Micro/3 (Walmsley et

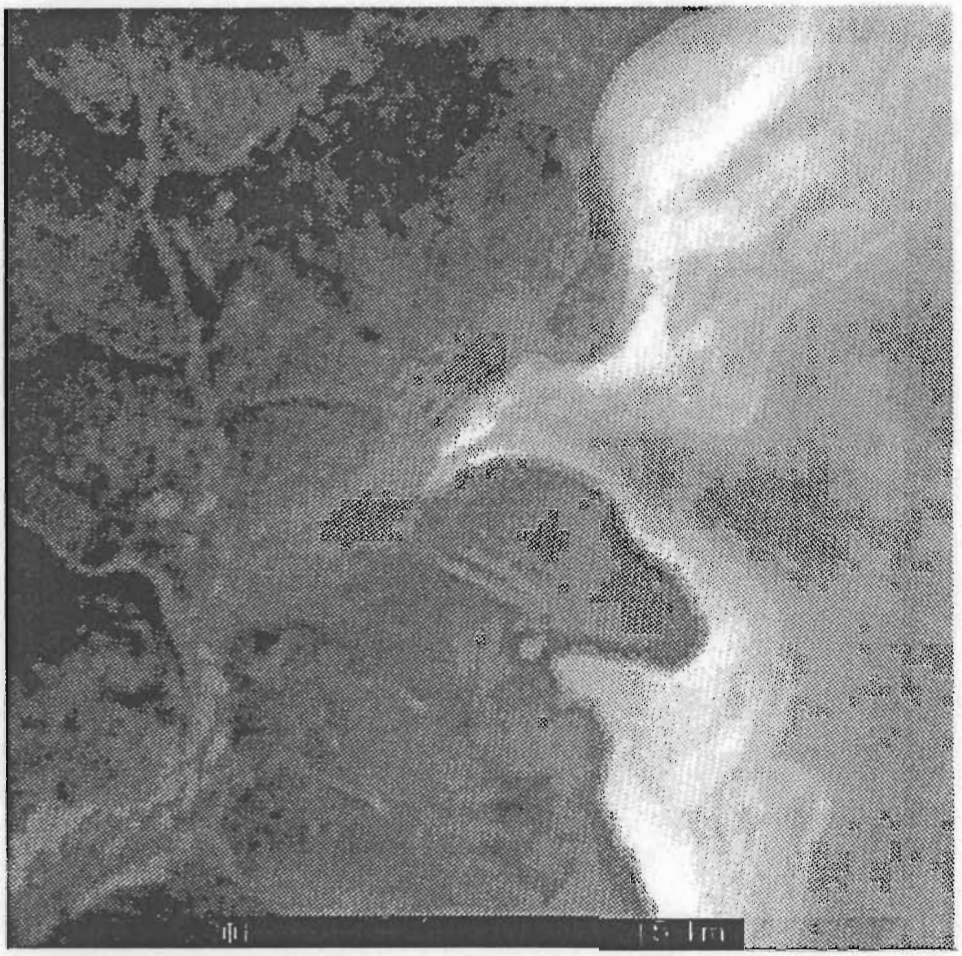

**Figure 3.3. LANDSAT MSS subscene (Band 4) for 19 August 1988.** The area is that shown in Fig. 1.2b.

al., 1990) is integrated as part of the ASEBM.

The wind model is applied to the study area, with reference to the wind measurements from the Blockade Bend autostation, to estimate the wind modification by the terrain over the whole area. The output of the MS-Micro/3 is a set of normalized windspeed files for different upwind directions (Appendix D).

One of the most important requirements for neutral stratification by the wind model is moderate to strong wind. Taylor and Lee (1984) proposed a low limit of windspeed of 3.0 $ms^{-1}$ at 10 m over the surface. This requirement is usually met in the study area, as evidenced by the strong wind measurements at the Blockade Bend. However, in areas where wind is light, the wind model should be used with caution.

## 3.4 Computation of Radiation Loading

It is evident from the discussion in Chapter 2 that the net radiation is the most important surface energy component in both melting and post-melting periods. Therefore, the determination of how this component varies topographically is fundamental to understanding the spatial variability of the surface energy budget. As shown in equation 2.2, the net radiation is composed of net solar radiation $K^*$ ($=(1-\alpha)\,K\downarrow$) and net long-wave radiation $L^*$. Among these components, the spatial variability of short-wave global radiation $K\downarrow$ is the most important (Garnier and Ohmura, 1968; Swift, 1976), while the effects of the spatial variability of long-wave radiation on the surface energy budget are

less important over the same type of terrain. Therefore, $L^*$ can be assumed to be homogeneous over a limited area (several kilometres).

For the study area, the net long-wave radiation ($L^*$) over the tundra is assumed to be homogeneous, and the value is estimated from the Blockade Bend station, as done in Chapter 2. However, it is apparent that $L^*$ over the glacier differs from the tundra because of the difference in surface temperatures (Ohmura, 1982). Therefore, over the glacier, we only assume that the long-wave downward radiation ($L\downarrow$) is the same as that at the autostation site, which is an acceptable assumption over the limited area. The long-wave upward radiation ($L\uparrow$) over the glacier is calculated using the Stephen-Boltzman law. The assumptions made here are applied to the study area because of its distinctive terrain features. In other areas where the surfaces are relatively homogeneous, no spatial variations in $L^*$ need assumed.

### 3.4.1 Spatial Variation of Solar Radiation

The global solar radiation $K\downarrow$ is composed of the direct-beam (S) and diffuse radiation (D). Both of the components of $K\downarrow$ contribute to the spatial variability of solar receipt at the surface, although the contribution of the diffuse radiation is much less than the direct-beam component. The total solar radiation incident on a slope can be formulated as:

$$K_s\downarrow = S\cos\Theta/\cos Z + D(1+\cos\beta)/2 + \alpha K\downarrow(1-\cos\beta)/2 \quad \text{.....(3.2)}$$

where $K_s\downarrow$ is the total solar radiation incident on a slope, S and D are the direct-beam and diffuse radiation received by a nearby horizontal surface, $\Theta$ is the angle between the direct-beam and a normal to the slope surface, Z is the solar zenith angle, and ß is the slope angle (Oke, 1987). The first term on the right of the equation 3.2 is the direct-beam part, the second is the diffuse radiation viewed by the slope, and the third is the reflected short-wave radiation seen by the slope. $\Theta$ is a function of slope angle, slope aspect, solar zenith and azimuth angles. It can be written as:

$$\cos\Theta = \cos\beta\cos Z + \sin\beta\sin Z\cos(\Omega - \Omega') \quad \text{.....(3.3)}$$

where $\Omega$ and $\Omega'$ are the solar azimuth angle and slope aspect, respectively.

Once the spatial variation of the global solar radiation ($K_s\downarrow$) is determined, the spatial pattern of the net solar radiation can be calculated as the product of the surface albedo and the global solar radiation.

### 3.4.2 Separating Direct-beam from Diffuse Radiation

As shown in equation 3.2, the calculation of solar radiation incident on an inclined surface requires measurements of direct-beam and diffuse radiation from a nearby

horizontal surface. We know that the surface at the reference autostation is horizontal. Therefore, assuming the homogeneity of the horizontal components of both the direct and diffuse radiation within the study area, we can calculate the spatial variability of solar radiation based on the measurement from that autostation. Since only the global solar radiation is measured at that autostation, a separation of direct from diffuse radiation is necessary. The methodology of separating the components of solar radiation is well establish by Liu and Jordan (Iqbal, 1983). It can be expressed as:

$$\frac{D}{S} = A + B \cdot CI \quad \text{.....(3.4)}$$

where A and B are empirical constants, and the clearness index CI is as defined in 2.2.2. The hourly radiation data for 1988 and 1989 at Resolute, N.W.T. (74°43'N, 94°27'W) have been used to derive the empirical relationship as in equation 3.4 on a monthly basis. The statistical relationships derived from May through August are shown in Appendix C. These empirical formulae are assumed to apply in our study area and are used to separate direct from diffuse radiation.

It should be noted that the above procedure can be excluded when both the direct and diffuse radiation are measured at the reference station. It is not a part of the ASEBM, but only a procedure of acquiring the meteorological information required by the ASEBM.

## 3.5 Computation of Subsurface Heat Flux

The explicit formulation of soil heat flux ($Q_G$) as in equation 2.16 is impossible in the ASEBM because of the lack of information on the spatial patterns of the surface thermal characteristics and the soil temperature profiles. Therefore, simplification is required to estimate this energy component. The ASEBM uses the parameterization proposed by Gadd and Keers (1970) in GCM studies:

$$Q_G = \mu Q^* \quad \text{.....(3.5)}$$

where $\mu$ is assigned a value of 0.1 for $Q^* > 0$ and 0.5 for $Q^* < 0$. However, this parameterization is only valid over the bare ground. Over the tundra in the study area, equation 3.5 gives reasonable estimates of the soil heat flux during the early summer (June, July). However, due to the significant cooling of the tundra surface in August, the soil heat flux is upward most of the time during a day, and equation 3.5 is no longer valid. Since the ASEBM is applied to August, 1991, we simply assume the soil heat flux over the tundra in the study area has the values of the reference station, the Blockade Bend site, as calculated in Chapter 2. Over the ice sheet, $Q_G$, the subsurface heat flux is the total energy used to heat and melt the ice (sensible plus latent), which is about 6 to 7 times larger than the soil heat flux over the bare tundra (Ohmura, 1982b). To estimate this component over the glacier in the study area, equation 1.1 is solved

excluding the soil flux term $Q_G$, and the solution to equation 1.1 is the ice surface temperature. If this intermediate surface temperature is higher than 0°C, sufficient ice is melted to bring the temperature to 0°C again. In this case, the surface temperature is reset to 0°C, and equation 1.1 is solved again, and $Q_G$ is obtained as a remainder to the equation. If the intermediate ice surface temperature is calculated below freezing, no subsurface heat flux is assumed.

If the ASEBM is used for places with different terrain features from those in the study area, the simplification and parameterization made here may be modified. The differences in the assumptions will lead to different magnitudes of the available energy ($Q^* - Q_G$) for convective heat exchange processes.

## 3.6 Computation of Convective Heat Fluxes

The computation of convective heat fluxes in the study area differs between the tundra and the glacier. Over the tundra surfaces, the convective fluxes are determined by the Bowen ratio approach, while over the glacier they are calculated by the aerodynamic method described in 2.2.1.3.

The Bowen ratio approach estimates the convective fluxes from the Bowen ratio (ß) and the available energy ($Q^* - Q_G$), such that:

$$Q_E=(Q^*-Q_G)/(1+\beta).....(3.6)$$

Once $Q_E$ is known, $Q_H$ can be derived from the definition of the Bowen ratio. In equation 3.6, $Q^*$ and $Q_G$ have been estimated from 3.4 and 3.5. The Bowen ratio can be estimated from the classification of surface types over the tundra based on remotely sensed imagery. Typical values can be assigned to each of the surface types. During our study period (August 1991), however, the surface was expected to be wet all over the tundra, as evidenced by the large amount of rainfall. The surfaces are assumed to be homogeneous in terms of the Bowen ratio, with the values obtained from the reference station site.

Over the ice sheet, the aerodynamic methods are used. The air temperature and humidity at level Z in equations 2.4 and 2.5 are derived from the Barnes Ice Cap autostation. The air temperature within the glacier area is estimated from the readings at the Barnes Ice Cap autostation and then calibrated for the elevation difference at the adiabatic lapse rate (0.98°C/100m). The absolute air humidity is assumed to be the same as that at the autostation site, and the wind speed is retrieved from the results of the MS-Micro/3.

The reason for employing different approaches over different terrains is apparent. Over the tundra, the atmospheric conditions are not known with respect to the complex and inhomogeneous local topography. The meteorological variables measured at the

Blockade Bend station do not accurately represent the conditions at other sites. Over the more homogeneous and extensive glacier surface, it is possible to estimate the meteorological variables from the reference station on the ice cap nearby. Furthermore, the boundary condition on the glacier that $T_s$ never exceeds the freezing point simplifies the formulation of the surface energy balance, which makes the aerodynamic methods more suitable in this case.

The exact methods used for determining the convective heat fluxes may vary with the area to which the ASEBM is applied, depending on the availability of field measurements. The Bowen ratio approach is promising in the estimation of convective heat fluxes when the detailed field measurements are not available, since a simple map of the Bowen ratio can be derived from the remotely sensed data. The values of the Bowen ratio at the reference stations can be used to validate the estimation from the remotely sensed data.

## 3.7 Computation of Ground Surface Equilibrium Temperature

Over the glacier, the equilibrium surface temperature $T_s$ is retained as the solution to equation 1.1, and is always less than or equal to 0°C. Over the tundra, $T_s$ can be calculated as a solution to equation 3.7:

$$K_m L_v (r \cdot q_{s0}(T_g) - q_a) = Q_E \text{.....(3.7)}$$

where, $Q_E$ on the right side of the equation is calculated by the Bowen ratio approach as described in 3.6, and the term on the left side is the aerodynamic formulation of $Q_E$. Under neutral conditions, $K_m$ is a function of surface windspeed and roughness. The surface wind speed is estimated from the MS-Micro/3 in 3.3. By assuming that the absolute air humidity is homogeneous over the tundra, the only unknown in equation 3.7 is $T_g$. The numerical solution of $T_g$ can be obtained iteratively.

Although it is a simple estimation, equation 3.7 can allow for the effects of the surface wind speed, surface relative humidity and roughness. The ground surface temperature is actually solved as a function of the latent heat flux, the surface wind speed, and surface relative humidity as well as roughness length. In this study, no variations of surface roughness and relative humidity over the tundra are assumed. Therefore, the ground surface temperature in equation 3.7 is only a function of evaporation rate and the surface wind speed. If the evaporation rate is the same at two sites, the higher the wind speed, the lower the ground surface temperature. This is expected in an areas with relatively homogeneous surface moisture availability. More complicated situations can be modeled if the spatial variations of surface relative humidity and roughness are available to the ASEBM.

## 3.8 Model Structure

The ASEBM is composed of two core modules: the point module (SEB.EXE) and the areal module (ASEB.EXE) (Figure 3.4). SEB.EXE calculates the surface energy balance at the reference station, as described in Chapter 2. Then, based on the output from the SEB.EXE and the measurements from both reference stations (Bxxx.DAT, BICxxx.DAT), the maps of topography and surface properties (saved in TOPO.DAT), and the wind output from the MS-Micro/3 model (WINDxxx.DAT), the areal module ASEB.EXE is employed to estimate the spatial variability of the surface energy components. The output of ASEB.EXE are the daily total and three-hourly fields of surface energy flux terms and the equilibrium surface temperature.

Table 3.1 shows the contents of the input and output files of the ASEBM as used in this study. The input file (SEBxxx.DAT) for the point module contains the three hourly meteorological variables measured at Blockade Bend and parameters required for the calculation of the surface energy balance. The four input files for the areal module contain the maps of elevation, slope, aspect, surface albedo and roughness, three-hourly windspeed fields, three-hourly flux terms and Bowen ratio calculated at Blockade Bend, and three-hourly meteorological measurements at both the Blockade Bend and the Barnes Ice Cap autostations. The main output of the ASEBM is a set of data files of surface energy fluxes on a three hourly and daily basis. The daily files are grid-based files, which can be easily modified to the standard data files of the SURFER graphics package.

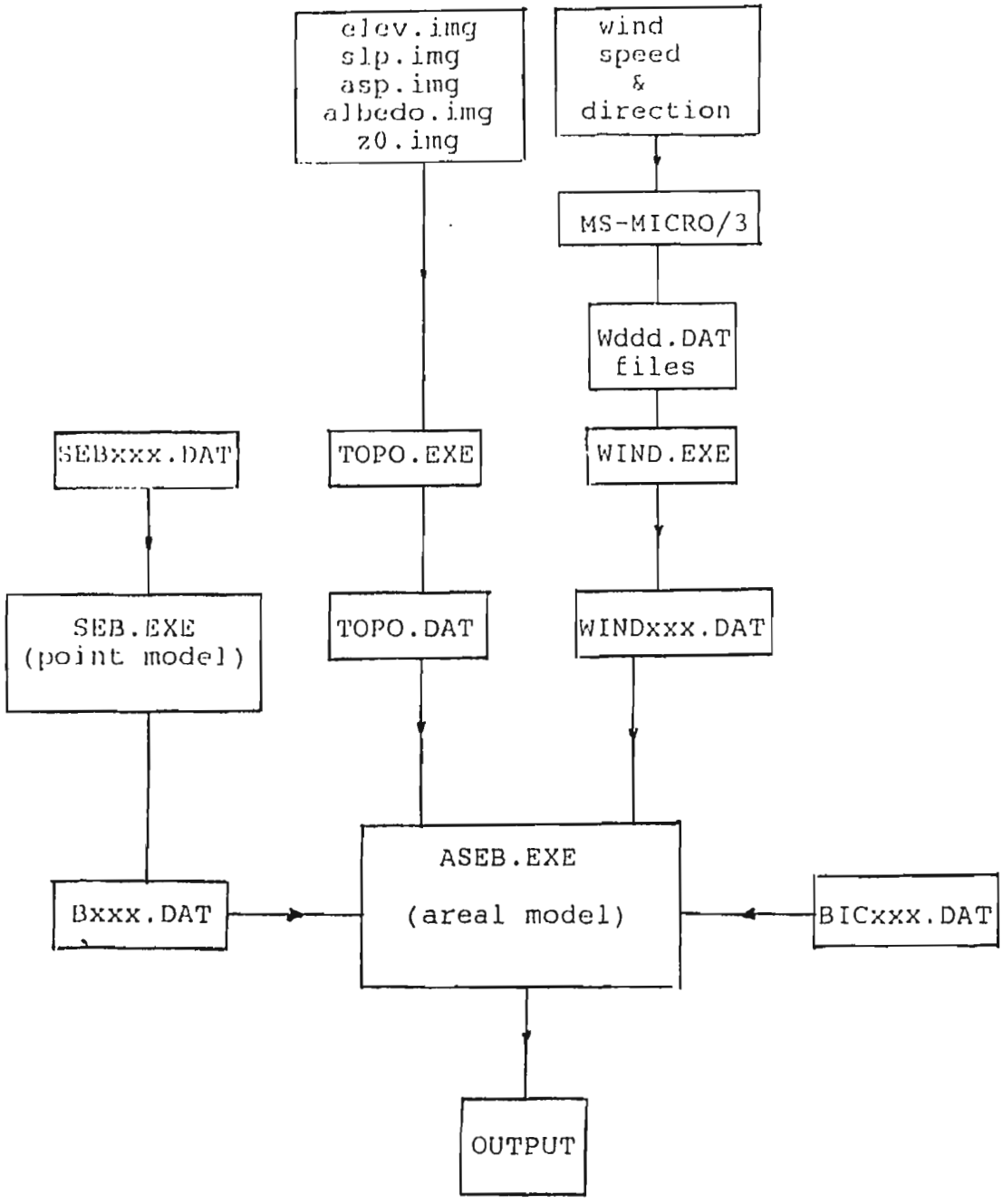


**Figure 3.4. Simplified flow chart of using the ASEBM**

**Table 3.1 Input and output to the ASEBM**

| | |
|---|---|
| **Input to the Point Module (SEB.EXE)** | |
| Temporal Data: | Julian date |
| Meteorological Variable: | $K\downarrow, T_a, T_0, T_{10}, P, V, RH$ (Blockade Bend) |
| Parameters: | r (surface relative humidity)<br>$k_s$ (thermal conductivity) |
| (File: SEBxxx.dat, xxx: Julian date) | |
| **Input to the Areal Module (ASEB.EXE)** | |
| File names | Contents |
| TOPO.DAT | maps of elevation, slope, aspect surface albedo and roughness. |
| WINDxxx.DAT | normalized wind speed |
| Bxxx.DAT | output from SEB.EXE: Bowen ratio, S, D, $L\downarrow$, $L^*$, $Q_G$, P, $q_a$, U, SZA (solar zenith angle), SAA (solar azimuth angle). |
| BICxxx.DAT | Meteorological Variables (Barnes Ice Cap): $T_a$, RH |
| **Output of the ASEBM** | |
| **Contents** | **File names** |
| **daily files** | |
| Net radiation | D_QSTAR.DAT |
| Sensible heat flux | D_QH.DAT |
| Latent heat flux | D_QE.DAT |
| Subsurface heat flux | D_QG.GRD |
| Equilibrium surface temperature | D_TG.GRD |
| **three-hourly file** | |
| three-hourly flux terms and equilibrium temperature | DIURNAL.DAT |

The three hourly files are the mean values at gridpoints over the glacier and the tundra, respectively. The format of the input and output files is shown in Appendix A. The source codes for the executable programs in Figure 3.4 are listed in Appendix B.

It should be noted that, although the content of the input files containing the meteorological measurements and the surface energy balance calculation at reference stations may be slightly different from Table 3.1 if the ASEBM is applied elsewhere, depending on availabilities of the reference stations and how the measurements of the reference stations are to be used, the procedures for using the ASEBM are the same. The surface energy balance is calculated only from one main reference station in our study, calculation from several reference stations may be accommodated by the ASEBM.

# *Chapter 4 APPLICATIONS*

## 4.1 Study Cases

Before using the ASEBM, a suitable resolution for experiments should be chosen for the study area. In this experiment, we use a resolution of 500 m x 500 m. Therefore, there are 576 grid points (areas) in our 144 $km^2$ study area.

The ASEBM is applied to selected days during the post-melting period and is limited to early August of 1991 by the availability of the measurements (see Chapter 2). Therefore, experiments are carried out for two days (218, 223) selected for calculating the surface energy balance during the post-melting period in Chapter 2.

It is noted that the amount of precipitation recorded in August of 1991 is high (Table 2.1(b)). Days with rainfall are very common during the month. The two days chosen for our experiments are 6 August (218), with no precipitation, and 11 August (223), with precipitation of 2.0 mm.

The meteorological variables for the two days from the Blockade Bend autostation are summarized in Table 4.1. 6 August received much more solar radiation in terms of both higher values of global solar radiation and the daily clearness index. The daily air

**Table 4.1**

**Daily means/totals of meteorological variables**

**for 6 and 11 August, 1991**

| date | K↓ ($MJm^{-2}day^{-1}$) | CI | $T_a$ (°C) | V ($ms^{-1}$) | RH | Precp. (mm) |
|---|---|---|---|---|---|---|
| 6 Aug. | 19.5 | 0.46 | 10.7 | 6.6 | 0.70 | 0 |
| 11 Aug. | 12.4 | 0.35 | 4.9 | 9.0 | 0.81 | 2.0 |

temperature is much higher on 6 August than 11 August. Moderate winds are found on both days, which well meet the requirement of neutral conditions by the wind model.

## 4.2 Results

### 4.2.1 Area-averaged Surface Energy Components

The daily areal averages of surface energy components over the glacier and tundra are obtained by summing and averaging the three-hourly values. Table 4.2 shows the daily total of flux terms and equilibrium surface temperature over tundra and glacier for both days. The net radiation is much higher on 6 August than 11 August. The net radiation over the tundra is nearly 2 $MJm^{-2}day^{-1}$ higher than over the glacier on 6 August, and, on 11 August, the difference is over 3 $MJm^{-2}day^{-1}$. Over the tundra, the convective fluxes act as an energy sink for both days, and the latent heat flux is more effective in dissipating energy than the sensible heat flux. Over the glacier, the sensible heat flux acts as an important energy source, and the latent heat flux is negligibly small. The ground heat flux at all points over the tundra is assumed to be the same as at the Blockade Bend autostation, and it acts as a small energy source for both days. Over the glacier, the subsurface heat fluxes are the largest energy components, representing the energy loss associated with the melting and/or warming of the glacier ice. This flux term is about twice as large on 6 August as on 11 August. In terms of daily average, the equilibrium

**Table 4.2. Daily totals of surface energy flux terms**

| Date | $Q^*$ | $Q_H$ | $Q_E$ | $Q_G$ | $T_g$ |
|---|---|---|---|---|---|
| | $MJm^{-2}day^{-1}$ | | | | (°C) |
| tundra | | | | | |
| 6 Aug. | 9.91 | 2.75 | 7.43 | -0.27 | 12.8 |
| 11 Aug. | 6.66 | 0.12 | 9.32 | -2.78 | 5.6 |
| glacier | | | | | |
| 6 Aug. | 8.11 | -5.87 | -0.51 | 14.51 | 0 |
| 11 Aug | 3.58 | -4.82 | 1.05 | 7.35 | 0 |

surface temperature on the tundra has a value of 12.8°C on 6 August, and 5.6°C on 11 August. As for the glacier, the daily averages are 0°C. The diurnal variations in energy fluxes over the tundra and glacier are shown in Figures 4.1 and 4.2.

It was noted that, on the glacier net radiation and convective fluxes act as energy source for ice melt. The relative ranking of importance of net radiation and convective fluxes differed in two days. On 6 August, about 56% of the melt energy was supplied by the net radiation, while on 11 August, the net radiation only accounted for 49% of the melt energy. This demonstrates that the relative importance of the different flux terms varies with weather conditions.

### 4.2.2 Spatial Variations in Surface Energy Components

Figure 4.3 shows the spatial variations in daily totals of global solar radiation for the two days. Similar spatial patterns can be seen for both days: relatively high values correspond with favourable slopes and aspects, and the range of variation over the glacier (about 0.5 $MJm^{-2}day^{-1}$) is lower than on the tundra (2 - 3 $MJm^{-2}day^{-1}$). This indicates that most of the spatial variability exists over the tundra area, while the glacier surfaces are relative homogeneous in terms of the global solar radiation. The values over the glacier are high due to the nearly flat surfaces. In spite of the similarities of the spatial patterns for the two days, it is noted that the absolute range of spatial variation is higher on 6 August than on 11 August. This indicates that, although the topographically-induced

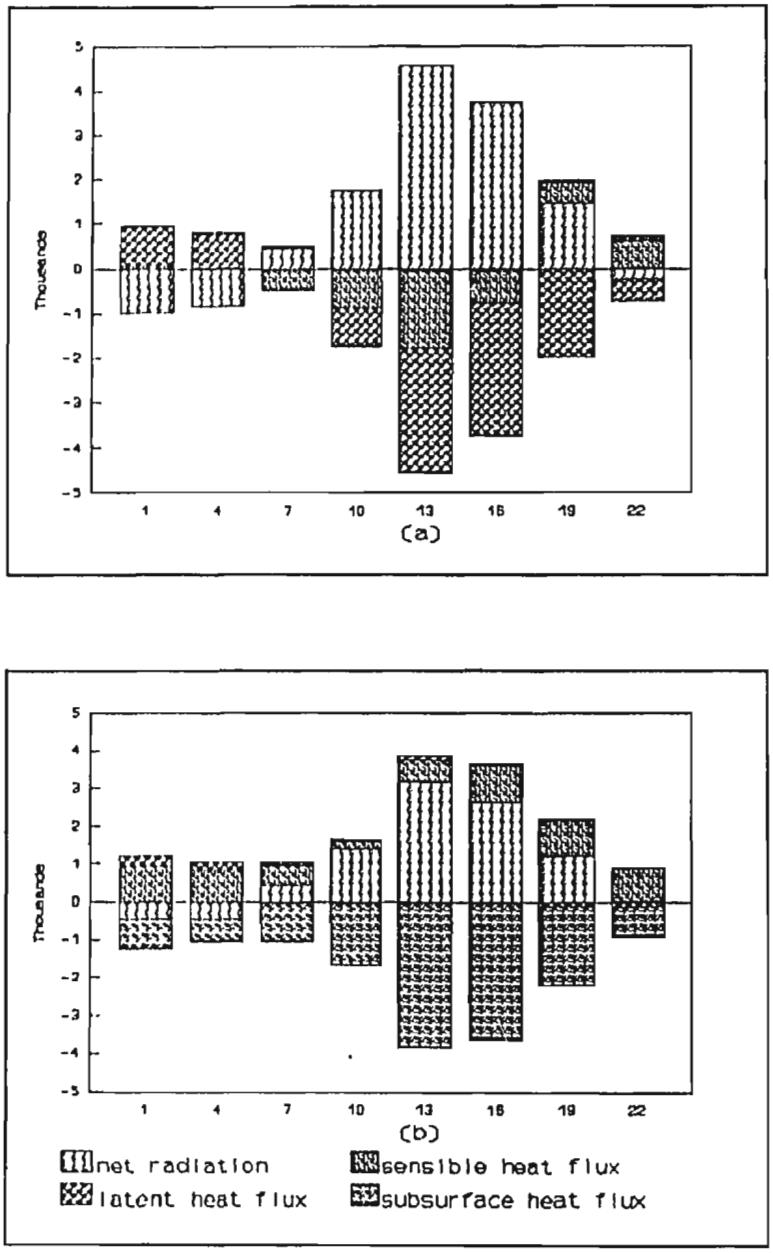


**Figure 4.1. Diurnal (UTC) variation of surface energy components on 6 August, 1991: (a) over the tundra; (b) over the glacier. The positive fluxes are the energy source to the surface, and the negative fluxes are the energy sink.**

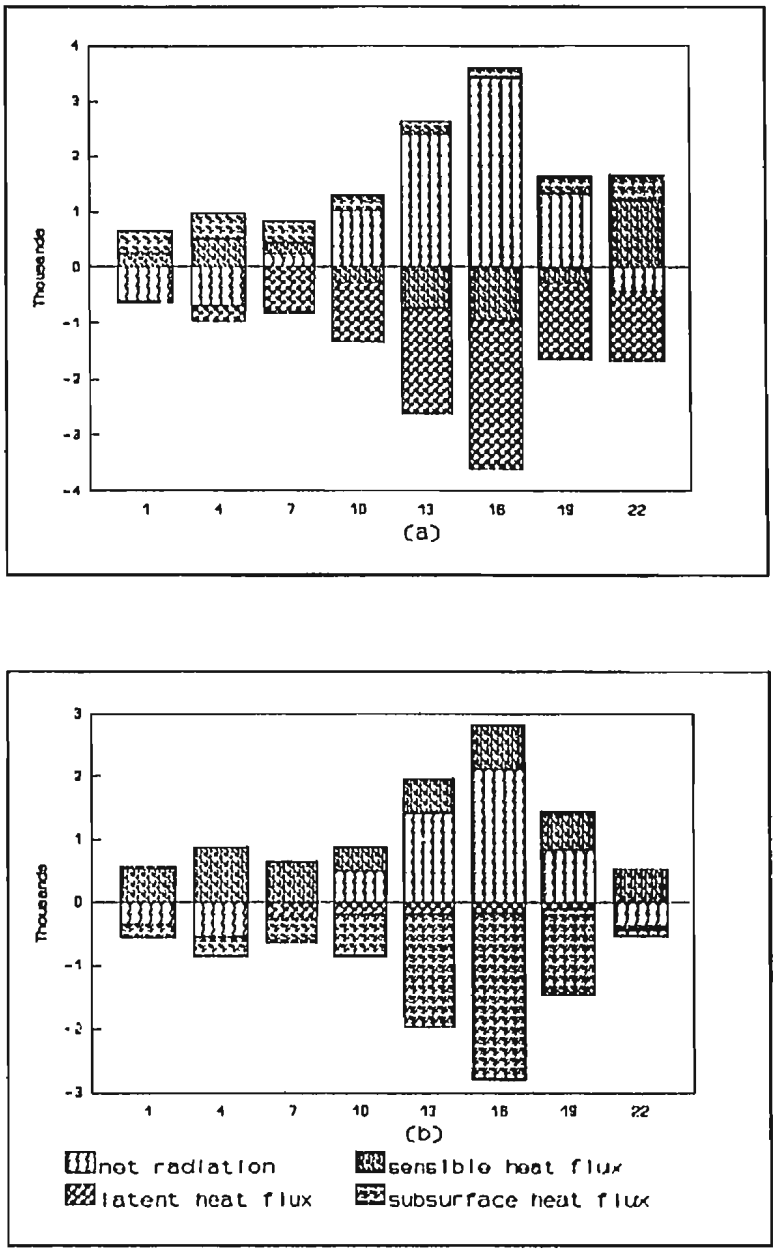


**Figure 4.2.** Diurnal (UTC) variations in surface energy components on 11 August, 1991: (a) over the tundra; (b) over the glacier. The positive fluxes are the energy source to the surface, and the negative fluxes are the energy sink.

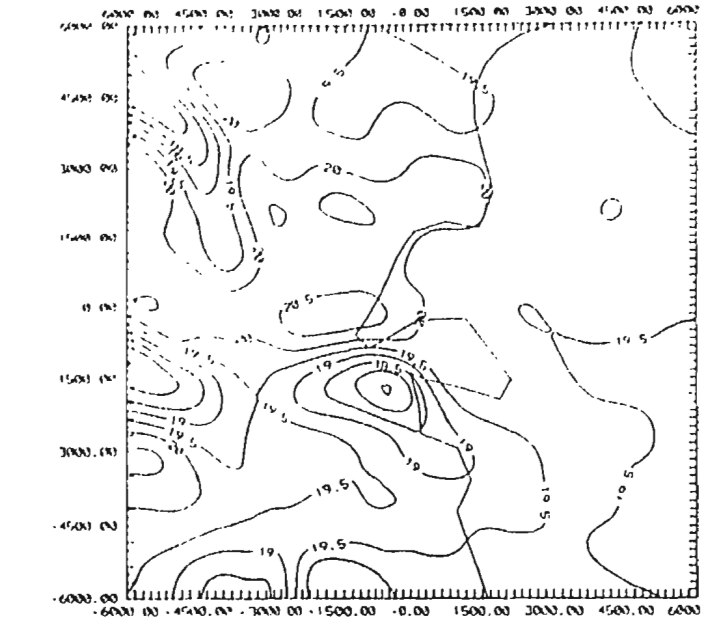

(a)

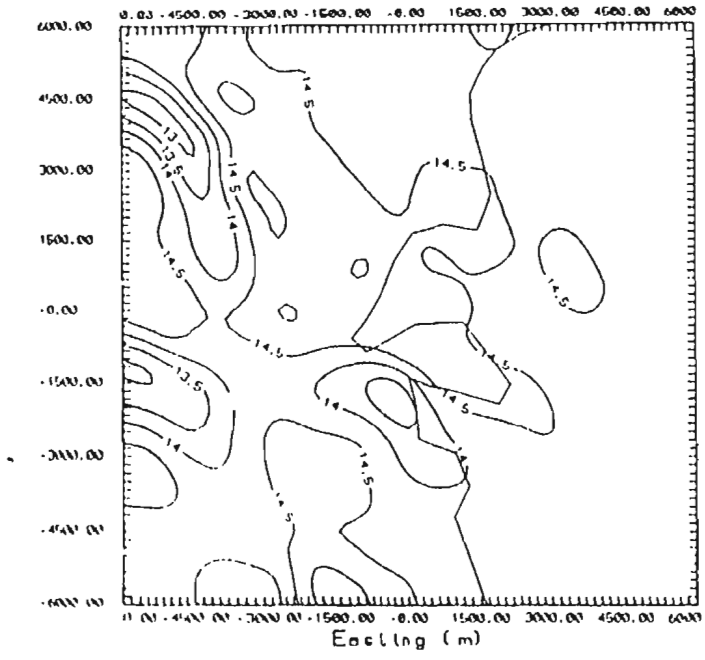


(b)

Figure 4.3. Spatial variations in global solar radiation ($MJm^{-2}day^{-1}$): (a) 6 August; (b) 11 August.

variability is similar in pattern, it may differ in magnitude, depending on the weather conditions.

Figure 4.4 shows the daily totals of net solar radiation. For both days, the ranges of variations over the tundra are reduced compared to the global solar radiation. This is expected as a result of the nearly homogeneous surface albedo over the tundra. Over the glacier, however, although the values decrease significantly compared to the tundra, the spatial variability becomes large compared to the global solar radiation. This is the result of the high spatial variations in surface albedo over the glacier, as shown in Figure 3.3. The most distinctive feature of the spatial variation in the net solar radiation is that the amount of radiation received over the glacier is much lower than that over the tundra. This results in the steep gradients near the glacier margin. The maximum differences between the glacier and tundra reach about 11 $MJm^{-2}day^{-1}$ on 6 August and 8 $MJm^{-2}day^{-1}$ on 11 August.

Similar spatial characteristics of net radiation are found between the two days (Figure 4.5). Although the values over the glacier are still lower than over the tundra, the maximum range decreases to 6 $MJm^{-2}day^{-1}$ for both days. This is because of the relatively high net long-wave radiation loss over the tundra compared to the cold glacier surfaces.

Figure 4.6 shows the daily totals of the sensible heat flux. The most distinctive spatial feature of the sensitive heat flux is that it acts as a significant energy source over the glacier, but is a small energy sink over most of the tundra. The spatial patterns differ significantly between the two days, especially over the tundra.

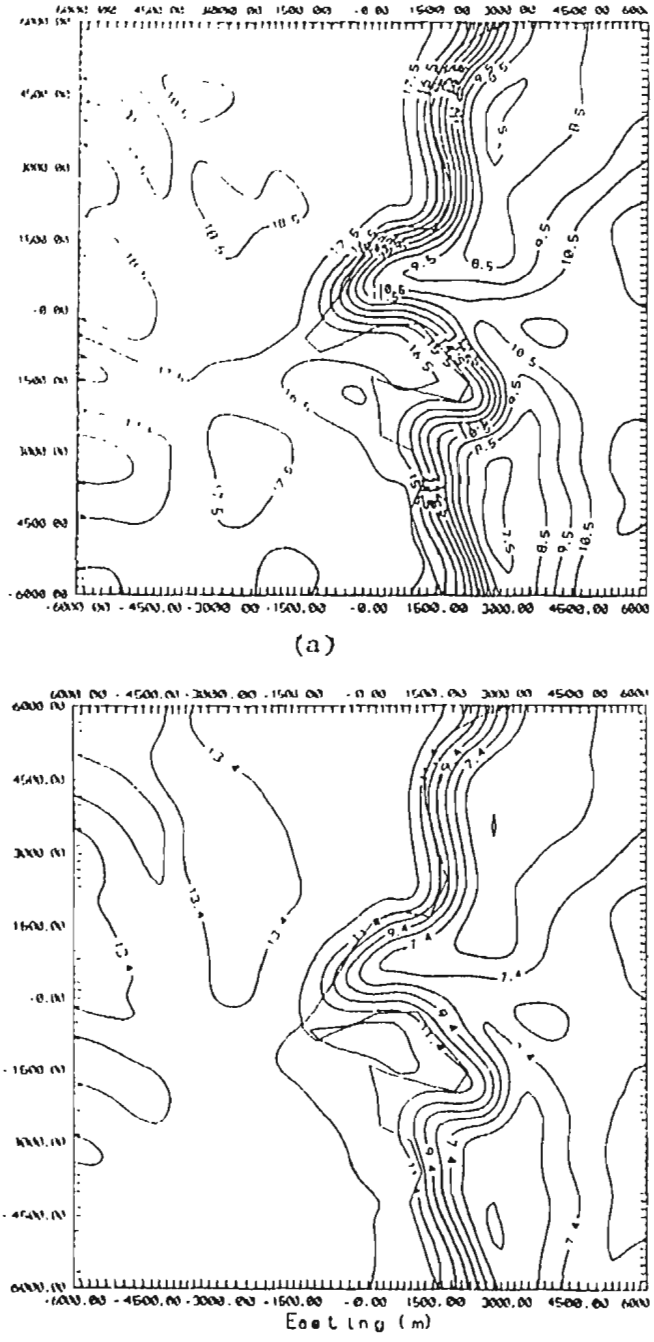


Figure 4.4. Spatial variations in net solar radiation ($MJm^{-2}day^{-1}$): (a) 6 August; (b) 11 August.

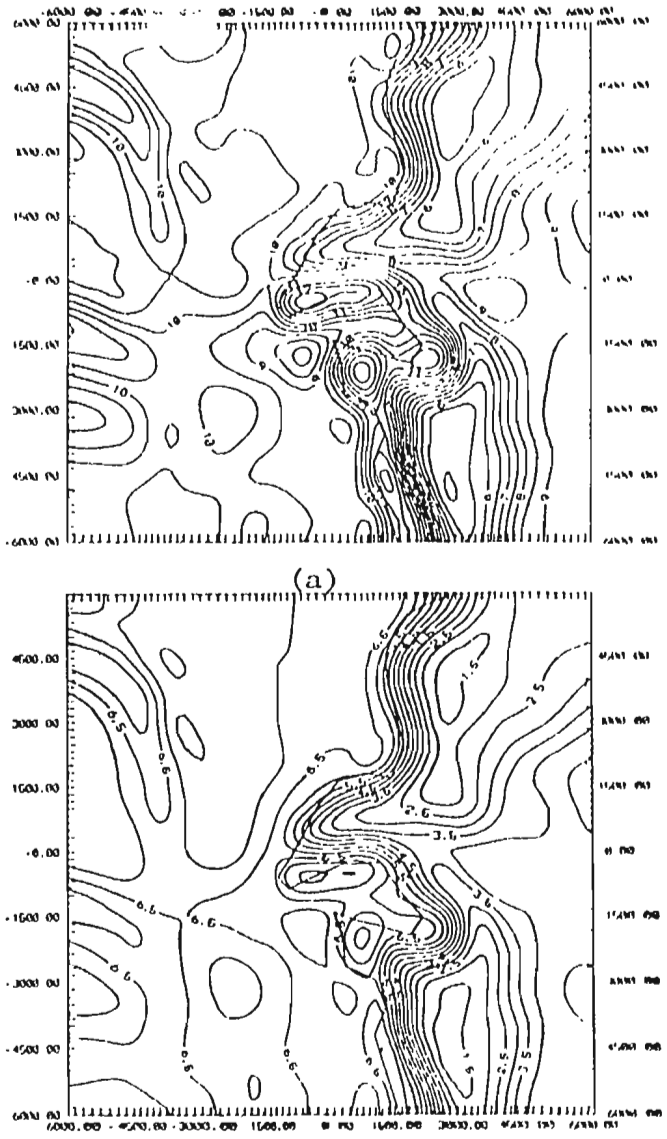

(a)

(b)

Figure 4.5. Spatial variations in net radiation ($MJm^{-2}day^{-1}$): (a) 6 August; (b) 11 August.

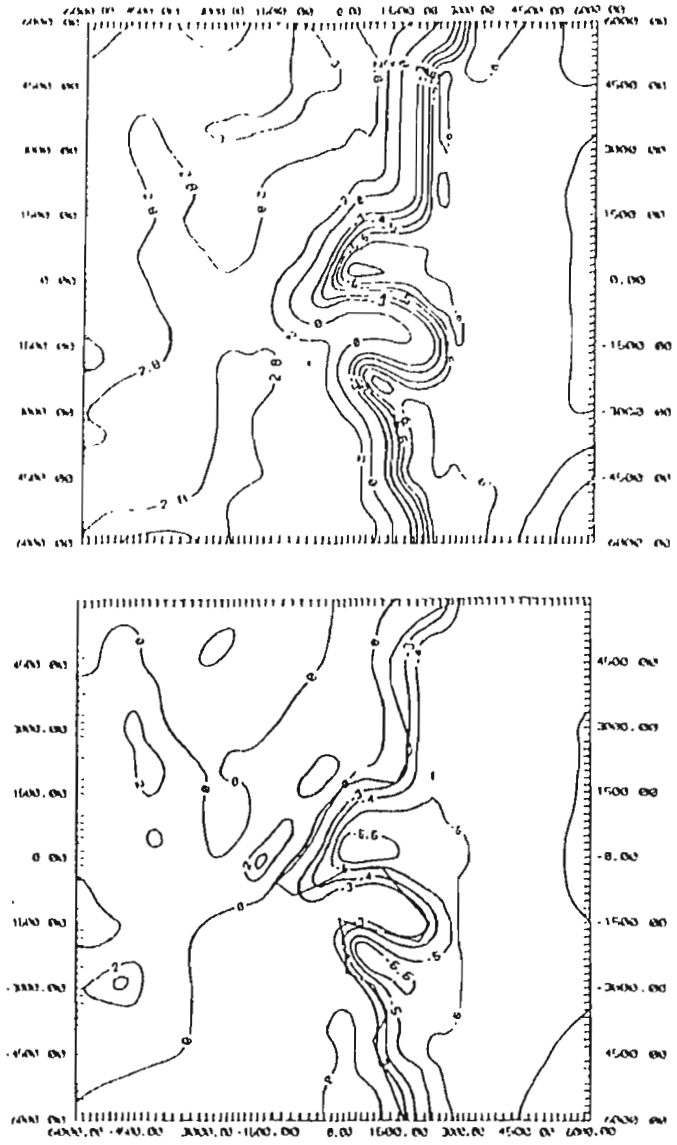

**Figure 4.6.** Spatial variations in sensible heat flux ($MJm^{-2}day^{-1}$): (a) 6 August; (b) 11 August.

The latent heat of evaporation is negligibly small over the glacier but very high over the tundra (Figure 4.7). This demonstrates that, for both days, latent heat flux was an effective way of dissipating energy over the tundra. However, the spatial patterns of the two days differ significantly.

The subsurface heat flux over the tundra is a small energy source for the two days. Since we have assumed a homogeneous value over the tundra, Figure 4.8 only shows the values over the glacier by masking off the tundra area. It is noted that over the glacier this flux term is a significant energy sink. The energy goes to warm and melt the glacier ice. Although the patterns are similar over the glacier, the magnitude of this flux differs dramatically between the two days. Much more ice-melt is expected on 6 August than on 11 August.

The equilibrium surface temperatures are at the melting point over the glacier in terms of daily average. Therefore, Figure 4.9 only shows the surface temperatures over the tundra area. A large temperature gradient exists near the glacier margin, but relatively small differences (1 - 2°C) are found over other parts of the tundra.

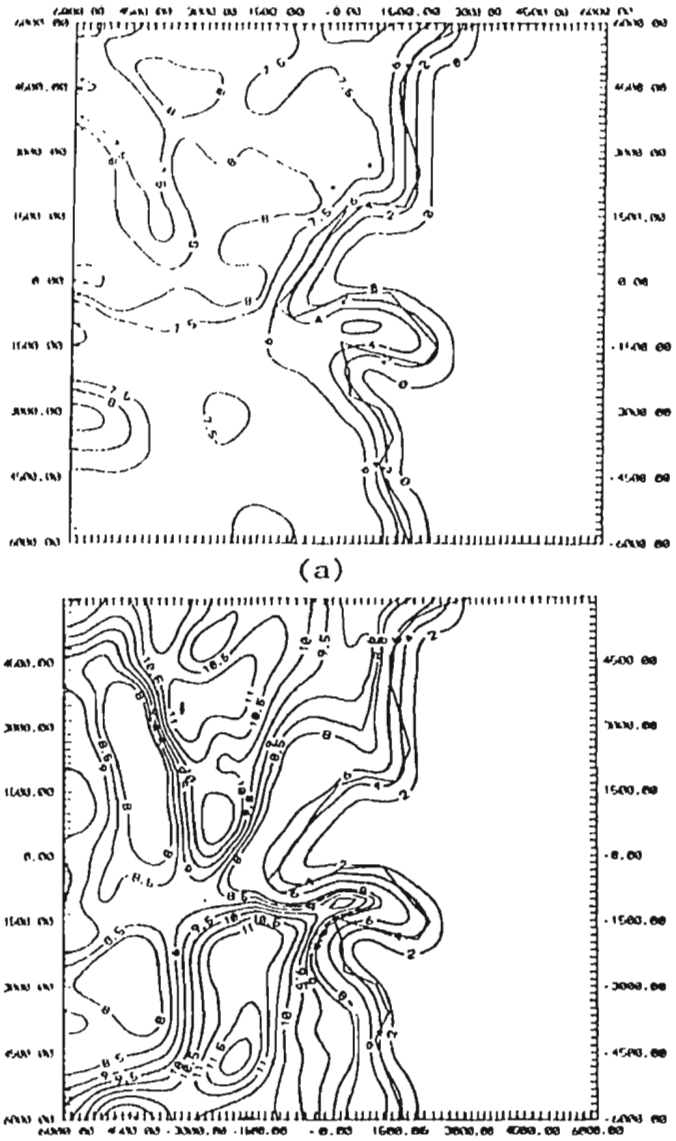

(a)

(b)

**Figure 4.7. Spatial variations in latent heat flux ($MJm^{-2}day^{-1}$): (a) 6 August; (b) 11 August.**

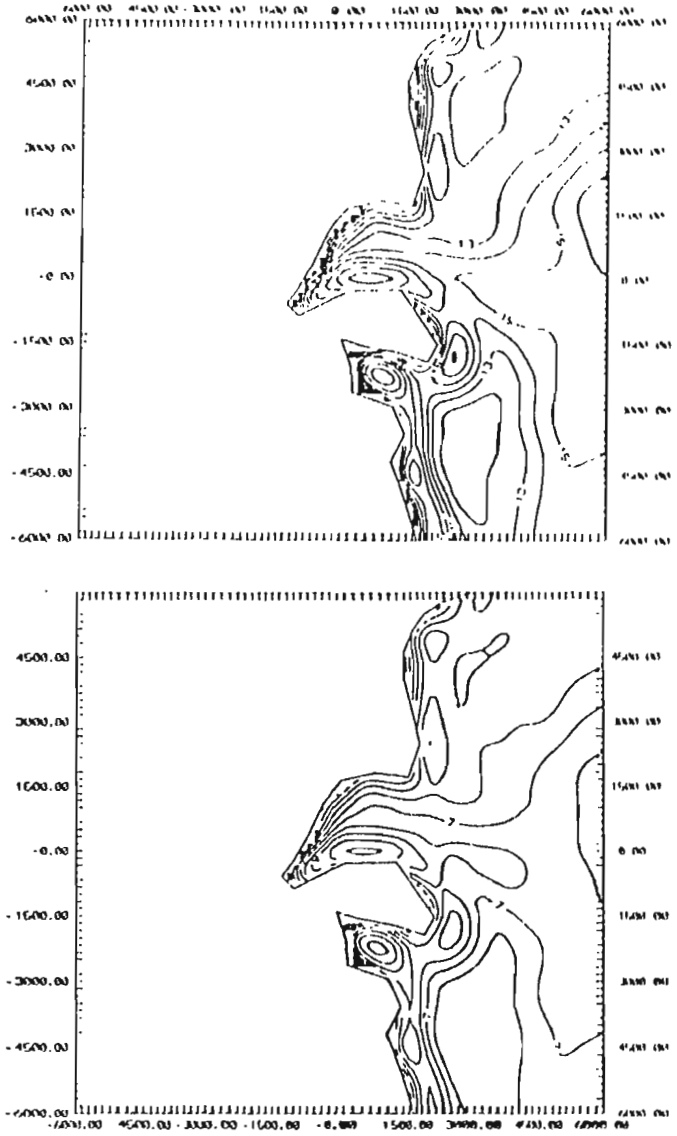

**Figure 4.8.** Spatial variations in subsurface heat flux over the glacier ($MJm^{-2}day^{-1}$): (a) 6 August; (b) 11 August.

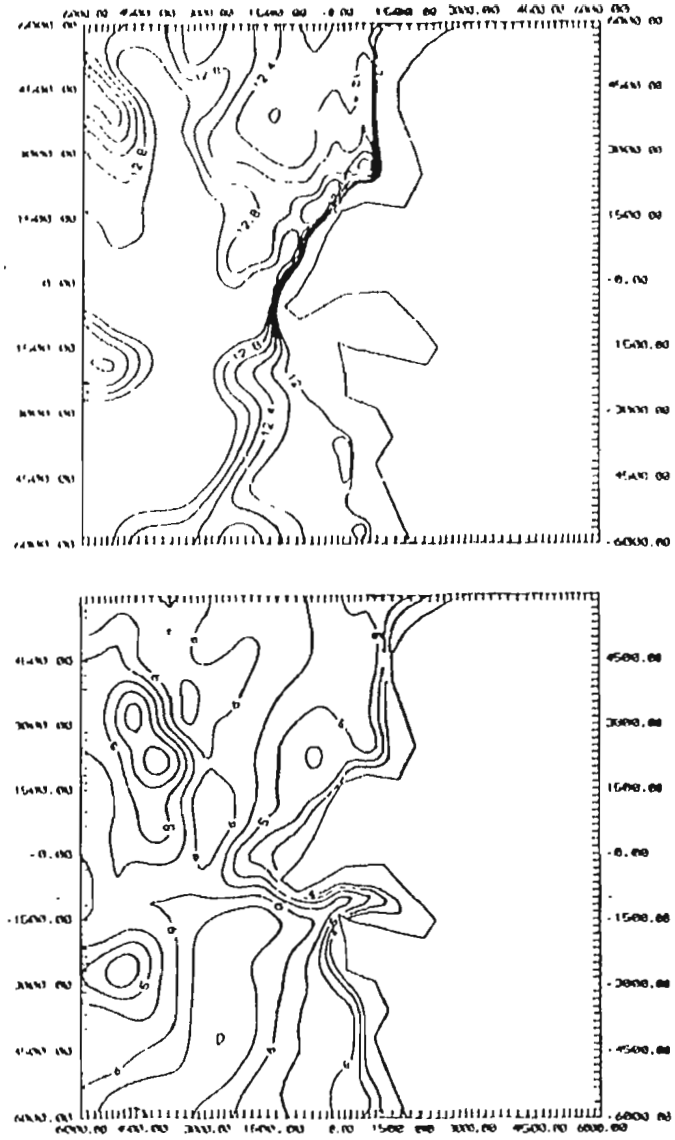

**Figure 4.9. Spatial variations in surface equilibrium temperature (°C): (a) 6 August; (b) 11 August.**

## 4.3 Advection Considerations

The ASEBM is a two-dimensional model, and it does not include the advective effects. Since there is no simple way to parameterize the advective term, estimates based the approaches described in Stull (1988) have been made to evaluate its influence.

In the study area, where tundra and ice-cap are juxtaposed, when the air flows from the upwind tundra (rough surface) to the downwind smooth ice-cap (in most cases), an internal boundary layer (IBL) is developed immediately above the ice surface. Within the IBL, the air is modified and adjusted to the glacier surface, that is, it does not 'feel' the influence of warm advection from the upwind tundra. This advective effect is known as 'fetch effect' and the depth of IBL is usually parameterized as a power of the fetch:

$$\frac{\delta}{z_{02}} = a_{IBL}\left(\frac{x}{z_{02}}\right)^{b_{IBL}} \quad \text{....(4.1)}$$

where,

$$a_{IBL} = 0.75 + 0.03\ln\left(\frac{z_{02}}{z_{01}}\right) \quad \text{.....(4.2)}$$

where $z_{01}$ and $z_{02}$ are the roughness lengths upwind and downwind of the border. x is the

fetch, and the power, $b_{IBL}$, is equal to 0.8 for neutral conditions (Stull, 1988). Given that the roughness length of tundra is 0.1 cm and 0.001 cm over glacier, the parameter $a_{IBL}$ will be 0.612. Under neutral conditions, the IBL over the ice will increase to a depth of 10 m at the fetch of 584 m downwind of the border. Therefore the extent of the glacier area which is influenced by the advection from the tundra is small. (Remember that the grid space is 500 m and assume that the advection is effective when the IBL is less than 10 m).

Due to the distinctive difference of surface thermal characteristics between the tundra and glacier ice, a stable thermal IBL (TIBL) will be developed and embedded in the IBL under the above case where the air flows from warm tundra to cold ice surface. The growth rate of the TIBL with fetch is much smaller. Garratt (1987) proposed that the depth of the TIBL increases with the square root of fetch distance:

$$h=0.014U[x\bar{\theta}/g\Delta\theta]^{0.5}.....(4.3)$$

where U is the wind speed of the flow, $\Delta\theta$ is the temperature difference between the air and the ice surface, and $\bar{\theta}$ is the mean potential temperature. Assume, for example, that the mean wind speed is 10 m/s, the temperature difference 10 °C, and the potential temperature 283°K. The result shows that the fetch of about 2 km is required to develop a TIBL to a height of 10 meters.

Conversely, if the air flows off the ice-cap, it slows down due to the increased

roughness. The horizontal convergence results in upward motion of the air which contributes to the development of a deeper IBL. The growth rate of IBL is much larger. The fetch distance is about 116 m at which the IBL reaches 10 m.

In all, although the advective effects exist in the studied case, the influence is negligible in terms of the grid space of the model. If a more detailed surface energy balance calculation is required at much smaller scale along the border where the advective effects are the most effective, an extension of the ASEBM model may be required. A three-dimensional model can be introduced to explicitly simulate the advective influence by calculating the horizontal fluxes and their convergence. However, this would introduce a much higher order of complexity and is beyond the scope of this thesis.

# *Chapter 5 CONCLUSION*

The purpose of this study was to develop an approach to the physically-based areal extrapolation of the surface energy budget terms based on field measurements, topographical information and remotely sensed data. The methodology is demonstrated through the application of the ASEBM to two contrasting days, and the results from the ASEBM are encouraging. This demonstrates that the methodology underlying the model is useful in studies concerning the spatial patterns of the surface energy balance.

The uncertainties in the results from the ASEBM applied to the study area should be pointed out. Firstly, the main reference station used in the ASEBM, Blockade Bend, was not designed to provide complete data for surface energy balance calculations. Thus, the simple calculation based on the limited meteorological variables may be not very accurate. It follows that the areal extrapolation based on the crude point estimates will result in uncertainties. Secondly, the LANDSAT image used to estimate the surface albedo is from 19 August 1988, which is not from the actual experimental period. Possible differences in terms of atmospheric and surface conditions may exist between the selected days of the experiment and the day the image was taken. To allow for changing atmospheric and surface conditions, remotely sensed data should ideally be from the same period as the meteorological observations. This is also important in

determining other surface properties besides surface albedo. Thirdly, the assumption of no spatial variation of soil heat flux over the tundra excludes the contribution of this energy flux to the spatial variation of surface energy available for the convective heat exchanges.

It should be noted that these uncertainties related to the acquisition of information are not a fundamental limitation on the ASEBM, since more complete measurements at the reference station(s) and detailed surface properties estimated from real-time remotely sensed data can be easily accommodated into the ASEBM as they become available.

A more complete energy budget measurement system at the reference station used in the ASEBM should include global solar radiation ($K\downarrow$) and the reflected solar radiation ($K\uparrow$) measured by a pyranometer, $Q^*$ by a net radiometer, and $Q_G$ by heat flux plates, as well as vertical temperature and vapour pressure gradients, and the surface wind profile. The sampling interval should be as short as possible.

The logic underlying the ASEBM is rather simple. Its purpose is to make use of the available information (field measurements, topographical information and remotely sensed data) to have a better understanding of the spatial patterns of the surface energy balance. Although the ASEBM itself was established for the Baffin Island study area, it can be applied with little modification to other places where the required information is available.

# *REFERENCES*


Andrews, R. H., 1964: Meteorology and heat balance of the ablation area, White Glacier, Canadian Arctic Archipelago - summer 1960 (Lower Ice Station: 79°26'N, 90°39'W, 208 m), *Axel Heiberg Island Research Reports, Meteorology No* 1, McGill University, Canada, pp. 107.

Brest, L. C. and S. M. Goward, 1987: Deriving surface albedo measurements from narrow band satellite data. *Int. J. Remote Sensing,* **8**: No. 3, pp. 351-367.

Duguay, R. C. and E. F. LeDrew, 1991: Mapping surface albedo in the east slope of the Colorado Front Range, U.S.A., with Landsat thematic mapper. *Arctic and Alpine Research* **23**: No. 2, pp. 213-223.

Eastman, J.R., 1990: *IDRISI, a grid-based geographic analysis system.* Graduate School of Geography, Clark University, 364pp.

Gadd, A. J. and J. F. Keers, 1970: Surface exchanges of sensible and latent heat in a 10-level model atmosphere. *Quart. J. Roy. Meteor. Soc.*, **96**, 297-308.

Garnier, B.J. and Atsumu Ohmura, 1968: A method of calculating the direct shortwave radiation income of slopes. *J. Appl. Meteor.*, **7**: 796-800.

Garratt, J.R., 1983: Surface influence upon vertical profiles in the nocturnal boundary layer. *Boundary Layer Meteor.*, **26**, 69-88.

Havens, J. M., 1964: Meteorology and heat balance on the accumulation area, McGill

Ice Cap, Canadian Arctic Archipelago - summer 1960 (Upper Ice Station I: 79°41'N, 90°27'W, 1530 m), *Axel Heiberg Island Research Reports, Meteorology, No.* 2, McGill University, Canada, pp. 87.

Iqbal, Muhammad, 1983: *An Introduction to Solar Radiation*. Toronto, Academic Press, 390pp.

Jackson, P.S. and Hunt, J.C.R., 1975: Turbulent wind flow over a low hill. *Q.J.R. Meteorol. Soc.* 101, 929-955pp.

Jacobs, J.D., 1974: *Solar and Atmospheric Radiation Data for Broughton Island Eastern Baffin Island, Canada, 1971-1973.* Occasional Paper No. 11, Institute of Arctic and Alpine Research, Univ. of Colorado.

Jacobs, J.D., 1991: Climate autostations on Barnes and Penny Ice Caps. *Research Note 91/2, Baffin Island and Labrador Mesoclimate Program,* Dept. of Geography, Memorial Univ. of Nfld, St. John's, NF., Canada, 20 pp.

Jacobs, J.D., Headley, A.N. and Wang, H., 1993: Climate autostation operations at remote integrated studies sites in Baffin Island, N.W.T., 1987-1992. *Canadian Climate Centre Report No. 93-4*, AES, Downsview, Ontario.

Jacobs, J.D., Heron R., and Luther, J. Recent changes on the northwest margin of the Barnes Ice Cap, Baffin Island, Canada. *Arctic and Alpine Research* (in review).

Maxwell, J.B., 1980: *The Climate of the Canadian Arctic Islands and Adjacent Waters, Vol. 1.* AES, Climatological Studies No. 30, Downsview, Ontario.

Munro, D. S., 1990: Comparison of melt energy computations and ablatometer

measurements on melting ice and snow. *Arctic and Alpine Research,* **22**: No. 2, pp. 153-162.

Musick, B. H., 1986: Temporal change of Landsat MSS albedo estimates in arid rangeland. *Remote Sensing of Environment* **20**: pp. 107-120

Myrup, L. O., 1969: A numerical model of the urban heat islands. *J. Appl. Meteor.*, **8**, 908-918.

Oerlemans, J. and Vugts, H.F., 1993: A meteorological experiment in the melting zone of the Greenland Ice Sheet. *Bulletin American Meteorological Society*, Vol.**74**, No.3, 355-365pp.

Ohmura, A. and Muller, F., 1976: Heat balance measurement on arctic tundra, Axel Heiberg Island, Canadian Arctic Archipelago. *International Geography,* **2**: 80.

Ohmura, A., 1982a: A historical review of studies on the energy balance of Arctic tundra. *Journal of Climatology,* **2**: 185-195.

Ohmura, A., 1982b: Climate and energy balance on the Arctic tundra. *Journal of Climatology,* **2**: 65-84.

Oke, T.R., 1987: *Boundary Layer Climates.* The University Press, Cambridge, 435pp.

Otterman, J. and R. S. Fraser, 1976: Earth-atmosphere system and surface reflectivities in arid regions from Landsat MSS data. *Remote Sensing of Environment,* **5**, pp. 247-266.

Outcalt, S.I., 1972: The development and application of a simple digital surface-climate simulator. *J. Appl. Meteor.*, **11**, 629-636.

Petzold, E. D., 1974: Solar and net radiation over snow. *Climatological Research Series No.* **9**, Dept. of Geography, McGill University, Canada, pp. 77.

Price, G. A. and T. Dunne: 1976: Energy balance computations of snowmelt in a subarctic area. *Water Resources Research,* **12**: No. 4, pp. 686-694.

Rott, Helmut and Friedrich Obleitner, 1992: The energy balance of dry tundra in west Greenland. *Arctic and Alpine Research,* **24**: No. 4, pp. 352-362.

Rouse, W. R. and Stewart, R. B., 1972: A simple model for determining evaporation for high latitude upland site. *J. Appl. Meteor.*, **11**, 106.

Stewart, R. B. and Rouse, W., 1976: Simple models for calculating evaporation from dry and wet tundra surfaces, *Arctic and Alpine Research,* **8**: 135.

Stull, B. R., 1988: *An Introduction to Boundary Layer Meteorology.* Boston, Kluwer Academic Publishers. pp. 666.

Swift,, W. L., $J_R$.: 1976: Algorithm for solar radiation on mountain slopes. *Water Resources Research,* **12**: No. 1, 108-112.

Taylor, P.A., 1977: Some numerical studies of surface boundary-layer flow over gentle topography. *Boundary Layer Meteorol.* **11**, 439-465pp.

Taylor, P.A. and Lee, R.J., 1984: Simple guidelines for estimating wind speed variations due to small scale topographic features. *Climatological Bulletin.* **18(2)**, 3-32.

Walmsley, L. J., Taylor, P.A., and T. Keith, 1986: A simple model of neutrally stratified boundary-layer flow over complex terrain with surface roughness modulations (MS3DJH/3R), *Boundary-Layer Meteor.*, **36**: pp. 157-186

Walmsley, L. J., D. Woolridge and J. R. Salmon, 1990: *MS-Micro/3 user's guide.* Report ARD-90-008. Atmos. Environ. Service, Downsview, Ontario, Canada.

Weick, J. E. and W. R. Rouse, 1991a: Advection in the coastal Hudson Bay lowlands, Canada. I. The terrestrial surface energy balance. *Arctic and Alpine Research,* **23**: No. 3, pp. 328-337.

Weick, J. E. and W. R. Rouse, 1991b: Advection in the coastal Hudson Bay lowlands, Canada. II. Impact of atmospheric divergence on the surface energy balance. *Arctic and Alpine Research*, **23**: No. 3, pp. 338-348.

Weller, G. et al., 1972: The tundra microclimate during snow-melt at Barrow, Alaska. *Arctic,* **25**: 291-300

Weller, G. and Holmgren, B. 1974: The microclimates of the Arctic tundra. *J. Appl. Meteorol.*, **13**, (12), 854.

# APPENDIX A

Input and Output Files of the ASEBM

## A.1 Input files of the ASEBM

### A.1.1 SEBxxx.dat

SEBxxx.dat (Surface energy balance on Julian date xxx) is the input file for point module SEB.EXE. SEB218.dat (6 August) and SEB223.DAT (11 August), as shown in Table A.1. Each file has eight rows and seven columns. Each column represents a variable, and each row indicates each of the eight measurements of the day.

### A.1.2 Bxxx.dat

Bxxx.dat is the output file from SEB.EXE. It is also one of the input files to ASEB.EXE. B216.DAT is shown in Table A.2 Each row is accompanied by an explanation of its contents.

### A.1.3 TOPO.DAT

Five base maps (elevation, slope, aspect, roughness and albedo) are conformed to a resolution of 500 m x 500 m. Then, TOPO.EXE is invoked to read these five maps into a single file --- TOPO.DAT. Part of the TOPO.DAT is listed as

**TABLE A.1. Input file SEBxxx.DAT**

SEB218.DAT

| $K\downarrow$ ($KJm^{-2}/3h$) | $T_{10}$ (°C) | $T_0$ (°C) | $T_a$ (°C) | V ($ms^{-1}$) | RH | P (mb) |
|---|---|---|---|---|---|---|
| 0 | 14.91 | 9.95 | 10.27 | 7.8 | 89.2 | 961 |
| 83 | 14.15 | 8.48 | 8.52 | 7.4 | 92.0 | 962 |
| 1482 | 13.60 | 9.28 | 7.79 | 5.5 | 88.3 | 963 |
| 3286 | 13.80 | 13.79 | 8.71 | 2.9 | 81.4 | 964 |
| 6442 | 15.50 | 19.76 | 11.12 | 5.8 | 66.5 | 965 |
| 5180 | 17.80 | 20.76 | 13.31 | 8.3 | 49.6 | 966 |
| 2532 | 18.37 | 15.84 | 13.66 | 7.9 | 44.0 | 966 |
| 509 | 17.25 | 11.20 | 12.33 | 6.8 | 47.5 | 966 |

Input file SEB223.DAT

| | | | | | | |
|---|---|---|---|---|---|---|
| 0 | 12.72 | 5.17 | 6.35 | 5.8 | 90.9 | 948 |
| 41 | 11.68 | 3.18 | 4.52 | 11.5 | 85.8 | 950 |
| 1124 | 10.66 | 3.63 | 3.52 | 11.7 | 82.2 | 953 |
| 2060 | 10.44 | 4.78 | 3.68 | 7.5 | 79.5 | 955 |
| 3664 | 11.01 | 8.09 | 4.92 | 9.1 | 76.5 | 956 |
| 4732 | 12.14 | 11.43 | 6.27 | 10.0 | 73.1 | 956 |
| 2321 | 12.73 | 8.25 | 5.75 | 8.6 | 78.8 | 956 |
| 296 | 11.83 | 3.61 | 4.24 | 7.5 | 86.6 | 955 |

**TABLE A.2. Input file B218.DAT**

---

218 (Julian date)
0.750 (relative surface humidity)

---

961 962 963 964 965 966 966 966 (air pressure in mb)

---

0.0072 0.0066 0.0060 0.0059 0.0057 0.0049 0.0044 0.0044 (absolute air humidity)

---

7.27 6.89 5.12 2.70 5.40 7.73 7.36 6.33 (wind speed at 2 m in m/s)

---

0.10 0.01 -30.31 1.00 0.64 0.26 -0.22 -1.32 (Bowen ratio)

---

0.00 1.55 509.30 1298.04 4690.18 3224.78 1141.63 132.28
(direct-beam radiation in $KJm^{-2}/3h$)

---

0.00 81.45 972.70 1987.96 1751.82 1955.22 1390.37 376.72
(diffuse radiation in KJn. /3h)

---

2963.7 2949.6 3112.0 3137.0 3209.0 3236.2 3217.6 3162.7
(long-wave downward radiation in $KJm^{-2}/3h$)

---

-970.2 -903.3 -832.0 -1166.1 -1257.7 -1026.0 -850.5 -707.09
(net long-wave radiation in $KJm^{-2}/3h$)

---

-53.57 -61.24 -37.46 27.77 38.71 -22.90 -65.21 -91.39 ( $Q_G$ in $KJm^{-2}/3h$)

---

1.57 1.52 1.34 1.09 0.94 1.01 1.24 1.48
(solar zenith angle at middle time of each 3-hly interval in radius)

---

5.76 0.74 1.32 2.08 2.95 3.87 4.67 5.39
(solar azimuth angle at middle time of each 3-hly interval in radius)

---

in Table A.3. There are five columns in TOPO. The number of rows in the file is the number of grid points within the study area. With a resolution of 500 m x 500 m, there are 576 grid points inside the study area, and therefore the number of rows in TOPO.DAT is 576. Only the first 15 rows are listed here, however

### A.1.4 BICxxx.DAT

BICxxx.DAT (Barnes Ice Cap measurements at Julian date xxx) contains measurements of air temperature and humidity from the Barnes Ice Cap autostation for a day. It is composed of two rows, one is for air temperature and the other for relative humidity (Table A.4)

### A.1.5 WINDxxx.DAT

WINDxxx.DAT contains the normalized windspeed of each grid point for every upwind direction, and it is created from 8 separate files (see Appendix D) by invoking WIND.EXE (The process of applying the MS-Micro/3 is discussed in Appendix D). It is composed of 8 columns and 576 rows. Each column corresponds to each incident direction of upwind of the day. The First 18 rows of file WIND218.DAT is presented in Table A.5.

**TABLE A.3.** Input file TOPO.DAT

| elevation (m) | slope (radius) | aspect (radius) | albedo | roughness (m) |
|---|---|---|---|---|
| 373.6848145 | 0.0823765 | 4.4143982 | 0.0732520 | 0.0010000 |
| 386.6896057 | 0.0865429 | 5.5021915 | 0.0675610 | 0.0010000 |
| 380.6951904 | 0.0806678 | 0.2419476 | 0.0707859 | 0.0010000 |
| 384.6575928 | 0.1035567 | 4.4344487 | 0.0788888 | 0.0010000 |
| 427.0248108 | 0.0995933 | 4.9077706 | 0.0770731 | 0.0010000 |
| 465.2304688 | 0.0912758 | 5.0782428 | 0.0736314 | 0.0010000 |
| 488.7297974 | 0.0403463 | 4.7965345 | 0.0689160 | 0.0010000 |
| 503.2952271 | 0.0379197 | 4.2759380 | 0.0757452 | 0.0010000 |
| 511.2511902 | 0.0300411 | 3.9103434 | 0.0763956 | 0.0010000 |
| 518.2920532 | 0.0409223 | 4.9602404 | 0.0806503 | 0.0010000 |
| 536.9559326 | 0.0525066 | 5.0106487 | 0.0826557 | 0.0010000 |
| 552.1901245 | 0.0464376 | 4.5620708 | 0.0859619 | 0.0010000 |
| 542.5439453 | 0.0509164 | 1.8279414 | 0.0895391 | 0.0010000 |
| 530.2504883 | 0.0426206 | 2.5883374 | 0.1010295 | 0.0010000 |
| 535.4116821 | 0.0503947 | 3.9147010 | 0.1030349 | 0.0010000 |

.....

TABLE A.4. Input file BICxxx.DAT

| | $T_a$ (°K) | RH |
|---|---|---|
| BIC218.DAT | 276.72 | 0.903 |
| | 276.07 | 0.904 |
| | 274.95 | 0.906 |
| | 274.39 | 0.907 |
| | 274.95 | 0.905 |
| | 276.04 | 0.790 |
| | 276.71 | 0.662 |
| | 276.88 | 0.650 |
| BIC223.DAT | 274.24 | 0.905 |
| | 272.93 | 0.908 |
| | 271.58 | 0.899 |
| | 271.33 | 0.888 |
| | 272.05 | 0.882 |
| | 272.58 | 0.872 |
| | 272.71 | 0.877 |
| | 272.68 | 0.890 |

## A.2 Output files of the ASEBM

### A.2.1 Bxxx.DAT (Output from SEB.EXE)

This file also acts as an input file to ASEB.EXE. The format of the file is described in A.1.2.

### A.2.2 D_QSTAR.DAT (Output from ASEB.EXE)

This file contains grid values of daily total net radiation saved as a column, which is compatible to the IDRISI image file (Eastman, 1990). The format of the file makes the file adaptable for further spatial manipulations in IDRISI. D_QSTAR.DAT can also be easily modified to a standard format of SURFER data file by invoking a program called 'COMBINE.EXE' (see Appendix B.5). 'COMBINE.EXE' accomplishes the task by adding two coordinate columns to D_QSTAR.DAT.

**Table A.5. WIND218.DAT**

| | | | | | | | |
|---|---|---|---|---|---|---|---|
| 1.09 | 1.06 | 1.03 | 1.04 | 1.09 | 1.11 | 1.11 | 1.10 |
| 1.10 | 1.11 | 1.05 | 0.98 | 1.08 | 1.12 | 1.12 | 1.10 |
| 1.12 | 1.19 | 1.14 | 1.00 | 1.05 | 1.12 | 1.12 | 1.09 |
| 1.17 | 1.27 | 1.26 | 1.16 | 0.97 | 1.12 | 1.12 | 1.09 |
| 1.23 | 1.29 | 1.30 | 1.25 | 1.04 | 1.12 | 1.12 | 1.08 |
| 1.29 | 1.27 | 1.33 | 1.22 | 1.15 | 1.14 | 1.14 | 1.10 |
| 1.30 | 1.34 | 1.31 | 1.20 | 1.15 | 1.15 | 1.15 | 1.16 |
| 1.35 | 1.30 | 1.27 | 1.24 | 1.11 | 1.16 | 1.16 | 1.13 |
| 1.39 | 1.31 | 1.33 | 1.26 | 1.08 | 1.17 | 1.17 | 1.11 |
| 1.38 | 1.37 | 1.33 | 1.29 | 1.18 | 1.32 | 1.32 | 1.22 |
| 1.36 | 1.44 | 1.33 | 1.24 | 1.20 | 1.34 | 1.34 | 1.33 |
| 1.42 | 1.39 | 1.32 | 1.30 | 1.25 | 1.38 | 1.38 | 1.27 |
| 1.38 | 1.30 | 1.26 | 1.21 | 1.14 | 1.34 | 1.34 | 1.20 |
| 1.36 | 1.38 | 1.34 | 1.17 | 1.21 | 1.41 | 1.41 | 1.28 |
| 1.38 | 1.31 | 1.34 | 1.24 | 1.17 | 1.36 | 1.36 | 1.31 |
| 1.27 | 1.30 | 1.40 | 1.30 | 1.24 | 1.40 | 1.40 | 1.27 |
| 1.26 | 1.27 | 1.27 | 1.22 | 1.17 | 1.46 | 1.46 | 1.27 |
| 1.23 | 1.23 | 1.23 | 1.29 | 1.14 | 1.40 | 1.40 | 1.16 |

.....

### A.2.3 D_KD.DAT, D_KSTAR.DAT, D_QH.DAT, D_QE.DAT and D_QG.DAT (Output from ASEB.EXE)

These five files are have the same format as D_QSTAR.DAT (see A.2.2) except that they have the daily totals of global solar radiation, net solar radiation, sensible heat, latent heat and subsurface heat fluxes.

### A.2.4 D_TG.DAT (Output from ASEB.EXE)

This file has the same format as D_QSTAR.DAT described in A.2.2 except that it contains the daily averages of ground surface temperature for each of the grids.

### A.2.5 DIURNAL.DAT (Output from ASEB.EXE)

This file contains three-hourly areally-averaged values of surface energy terms and equilibrium surface temperature over both the tundra and glacier. The file of 6 August is shown in Table A.6. There are 8 rows and ten columns in the file, with each row representing each of the 3-hour interval of the day. The subscript 't' and 'g' represent 'tundra' and 'glacier', respectively.

Table A.6. File DIURNAL.DAT of 6 August

| $Q^*_t$ | $Q^*_g$ | $QH_t$ | $QH_g$ | $QE_t$ | $QE_g$ | $QG_t$ | $QG_g$ | $T_t$ | $T_r$ |
|---|---|---|---|---|---|---|---|---|---|
| ---KJm$^{-2}$/3h--- | | | | | | | | °C | |
| -970.2 | -445.7 | -83.3 | -958.9 | -833.3 | -270.5 | -53.6 | 783.6 | 10.3 | 0 |
| -829.6 | -416.1 | -7.6 | -845.3 | -760.8 | -200.2 | -61.2 | 629.4 | 8.9 | 0 |
| 449.4 | 445.6 | 503.5 | -523.6 | -16.6 | -77.0 | -37.5 | 1046.2 | 10.1 | 0 |
| 1750.7 | 1424.1 | 861.5 | -207.0 | 861.5 | -19.3 | 27.8 | 1650.5 | 16.7 | 0 |
| 4559.9 | 3182.8 | 1764.4 | -574.3 | 2756.8 | -83.2 | 38.7 | 3840.2 | 19.5 | 0 |
| 3718.1 | 2645.8 | 772.0 | -956.0 | 2969.0 | -45.5 | -22.9 | 3647.3 | 15.9 | 0 |
| 1477.7 | 1225.7 | -435.2 | -974.2 | 1978.1 | 97.6 | -65.2 | 2102.3 | 12.7 | 0 |
| -242.3 | 50.3 | -622.5 | -849.1 | 471.6 | 89.1 | -91.4 | 810.3 | 7.9 | 0 |

# APPENDIX B

Source Code of the Programs in the ASEBM

## B.1 Source Code of SEB.EXE --- SEB.FOR

```
C-------------------------------------------------------
C SEB.EXE  (Point Module)
C-------------------------------------------------------
Compiled by VAX Fortran compiler
Created by H. Wang
C-------------------------------------------------------
        integer day
       real k,ks,lu,IC
       PARAMETER(N=8,DELTA=5.67E-11,k=0.4,rua=1.2,z=2.0,
      &
        Cp=1.01,fia=70.4,z0=0.001,albe=0.18,ZS=0.1,
      &          NEPS=5,Lv=2500,tmin=250.0,tmax=320.0,
     &          AA=1.222, BA=-1.235)
       REAL T10(N),T0(N),TAL(N),KD(N),RH(N),P(N),
     &      LD(N),UL(n),RI0(n),CLEAR(n),UA(n),
     &      Qstar(N),QH(N),QE(N),QG(N),Bowen(N),
     &      Ratio(N),StarL(N),ql(N),S(N),DD(N),SZA(N),
      &       SAA(N),MTime(N)
      character*14 infile,outfile
C             T10: soil temp. at 10 cm (C)
c             T0:  temp. at 0 cm (C)
c             TAL: air temp. at level of 2m (C)
c             KD:  global radiation (KJm-2/3h)
c             RH:  relative humidity at level of 2m
c             P:   air pressure (mb)
c             ql:  absolute air humidity (g/g)
c             LD:  downward long-wave radiation (KJm-2/3h)
c             StarL: net long-wave radiation (KJm-2/3h)
c             UL:  windspeed extrapolate to 2m from UA (m/s)
c             RI0: extraterrestrial radiation (KJm-2/3h)
c             CLEAR: clearness index (non-dimensional)
c             UA:  wind speed measured at 3.5 m
c             Bowen: Bowen ratio (non-dimensional)
c             Ratio: Qg/Q*   (non-dimensional)
c             S:   direct beam radiation (KJm-2/3h)
c             DD:  diffuse radiation (KJm-2/3h)
c             SZA: solar zenith angle (radius)
c             SAA: solar azimuth angle (radius)
```

```
c            Mtime: middle time of each 3-hly interval.
c                  (for calculating average SZA & SAA
c                   angles for each 3-hly interval.)
               goto 10
911   write(*,*)'ERROR:',infile,'not found or invalid.'
       write(*,*)'Try Again!'
10    write(*,*)'Enter input filename for meterological
     &          variables:'
         read(*,'(A)')infile
      write(*,*)'Enter output filename:'
         read(*,'(A)')outfile
      write(*,*)'Enter the Julian Day:'
         read(*,*)Day
      write(*,*)'Enter the conductivity of the
      &          soil(KJs-1K-1M-1):'
         read(*,*)ks
      write(*,*)'Enter the surface relative humidity: '
        read(*,*)X
      write(*,*)'Enter break value for clearness index:'
        read(*,*)CI
      open(4,file=infile,status='old',err=911)
        read(4,*)(kd(i),t10(i),t0(i),tal(i),
     &              ua(i),Rh(i),p(i),i=1,8)
         close(4)

         fi=fia*3.14/180.0
      open(10,file=outfile,status='new')
      write(10,500)day,x
      write(10,600)(p(i),i=1,8)
500    format(1x,i3/1x,f5.3)
600    format(1x,8f7.0)

      do 199 i=1,n
         t10(i)=t10(i)+273.16
         t0(i)=t0(i)+273.16
         tal(i)=tal(i)+273.16
         Rh(i)=Rh(i)/100.0
         ul(i)=ua(i)*log(z/z0)/log(3.5/z0)
199    continue
C-------------------------------------------------------------
C      CALCULATING THE DAY-DEPENDENT VARIABLES
```

```
C-------------------------------------------------------
      IC=4921.0     ! solar constant in KJM-2h-1
      GAR=2.0*3.14*(DAY-1)/365.0 ! day angle in radians
      CALL DAY_VAR(IC,GAR,E0,I0,ET,DEL)
     Call Cal_cle(fi,del,kd,et,i0,ri0,clear,sza,saa,mtime)
      call SD(kd,clear,AA,BA,s,dd)
c-------------------------------------------------------
         D_Qstar=0.0
       D_QH=0.0
       D_QE=0.0
       D_QG=0.0
      do 99 i=1,n
        net_k=kd(i)*(1.0-albe)
        ql(i)=rh(i)*qs(tal(i),p(i))
     IF(clear(i).lt.CI) Then
17                  trans1=trans(g,tal(i),t0(i),z,z0,rua,k,ul(i))
      lu=delta*t0(i)**4*3600.0*3.0
        QH(i)=cp*(t0(i)-tal(i))*trans1
        q0=x*qs(t0(i),p(i))
        QE(i)=lv*(q0-ql(i))*trans1
        QG(i)=ks*(t0(i)-t10(i))/ZS*3600.0*3.0
        Ld(i)=-(net_k-lu-QH(i)-QE(i)-QG(i))
        StarL(i)=Ld(i)-lu
        Qstar(i)=net_k-lu+Ld(i)
        Bowen(i)=QH(i)/QE(i)
        Ratio(i)=QG(i)/Qstar(i)
        D_Qstar=D_Qstar+Qstar(i)
        D_QH=D_QH+QH(i)
        D_QE=D_QE+ QE(i)
        D_QG=D_QG+QG(i)
        D_B=D_QH/D_QE
        D_R=D_QG/D_Qstar
     ELSE
C-------------------------------------------------------
C      ITERATIONS FOR SOLVING BALANCE EQUATION
C-------------------------------------------------------
         L=0
       DA=tmin ! initial minimum value for iteration
         DB=tmax ! initial maximum value for iteration
         A=net_k
       B=C_LD(Tal(i),P(i),Rh(i),delta)
```

```
C-------------------------------------------------------------
          C1=DELTA*DA**4*3600.0*3.0
          C2=DELTA*DB**4*3600.0*3.0
          D1=trans(g,tal(i),da,z,z0,rua,k,ul(i))
          D2=trans(g,tal(i),db,z,z0,rua,k,ul(i))
      E1=LV*(ql(i)-X*QS(DA,P(i)))
      E2=LV*(ql(i)-X*QS(DB,P(i)))
      F1=Ks/Zs*(T10(i)-DA)*3600.0*3.0
      F1=Ks/Zs*(T10(i)-DB)*3600.0*3.0
      FLGA=Ff(A,B,C1,D1,E1,F1,CP,Tal(i),DA)
      FLGB=Ff(A,B,C2,D2,E2,F2,CP,Tal(I),DB)
       FLG=FLGA*FLGB
C-------------------------------------------------------------
          IF(FLG.GT.0.0) THEN
             STOP 'Iteration doesn't work!'
          ELSEIF(FLG.EQ.0.0) THEN
             IF(FLGA.EQ.0.0) THEN
                T0(I)=DA
               GOTO 17
              ELSE
               T0(I)=DB
                GOTO 17
             ENDIF
          ELSEIF(FLGA.LT.0.0) THEN
                DA=DA
                DB=DB
          ELSE
                C=DA
                DA=DB
                DB=C
        ENDIF
C-------------------------------------------------------------
C  END of Initial Values Check
C-------------------------------------------------------------
        ABSD=ABS(DB-DA)
     MI=INT((NEPS+LOG10(ABSD))/LOG10(2.)) ! Maximum
                iterative Steps
87       DMI=(DA+DB)/2.
         C=DELTA*DMI**4*3600.0*3
         D=trans(g,tal(i),DMI,z,z0,rua,k,ul(i))
         E=LV*(ql(i)-X*QS(DMI,P(I)))
```

```
          F=Ks/Zs*(T10(I)-DMI)*3600.0*3
          FLGM=Ff(A,B,C,D,E,f,CP,TAL(I),DMI)
              IF(FLGM.GT.0.0) THEN
                    DB=DMI
                  ELSEIF(FLGM.LT.0.0)THEN
                 DA=DMI
                ELSE
                  T0(I)=DMI
                   GOTO 17
              ENDIF
               L=L+1       ! Iterative Step Index
            IF(L.EQ.MI) THEN
                T0(I)=(DA+DB)/2.
                goto 17
              ELSE
                GOTO 87
            ENDIF
        ENDIF
99      CONTINUE
        open(10,file=outfile,status='old')
         write(10,150)ql
         write(10,100)ul,bowen,s,dd,Ld,starL,qg,sza,saa
          close(10)
100     format(1x,8f10.2)
150     format(1x,8f10.4)
        STOP
        END
c-------------------------------------------------------
c  Function for calculating saturation absolute humidity
c-------------------------------------------------------
         Function qs(x,y)
        qs=6.112*exp(17.67*(x-273.16)/(x-29.66))*0.622/y
         return
        end
C *******************************************************
C  SUBROUTINE FOR CALCULATE DAY_DEPENDENT VARIABLES
C  *****************************************************
SUBROUTINE DAY_VAR(IC,GARMA,E0,I0,ET,DEL)
      REAL IC,I0
      E0=1.00011+0.034221*COS(GARMA)+0.00128*SIN(GARMA)+
     &       0.000719*COS(2*GARMA)+0.000077*SIN(2*GARMA)
```

```
c           /* eccentricity correction factor */
          I0=IC*E0
       ET=(0.000075+0.001868*COS(GARMA)-0.032077*SIN(GARMA)-
      &    0.014615*COS(2*GARMA)-0.04089*SIN(2*GARMA))*229.18
c           /* equation of time */
       DEL=0.006918-0.399912*COS(GARMA)+0.070257*SIN(GARMA)-
      &        0.006758*COS(2*GARMA)+0.000907*SIN(2*GARMA)-
      &        0.002697*COS(3*GARMA)+0.00148*SIN(3*GARMA)
c           /* declination */
       RETURN
       END
C ******************************************************
C  Subroutine for clearness index CLEAR(N)
C ******************************************************
        SUBROUTINE Cal_cle(FIA,DEL,KD,ET,I0,RI0
     &              ,CLEAR,sza,saa,mtime)
       DIMENSION RI0(8),CLEAR(8),sza(8),saa(8)
       REAL KD(8),I0,LAT1,LAT2,mtime(8)
      APT11=(3.0-5.0)+ET/60.0   ! LAT1 of first time
     interval
      APT12=(6.0-5.0)+ET/60.0   ! LAT2 of first time
     interval
      TRAN=-TAN(FIA)*TAN(DEL)
      IF(ABS(TRAN).GT.1.0) THEN
        write(*,*)'No Sunset Condition!'
        write(*,*)'********************'
        RI0(1)=FUN_RI0(24.0+APT11,24.0,FIA,DEL,I0)+
     &          FUN_RI0(0.0,APT12,FIA,DEL,I0)
         mtime(1)=23.5+ET/60.0
         DO 39 I=2,8
            UST1=I*3.0
             UST2=(I+1)*3.0
               LAT1=(UST1-5.0)+ET/60.0
                  LAT2=(UST2-5.0)+ET/60.0
                   RI0(I)=FUN_RI0(LAT1,Lat2,FIA,DEL,I0)
                      mtime(i)=(LAT1+LAT2)/2.0
39        CONTINUE
        ELSE
                    SRH=ACOS(TRAN)
                    SRH=SRH*180./3.14
C                   /* NOTE: |SRH: SUN RISE HOUR ANGLE|*/
```

```
                        SSH=-SRH
C                /* NOTE: [SSH: SUN SET HOUR ANGLE]*/
                   SRLAT=12-SRH/15
C       /* NOTE: [SRLAT: SUN RISE (LOCAL APPARENT TIME)] */
                        SSLAT=12-SSH/15.
C       /* NOTE: [SSLAT: SUN SET (LOCAL APPARENT TIME)] */
        write(*,*)'Sunrise Local time=',srlat
        write(*,*)'Sunset Local time=',sslat
           IF(APT11+24.0.GT.SSLAT) THEN
               RI01=0.0
              ELSE
               RI01=FUN_RI0(APT11+24.0,SSLAT,FIA,DEL,I0)
                    ENDIF
           IF(APT12.GT.SRLAT)THEN
               RI02=FUN_RI0(SRLAT,APT12,FIA,DEL,I0)
                    ELSE
               RI02=0.0
           ENDIF
           RI0(1)=RI01+RI02

           if(RI0(1).eq.0.0) then
             mtime(1)=23.5+ET/60.0
              elseif(RI01.ge.RI02) then
                mtime(1)=(Apt11+24.+SSLAT)/2.0
              else
             mtime(2)=(SRLAT+APT12)/2.0
           endif
            DO 49 I=2,8
            UST1=I*3.0
            UST2=(I+1)*3.0
            LAT1=(UST1-5.0)+ET/60.0
            LAT2=(UST2-5.0)+ET/60.0
         IF(LAT1.GE.SRLAT.AND.LAT2.LE.SSLAT) THEN
C              /* daytime condition*/
              RI0(I)=FUN_RI0(LAT1,LAT2,FIA,DEL,I0)
              Mtime(i)=(Lat1+Lat2)/2.0
           ELSEIF(LAT1.LT.SRLAT.and.lat2.gt.srlat) THEN
C                    /* between sunrise condition*/
                   RI0(I)=FUN_RI0(SRLAT,LAT2,FIA,DEL,I0)
Mtime(i)=(SRLAT+LAT2)/2.0
            ELSEif(lat1.lt.sslat.and.lat2.gt.sslat) then C                    /* between
```

```
sunset time*/
                    RI0(I)=FUN_RI0(LAT1,SSLAT,FIA,DEL,I0)
Mtime(i)=(Lat1+SSLAT)/2.0
                          else
                Ri0(i)=0
                Mtime(i)=(Lat1+Lat2)/2.0
              ENDIF
49       CONTINUE
       ENDIF
        DO 59 I=1,8
          IF(RI0(I).EQ.0) THEN
             CLEAR(I)=-99.9
                              ELSE
                CLEAR(I)=KD(I)/RI0(I)
          ENDIF

59        CONTINUE
          call calangle(mtime,del,fia,sza,saa)
         RETURN
         END
C ********************************************************
C Subroutine for separating S(N) from D(N)
C ********************************************************
Subroutine SD(kd,clear,A,B,s,d)
          real kd(8),s(8),d(8),clear(8)
            do 29 i=1,8
              d(i)=A*kd(i)+B*clear(i)*kd(i)
              if(d(i).lt.0.0) then
                   d(i)=0.0
                elseif(d(i).gt.kd(i)) then
                   d(i)=kd(i)
              endif
              s(i)=kd(i)-d(i)
29           continue
       return
       end
C ********************************************************
C Subroutine for solar zenith & azimuth angles SZA,SAA
C ********************************************************
          Subroutine calangle(time,del,fia,sza,saa)
          dimension time(8),sza(8),saa(8)
```

```
          do 79 i=1,8
            ht=15.0*(12.0-time(i))*3.14/180.0
          ang1=sin(del)*sin(fia)+cos(del)*cos(fia)*cos(ht)
                                  sza(i)=Acos(ang1)
          ang2=(sin(del)*cos(fia)-cos(del)*sin(fia)*
     &          cos(ht))/sin(sza(i))
          saa(i)=Acos(ang2)
              if(time(i).ge.12.0) then
                saa(i)=2*3.1416-saa(i)
              endif
79          continue
        return
        end
C*********************************************************
C       FUNCTION FOR ITERATION
C*********************************************************
          FUNCTION Ff(A,B,C,D,E,f,CP,TA,T0)
        Ff=((A+B-C+f)/D+E)/CP+TA-T0
        RETURN
        END
C*********************************************************
C   FUNCTION FOR CALCULATING THE EXTRATERRESTRIAL RADIATION
C   DURING PERIOD OF T1 AND T2
C*********************************************************
          FUNCTION FUN_RI0(T1,T2,FIA,DEL,dI0)

          FUN_RI0=-12./3.14*dI0*(SIN(DEL)*SIN(FIA)*
     &       3.14/12.*(T1-T2)+
     &       COS(DEL)*COS(FIA)*(SIN(3.14-3.14/12.*t2)-
     &       SIN(3.14-3.14/12.*t1)))
        RETURN
        END
C*********************************************************
C  FUNCTION FOR RICHARDSON NUMBER
C*********************************************************
FUNCTION RICHARD(G,TZ,T0,Z,Z0,U)
          RICHARD=g*(tz-t0)*(z-z0)*2.0/(tz+t0)/u**2
        RETURN
        END
c*********************************************************
c  FUNCTION FOR TRANSFER COEFFICIENT CORRECTIONS
```

```
C************************************************************
            function  trans(g,ta,t0,z,z0,rua,k,u)
            real k
          transN=rua*k**2*u/(log(z/z0))**2*3600.0*3.0   !   Neutral
          Ri=Richard(g,ta,t0,z,z0,u)
         if(Ri.ge.0.0) then
           trans=transN/(1+10.0*Ri)
          else
           trans=transN*(1-10.0*Ri)
         endif
       Return
       End
C************************************************************
C FUNCTION FOR CALCULATING LONGWAVE DOWNWARD RADIATION
C  ************************************************************
          FUNCTION C_LD(TA,P,RH,DELTA)
         E=0.70+5.95E-5*QS(TA,P)*RH*P/0.622*EXP(1500.0/TA)
          C_LD=E*DELTA*TA**4*3600.0*3
       RETURN
       END
```

## B.2 Source Code of ASEB.EXE --- ASEBM.FOR

```
C-------------------------------------------------------
C ASEB.EXE
C-------------------------------------------------------
Compiled by VAX FORTRAN compiler
Created by H. Wang in Feb., 1993
C=======================
C definition of variables
C=======================
       integer day
       real    Lv,k,Km
       parameter(N=576,Tmax=320,Tmin=230.0,Lv=2500.0,
     &   elevblk=420.0,rua=1.2,
     &   g=9.8,NEPS=5,Cp=1.01,Delta=5.67E-11,z=2.0,k=0.4,
      &   elevbic=1085.0)
       character*15 infile1,infile2,infile3,infile4,outfile
```

```
      real    Qstar(8,N),Kd(8,N),Kstar(8,N),
     &        Qh(8,N),QE(8,N),QG(8,N),Tg(8,N),
     &        WS(8,N),Pa(8,N)
      real    DQstar(N),DKstar(N),DQh(N),DQe(N),
     &        DQg(N),DTg(N),DKD(N)
      real    elev(N),slp(N),asp(N),albe(N),z0(N)
      real    bowen(8),s(8),d(8),Ld(8),Lstar(8),
     &        Qgblk(8),sza(8),saa(8),w(8)
      real    tQstar(8),tQH(8),tQE(8),tQG(8),tTg(8)
      real    gQstar(8),gQH(8),gQE(8),gQG(8),gTg(8)
      real    Pblk(8),qablk(8) ! pressure & humidity at BLK
      real    Tbic(8),RHbic(8),qabic(8) ! Air temp.
     & RH at Barnes Ice Cap
C=============================
C input and output file names
C=============================
      write(*,*)'Enter name of the file created by
     &          SEB.EXE:'
                read(*,'(A)')infile1
      write(*,*)'Enter name of the file of topographical
     &          and surface properties:'
                read(*,'(A)')infile2
      write(*,*)'Enter name of the file containing air
     &          temp. & humidity at the Barnes Ice Cap:'
                read(*,'(A)')infile3
      write(*,*)'Enter name of the windspeed file from MS-
     &          Micro/3:'
                read(* '(A)')infile4
      write(*,*)'Enter name of the output file:'
                read(*,'(A)')outfile
      GOTO 60
C================
C error messages
C================
99    write(*,*)'Error: file ',infile1,'not found or
     &          invalid.'
                stop
199   write(*,*)'Error: file ',infile2,'not found or
     &          invalid.'
                stop
299   write(*,*)'Error: file ',infile3,'not found or
```

```
     &            invalid.'
                  stop
399    write(*,*)'Error: file ',infile4,'not found or
     &            invalid.'
                  stop
C=============================================
C read in data from input files
C=============================================
60     open(2,file=infile1,status='old',err=99)
         read(2,*)day
         read(2,*)r
         read(2,*)Pblk,qablk,w,bowen,s,d,Ld,Lstar,
     &            Qgblk,sza,saa
       close(2)
       open(3,file=infile2,status='old',err=199)
       read(3,*)(elev(i),slp(i),asp(i),albe(i),z0(i),i=1,N)
         close(3)
       open(4,file=infile3,status='old',err=299)
       read(4,*)(Tbic(i),RHbic(i),i=1,8)
       close(4)
       open(5,file=infile4,status='old',err=399)
       read(5,*)((WS(i,j),i=1,8),j=1,N)
       close(5)
C=====================
C processing of data
C=====================
       do 50 i=1,8
       do 50 j=1,N
         Pa(i,j)=Pblk(i)-(elev(j)-elevblk)*rua*g/100.0
         WS(i,j)=WS(i,j)*w(i)
50     continue
       do 70 i=1,8
         esbic=es(Tbic(i))
         qsbic=0.622*esbic/(Pblk(i)-(elevbic-
     &   elevblk)*rua*g/100.0)
         qabic(i)=qsbic*RHbic(i)
         tQstar(i)=0.0
         tQH(i)=0.0
         tQE(i)=0.0
         tQG(i)=0.0
         tTg(i)=0.0
```

```
        gQstar(i)=0.0
        gQH(i)=0.0
        gQE(i)=0.0
        gQG(i)=0.0
        gTg(i)=0.0
70      continue
C=========================
C radiation calculation
C=========================
      M=8
      call radcal(s,d,slp,asp,sza,saa,albe,kd,m,N)
      do 90 i=1,8
        do 90 j=1,N
          Kstar(i,j)=(1-albe(j))*Kd(i,j)
90      continue
C=================================
C surface fluxes and temperature
C=================================
      Tx=Tmax
      Tm=Tmin
      Tx_Lu=Cal_Lu(Tx,Delta)
      Tm_Lu=Cal_Lu(Tm,Delta)
      Lt=0      ! grids in tundra
      Lg=0      ! grids in glacier
      do 20 j=1,N
        if(z0(j).eq.1.0E-5) then
         do 30 i=1,8
          Qstar_Tx=Kstar(i,j)+Ld(i)-Tx_Lu
          Qstar_Tm=Kstar(i,j)+Ld(i)-Tm_Lu
          call G_Ta(Tbic(i),Tgrid,elev(j),elevbic) ! Ta on glacier
          Tran_Tx=trans(g,Tgrid,Tx,z,z0(j),rua,k,ws(i,j))
          Tran_Tm=trans(g,Tgrid,Tm,z,z0(j),rua,k,ws(i,j))
          Qh_Tx=tran_Tx*(Cp*(Tx-Tgrid))
          Qh_Tm=tran_Tm*(Cp*(Tm-Tgrid))
          QE_Tx=tran_Tx*Lv*(qs(Tx,Pa(i,j))-qabic(i))
          QE_Tm=tran_Tm*Lv*(qs(Tm,Pa(i,j))-qabic(i))
          f_Tx=Qstar_Tx-Qh_Tx-QE_Tx
          f_Tm=Qstar_Tm-Qh_Tm-QE_Tm
          flag=f_Tx*f_Tm
          call Ev_flag(FLAG,f_Tx,f_Tm,Tx,Tm,Tg(i,j))
            if(Tg(i,j).eq.Tx) then
```

```
            Tg(i,j)=273.16
            Qstar(i,j)=Kstar(i,j)+Ld(i)-
     &              Cal_Lu(Tg(i,j),Delta)
        tran_Tg=trans(g,Tgrid,Tg(i,j),z,z0(j),
     &          rua,k,Ws(i,j))
        QH(i,j)=tran_Tg*(Tg(i,j)-Tgrid)*Cp
          QE(i,j)=tran_Tg*(qs(Tg(i,j),Pa(i,j))-qabic(i))*lv
        QG(i,j)=Qstar(i,j)-QH(i,j)-QE(i,j)
            elseif(Tg(i,j).eq.Tm) then
              Qstar(i,j)=Qstar_Tm
              QH(i,j)=QH_Tm
              QE(i,j)=QE_Tm
              QG(i,j)=0.0
            else
        call glacier(Tx,Tm,NEPS,Kstar(i,j),Ld(i),Delta,
     &           Cp,Lv,g,z,z0(j),WS(i,j),rua,k,
     &          Pa(i,j),qabic(i),Tgrid,Tg(i,j),
     &          Qstar(i,j),QH(i,j),QE(i,j),QG(i,j))
            endif
             Tx=Tmax
             Tm=Tmin
             gQstar(i)=Qstar(i,j)+gQstar(i)
             gQH(i)=QH(i,j)+gQH(i)
             gQE(i)=QE(i,j)+gQE(i)
             gQG(i)=QG(i,j)+gQG(i)
             gTg(i)=Tg(i,j)+gTg(i)
30          continue
          Lg=Lg+1

         else
           do 40 i=1,8
             Qg(i,j)=Qgblk(i)
          call
        tundra(Lstar( ),Kstar(i,j),bowen(i),
     &        Qstar(i,j),Qg(i,j),QH(i,j),QE(i,j))
         &        Km=rua*WS(i,j)*k**2/(log(z/0.001))**2
          call Tg_Cal(qablk(i),QE(i,j),Pa(i,j),
     &           r,Km,Lv,Tg(i,j),Tx,
     &            Tm,NEPS)
            Tx=Tmax
            Tm=Tmin
```

```
          tQstar(i)=Qstar(i,j)+tQstar(i)
          tQH(i)=QH(i,j)+tQH(i)
          tQE(i)=QE(i,j)+tQE(i)
          tTg(i)=Tg(i,j)+tTg(i)
40      continue
          Lt=Lt+1
         endif
20      continue
C=======================================================
C diurnal summaries of tundra vs. glacier
C=======================================================
        do 45 i=1,8
          tQstar(i)=tQstar(i)/Lt
          gQstar(i)=gQstar(i)/Lg
            tQH(i)=tQH(i)/Lt
            gQH(i)=gQH(i)/Lg
          tQE(i)=tQE(i)/Lt
          gQE(i)=gQE(i)/Lg
            tQG(i)=Qgblk(i)
            gQG(i)=gQG(i)/Lg
          tTg(i)=tTg(i)/Lt-273.16
          gTg(i)=gTg(i)/Lg-273.16
45      continue
C=======================================
C daily summaries of variables
C=======================================
       do 110 i=1,N
         DQstar(i)=0.0
         DKstar(i)=0.0
         DKd(i)=0.0
         DQh(i)=0.0
         DQe(i)=0.0
         DQg(i)=0.0
         DTg(i)=0.0
110     continue
       do 130 j=1,N
       do 120 i=1,8
         DQstar(j)=Qstar(i,j)+DQstar(j)
         DKstar(j)=Kstar(i,j)+DKstar(j)
         DQh(j)=Qh(i,j)+DQh(j)
         DQe(j)=Qe(i,j)+DQe(j)
```

```
        DQg(j)=Qg(i,j)+DQg(j)
        DTg(j)=Tg(i,j)+DTg(j)
        DKd(j)=Kd(i,j)+DKd(j)
120     continue
        DTg(j)=DTg(j)/8.0-273.16          ! converted to degree C
        DQstar(j)=DQstar(j)/1000.0    !  converted to MJm-2/day
        DKstar(j)=DKstar(j)/1000.0    !  converted to MJm-2/day
        DQh(j)=DQh(j)/1000.0
        DQe(j)=DQe(j)/1000.0
        DQg(j)=DQg(j)/1000.0
        DKd(j)=DKd(j)/1000.0
130     continue
C=============================================
C output of the ASEB.EXE
C=============================================
      open(10,file=outfile,status='new')
      write(10,101)(tQstar(j),gQstar(j),tQH(j),gQH(j),
     &              tQE(j),gQE(j),tQG(j),gQG(j),tTg(j),
     &              gTg(j), j=1,8)
      open(11,file='DKstar.dat',status='new')
      write(11,100)(DKstar(j),j=1,N)
      close(11)
      open(12,file='DKd.dat',status='new')
      write(12,100)(DKd(j),j=1,N)
      close(12)
      open(13,file='DQE.dat',status='new')
      write(13,100)(DQe(j),j=1,N)
      close(13)
      open(14,file='DQG.dat',status='new')
      write(14,100)(DQG(j),j=1,N)
      close(14)
      open(15,file='DTg.dat',status='new')
      write(15,100)(DTg(j),j=1,N)
      close(15)
100     format(1x,f8.1)
101     format(1x,10F8.1)
      STOP
      END
C=============================================
C definition of subroutines
C=============================================
```

```
C*************************************************
C  Subroutine for surface fluxes on tundra surfaces
C*************************************************
      subroutine  tundra(starL,starK,b,starQ,Qg,Qh,Qe)
        starQ=starL+starK
      avlbe=starQ-Qg
      qh=avlbe*b/(1.0+b)
      qe=avlbe-qh
      return
      end
C*****************************************
C Subroutine for surface temp. over tundra
C*****************************************
      subroutine Tg_Cal(qa,QE,Pa,r,Km,L,Tg,Tx,Tm,NEPS)
           real Km,L
          f_Tx=func1(L,Km,qa,Pa,r,QE,Tx)
          f_Tm=func1(L,Km,qa,Pa,r,QE,Tm)
          flag=f_Tx*f_Tm
          call Ev_flag(FLAG,f_Tx,f_Tm,Tx,Tm,Tg)
           if(Tg.ne.Tx.and.Tg.ne.Tm) then
          call iter(Tx,Tm,QE,qa,Pa,r,Km,L,Tg,NEPS)
           endif
      return
      end
C*******************************
C Subroutine for Evaluating FLAG
C*******************************
      subroutine Ev_flag(FLAG,f_Tx,f_Tm,Tx,Tm,Tg)
          if(flag.gt.0.0) then
            write(*,*)'Error: reset Tx and Tm!'
              stop
              elseif(flag.eq.0.0) then
                call find_Tg(f_Tx,f_Tm,Tx,Tm,Tg)
                goto 15
              elseif(f_Tx.lt.0.0) then
                tem=Tx
                Tx=Tm
                Tm=tem
              endif
15         return
          end
```

```
C*********************************************
C Function: f(Tg)=Lv*Km(q0-qa)-QE
C*********************************************
      function func1(L,Km,qa,Pa,r,QE,T)
          real L,Km
          es0=es(T)
          qs0=0.622*es0/Pa
          q0=r*qs0
          func1=L*Km*(q0-qa)*3600.0*3.0-QE
      return
      end
C*********************************************
C  function for saturated vapour pressure ES(T)
C*********************************************
      function es(t)
        es=6.112*exp(17.67*(t-273.16)/(t-29.66))
      return
      end
C*****************************************
C function for saturated absolute humidity
C*****************************************
      function qs(t,p)
        qs=0.622*es(t)/p
      return
      end
C*************************************************
C Subroutine for determine Tg when flag=0.0
C*************************************************
      subroutine find_Tg(f_Tx,f_Tm,Tx,Tm,Tg)
          if(f_Tx.eq.0.0) then
            Tg=Tx
              else
                Tg=Tm
          endif
      return
      end
C*******************************
C Subroutine of iteration for Tg
C*******************************
      subroutine iter(Tx,Tm,QE,qa,pa,r,Km,L,Tg,NEPS)
```

```
      real Km,L
      m_step=maxstep(Tx,Tm,NEPS)
      do 18 i=1,m_step
        Tg=(Tm+Tx)/2.0
        f_Tg=func1(L,Km,qa,Pa,r,QE,Tg)
          if(f_Tg.gt.0.0) then
            Tx=Tg
          elseif(f_Tg.lt.0.0) then
            Tm=Tg
          else
            goto 28
          endif
18      continue
28    return
      end
C**************************************
C Function for maximun iterative steps
C**************************************
      function maxstep(t1,t2,n)
        d12=ABS(t1-t2)
        maxstep=INT((n+LOG10(d12))/LOG10(2.0))
      return
      end
C************************************************************
C     FUNCTION FOR RICHARDSON NUMBER
C************************************************************
FUNCTION RICHARD(G,TZ,T0,Z,Z0,U)
        RICHARD=g*(tz-t0)*(z-z0)*2.0/(tz+t0)/u**2
      RETURN
      END
c************************************************************
c    FUNCTION FOR TRANSFER COEFFICIENT CORRECTIONS
C************************************************************
       function  trans(g,ta,t0,z,z0,rua,k,u)
      real k
      transN=rua*k**2*u/(log(z/z0))**2*3600.0*3.0 ! Neutral
      Ri=Richard(g,ta,t0,z,z0,u)
      if(Ri.ge.0.0) then
      trans=transN/(1+10.0*Ri)
       else
      trans=transN*(1-10.0*Ri)
```

```
        endif
        Return
        End
C**************************************
C Subroutine for solar radiation Kd(i,j)
C**************************************
       subroutine radcal(s,d,slp,asp,sza,saa,albe,Kd,M,N)
         real s(8),d(8),sza(8),saa(8)
         real slp(576),asp(576),albe(576)
         real Kd(m,N)
         do 38 i=1,m
         do 38 j=1,N
      cosCT=cos(slp(j))*cos(sza(i))+sin(slp(j))*sin(sza(i))*
      &           cos(saa(i)-asp(j))

         Kd(i,j)=s(i)*cosCT/cos(sza(i))+d(i)*
     &        (1+cos(slp(j)))/2.0+
     &        albe(j)*(s(i)+d(i))*(1-cos(slp(j)))/2.0
38       continue
       return
       end
C*****************************************
C Subroutine for air temperature over glacier
C*****************************************
       subroutine G_Ta(Tbic,Tgrid,elevgrid,elevbic)
          Tgrid=Tbic-0.98*(elevgrid-elevbic)/100.0
       return
       end
C*************************************************************
C   Subroutine for surface fluxes and temperature over glacier
C*************************************************************
         subroutine
       & glacier(Tx,Tm,n,kstar,ld,delta,Cp,L,g,z,z0,u,rua,k,
      & pa,qa,Tgrid,Tg,Qstar,QH,QE,QG )
        real L,Kstar,Ld,k
          m_step=maxstep(Tx,Tm,n)
          Do 48 i=1,m_step
           Tg=(Tx+Tm)/2.0
           Qstar=Kstar+ld-cal_Lu(Tg,delta)
           Tran_Tg=trans(g,Tgrid,Tg,z,z0,rua,k,u)
           Qh=Tran_Tg*Cp*(Tg-Tgrid)
```

```
          Qe=Tran_Tg*L*(qs(Tg,Pa)-qa)
          f_Tg=Qstar-QH-QE
              if(f_Tg.gt.0.0) then
                Tx=Tg
              elseif(f_Tg.lt.0.0) then
                Tm=Tg
              else
                goto 58
              endif
48         continue
58         if(Tg.gt.273.16) then
            Tg=273.16
            Qstar=kstar+ld-cal_lu(Tg,Delta)
            tran_Tg=trans(g,Tgrid,Tg,z,z0,rua,k,u)
            QH=tran_Tg*Cp*(Tg-Tgrid)
            QE=tran_Tg*L*(qs(Tg,pa)-qa)
            QG=Qstar-QH-QE
          elseif(Tg.le.273.16) then
            QG=0.0
          endif
          return
          end

C*****************************************
C Function for long-wave upward radiation
C*****************************************
      function Cal_Lu(t,c)
        Cal_Lu=c*t**4*3600.0*3.0
      return
      end
```

## B.3 Source Code of TOPO.EXE --- TOPO.FOR

```
c-------------------------------------------------------
c TOPO.EXE
c Preparing input file 'TOPO.DAT' for the ASEBM
c-------------------------------------------------------
        Dimension A(600,5)
        Character*16 file1,file2,file3,file4,file5,outfile
```

```
      Write(*,*)'----------------------------------------'
      Write(*,*)'THIS PROGRAM WILL CREATE "TOPO.DAT" '
      Write(*,*)'----------------------------------------'
      Write(*,*)'Enter the No. of grid cells in the ASEBM:'
      Read(*,*) N
     write(*,*)'Enter name of the DEM map:'
      read(*,'(A)') file1
     write(*,*)'Enter name of the SLOPE map:'
      read(*,'(A)') file2
     write(*,*)'Enter name of the ASPECT map:'
      read(*,'(A)') file3
     write(*,*)'Enter name of the Albedo map:'
      read(*,'(A)') file4
     write(*,*)'Enter name of the SURFACE ROUGHNESS map:'
      read(*,'(A)') file5
     write(*,*)'Enter name of the output file:'
      read(*,'(A)') outfile
     write(*,*)
        Write(*,*)'READING DATA.....'
C-------------------------------------------------------
C             READ IN DATA FILES
C-------------------------------------------------------
          Open(7,FILE=file1,STATUS='OLD',ERR=911)
        Read(7,*)(A(I,1),I=1,N)
        Close(7)
        Open(8,FILE=file2,STATUS='OLD',ERR=912)
        Read(8,*)(A(I,2),I=1,N)
        Close(8)
        Open(9,FILE=file3,STATUS='OLD',ERR=913)
        Read(9,*)(A(I,3),I=1,N)
        Close(9)
        Open(10,FILE=file4,STATUS='OLD',ERR=914)
        Read(10,*)(A(I,4),I=1,N)
        Close(10)
        Open(11,FILE=file5,STATUS='OLD',ERR=915)
        Read(11,*)(A(I,5),I=1,N)
        Close(11)
        Write(*,*)'FINISH READING.....'
         Goto 19
C -------------------------------------------------------
C             ERROR  MESSAGES
```

```
C-------------------------------------------------------
911         Write(*,*)'ERROR:', file1, 'NOT FOUND OR INVALID'
            STOP
912         Write(*,*)'ERROR:', file2, 'NOT FOUND OR INVALID'
            STOP
913         Write(*,*)'ERROR:', file3, 'NOT FOUND OR INVALID'
            STOP
914         Write(*,*)'ERROR:', file4, 'NOT FOUND OR INVALID'
            STOP
915         Write(*,*)'ERROR:', file5, 'NOT FOUND OR INVALID'
            STOP
C-------------------------------------------------------
C             WRITE OUT TO 'TOPO.DAT'
C-------------------------------------------------------
19          Open(12,File=outfile,Status='new')
           Write(12,100)(A(I,1)*0.3048,A(I,2)*3.14/180.0,
     &        A(I,3)*3.14/180.0, (A(I,J),J=4,5),I=1,N)
            Close(12)
           Write(*,*)'DONE!'
100         Format(1X,5F12.7)
           STOP
           END
```

## B.3 Source Code of WIND.EXE --- WIND.FOR

```
C=============================================================
================
C *Program: wind.exe; Source code: wind.for
C-------------------------------------------------------
C *The program will generate a windspeed file for a day
C  from 8 Wddd.dat (ddd: wind dir.in deg.) files created
C  by the MS-Micro/3.
C
C *The output file will be used as input to the ASEB.EXE
C-------------------------------------------------------
Compiled by VAX FORTRAN compiler
Created by H. Wang in March, 1993
C=============================================================
          parameter(l=24, n=576)  ! l x l grid lines
```

```
      dimension ws(8,n)
      integer a,b,c,d
      character*15 outfile
      character*15 infile(8)
      do 40 i=1,8
       write(*,*)'Enter name of No.',i,' wind file'
       read(*,'(A)')infile(i)
40     continue
      write(*,*)'Enter name of outfile:'
      read(*,'(A)') outfile
      goto 30
199    write(*,*)'Error: file',infile(i),' not found or
     &            invalid'
                stop
30     a=n-(l-1)
      b=n
      m=10
      do 10 i=1,8
        open(m,file=infile(i),status='old',err=199)
        read(m,*)(p,q,ws(i,j),j=1,n)
        close(m)
      m=m+1
10     continue
      open(19,file=outfile,status='new')
      do 60 i=1,l
        c=a-l*(i-1)
        d=b-l*(i-1)
        write(19,200)((ws(k,j),k=1,8),j=c,d)
60     continue
      close(19)
200    format(1x,8f6.2)
      stop
      end
```

## B.5 Source Code of COMBINE.EXE -- COMBINE.FOR

```
C==========================================================
==========
C combine.exe
C----------------------------------------------
Combines the grid coordinates with the field attri-
C butes to create a standard data file for SURFER
C----------------------------------------------
Compiled by VAX Fortran compiler
Created by H. Wang  ( March, 1993)
C----------------------------------------------
      character*15 infile, outfile
      write(*,*)'Enter name of the field file:'
      read(*,'(A)')infile
      write(*,*)'Enter output filename:'
      read(*,'(A)')outfile
      write(*,*)'Enter a multiply factor for attribute:'
        read(*,*)fct
      open(2,file='grid.dat',status='old')
      open(3,file=infile,status='old')
      open(4,file=outfile,status='new')
      do 10 i=1,576
      read(2,*) x, y
      read(3,*)z
      write(4,*) x, y,z*fct
10     continue
      stop
      end
```

# APPENDIX C

Separation of Diffuse from Direct Radiation

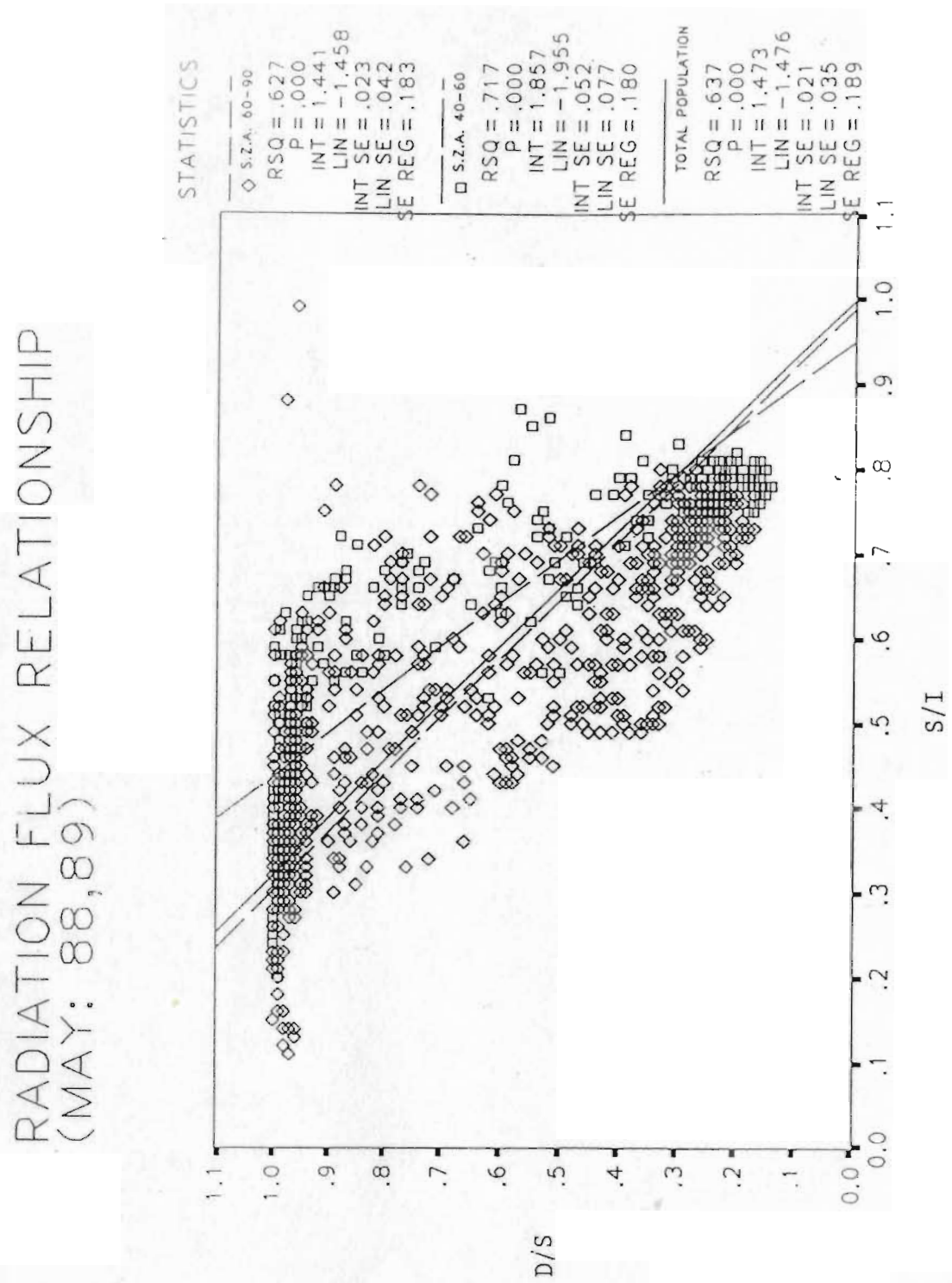


**Figure C.1. Variation of the hourly diffuse radiation as a function of the clearness index (May).**

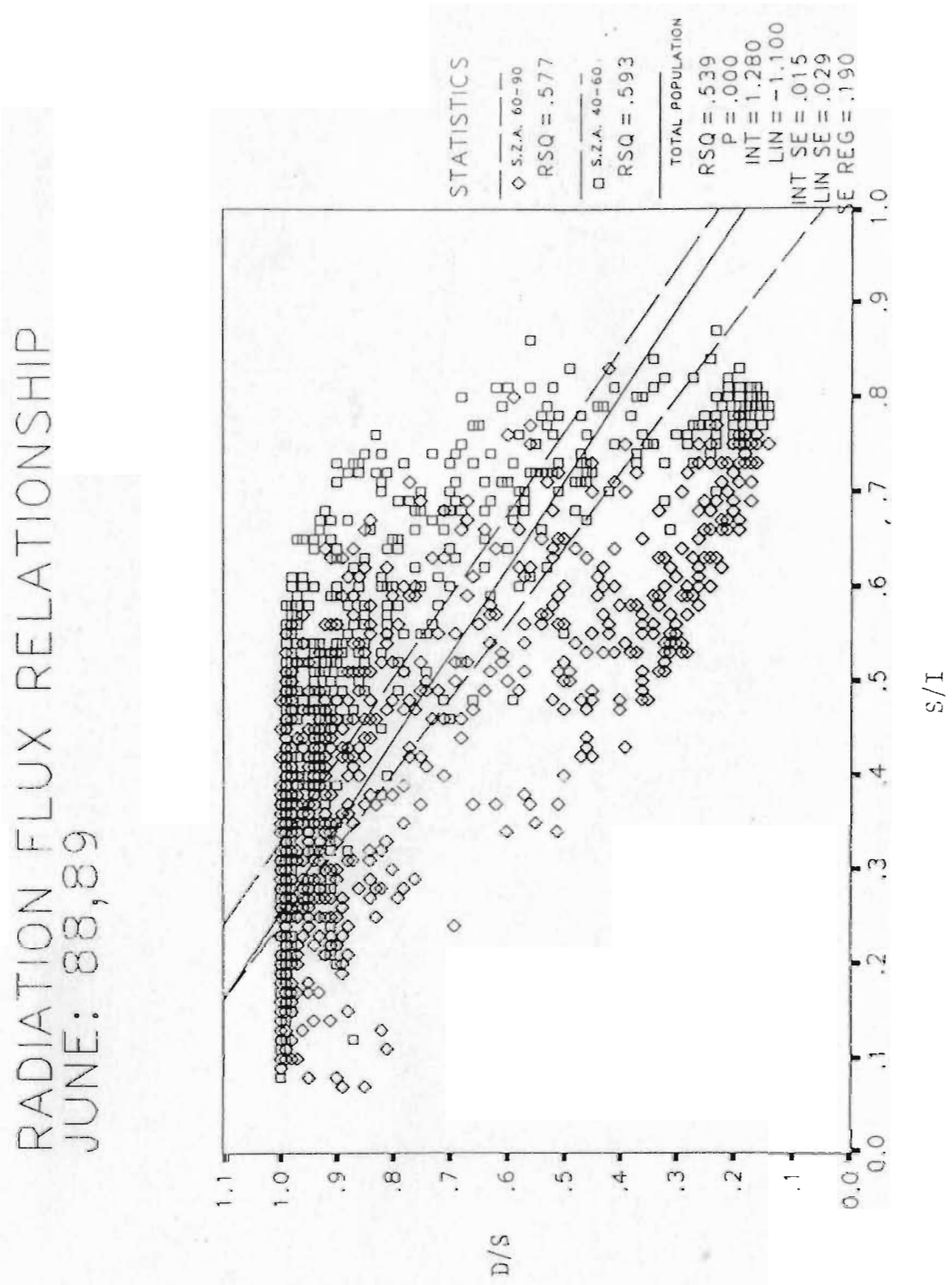


**Figure C.2. Variation of the hourly diffuse radiation as a function of the clearness index (June)**

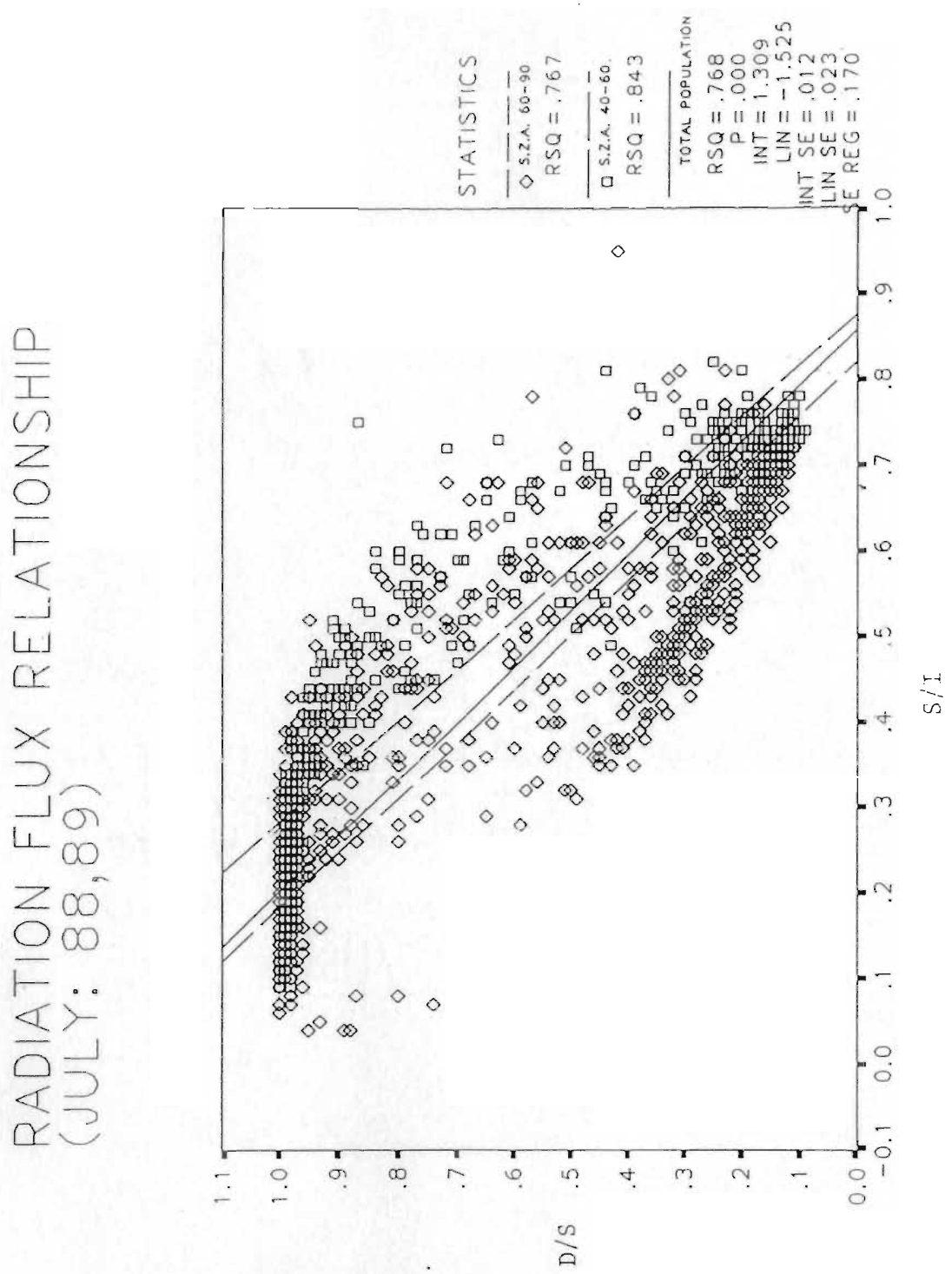


**Figure C.3. Variation of the hourly diffuse radiation as a function of the clearness index (July)**

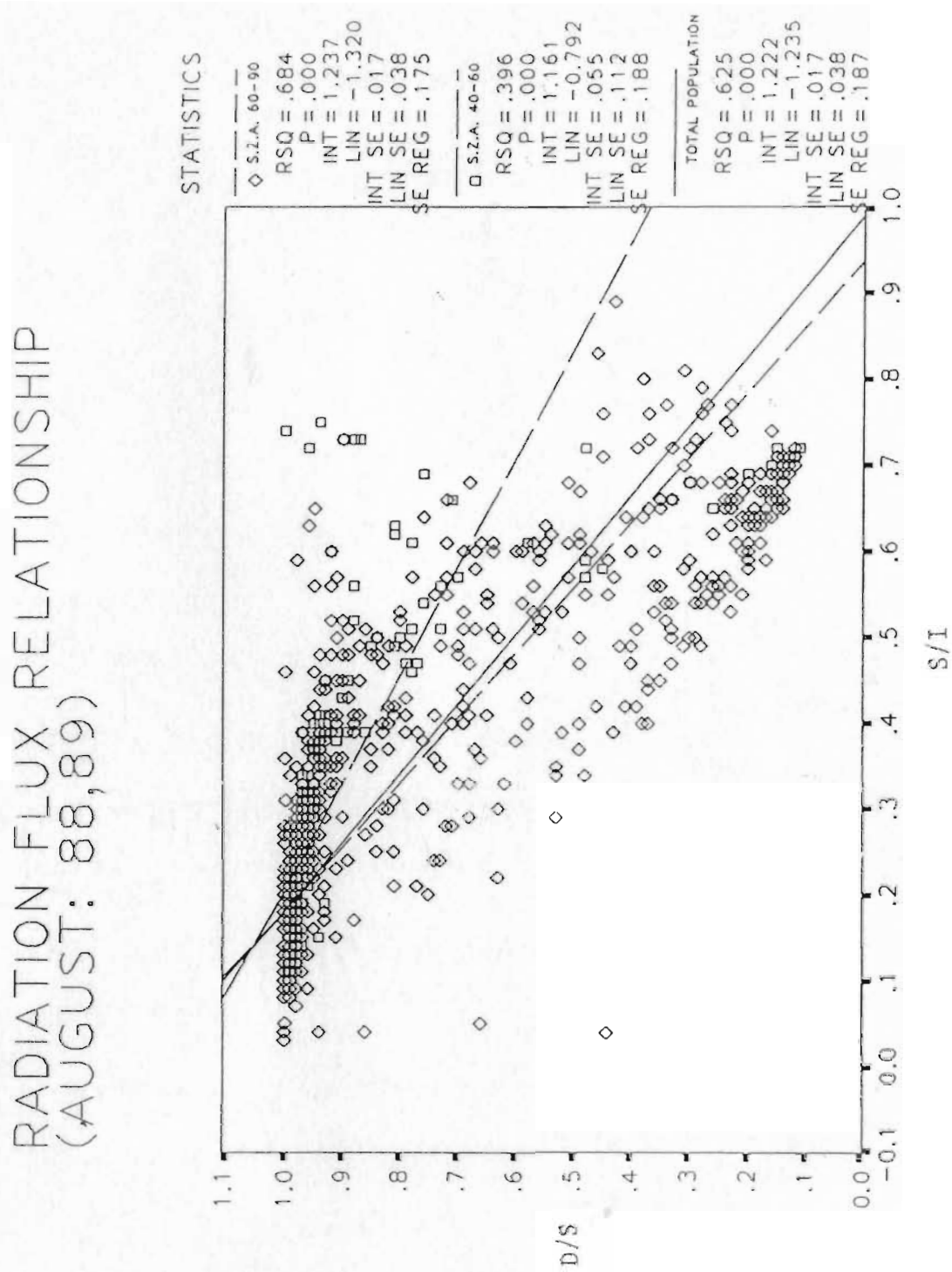


**Figure C.4. Variation of the hourly diffuse radiation as a function of the clearness index (August)**

# APPENDIX D

## Examples of the MS-Micro/3 Output

Details of the process of using the MS-Micro/3 is presented by Walmsley et al. (1990). As an example, the procedures of invoking the MS-Micro/3 on 11 August is presented as follows:

1. Run MSPAR.EXE to create a parameter files (MSMASTER.PAR) required by most of the other programs in the MS-Micro/3.
2. Run MSTG.EXE and MSRG.EXE to create topography and surface roughness grid files.
3. Run MS3R.EXE to calculate the normalized wind speed and the deviation of the wind direction.
4. Change the output files (Nddd.GRD) of the wind model into the standard SURFER data files (Wddd.DAT) via the 'Util' of the SURFER.
5. Eight Wddd.DAT files of the day is read into a single file by invoking WIND.EXE (See Appendix A.1.5).

The field of normalized windspeed only depends on the wind direction. Therefore, if the measured wind direction is the same, the resultant normalized windspeed field is

same. The wind measurement of 11 August is show in Table D.1. It is noted that some of the wind directions are only 1 degree apart. Thus we ignore the difference for those directions. That is, only five wind directions are calculated, as shown in the Table D.2.

The output are ten grid files of normalized windspeed and direction deviation. For the purpose of the ASEBM, only the normalized windspeed files are used. Figure D.1 to D.5 show the normalized windspeed for five different incident directions.

**Table D.1. Wind speed and direction (11 August, 91)**

| Measure time(UT) | Windspeed ($ms^{-1}$) | Wind Dir. (deg.) |
|---|---|---|
| 600 | 5.8 | 255 |
| 900 | 11.5 | 308 |
| 1200 | 11.7 | 303 |
| 1500 | 7.5 | 304 |
| 1800 | 9.1 | 309 |
| 2100 | 10.0 | 306 |
| 2400 | 8.6 | 306 |
| 300 | 7.5 | 287 |

## Table D.2. MSMASTER.PAR (11 August, 1991)

```
      MS-MICRO/3    MASTER PARAMETER SUMMARY

      Project Name, Date and Time  -
TEST CASE  93/03/12  12:08

      ------
            64         No. of X grid lines
            64         No. of Y grid lines
      -12000.0         Left boundary of domain (m)
       12000.0         Right boundary of domain (m)
      -12000.0         Lower boundary of domain (m)
       12000.0         Upper boundary of domain (m)
      ------
             5   No. of directions
      Dirn.  1          255  Direction (deg)
             1       420.00  Outer Level (m)
             1            2  Upstream roughness class
             1       0.1250  Relative frequency
             1        5.800  Average wind speed
      Dirn.  2          308  Direction (deg)
             2       420.00  Outer Level (m)
             2            2  Upstream roughness class
             2       0.2500  Relative frequency
             2       10.300  Average wind speed
      Dirn.  3          303  Direction (deg)
             3       420.00  Outer Level (m)
             3            2  Upstream roughness class
             3       0.2500  Relative frequency
             3        9.600  Average wind speed
      Dirn.  4          306  Direction (deg)
             4       420.00  Outer Level (m)
             4            2  Upstream roughness class
             4       0.2500  Relative frequency
             4        9.300  Average wind speed
      Dirn.  5          287  Direction (deg)
             5       420.00  Outer Level (m)
             5            2  Upstream roughness class
             5       0.1250  Relative frequency
             5        7.500  Average wind speed
      ------
      MS.TCN                 Topography contour file
      MS.RBS                 Roughness boundary file
      e:\restore\msprogPath for Scratch files.
      ------
             2   No. of roughness classes
      Class  1   1.00E-05    Roughness (m)
      Class  2   1.00E-03    Roughness (m)
      ------
            0.0          Origin x-shift (m)
            0.0          Origin y-shift (m)
         6000.0          Inner distance (m)
        10000.0          Outer distance (m)
```

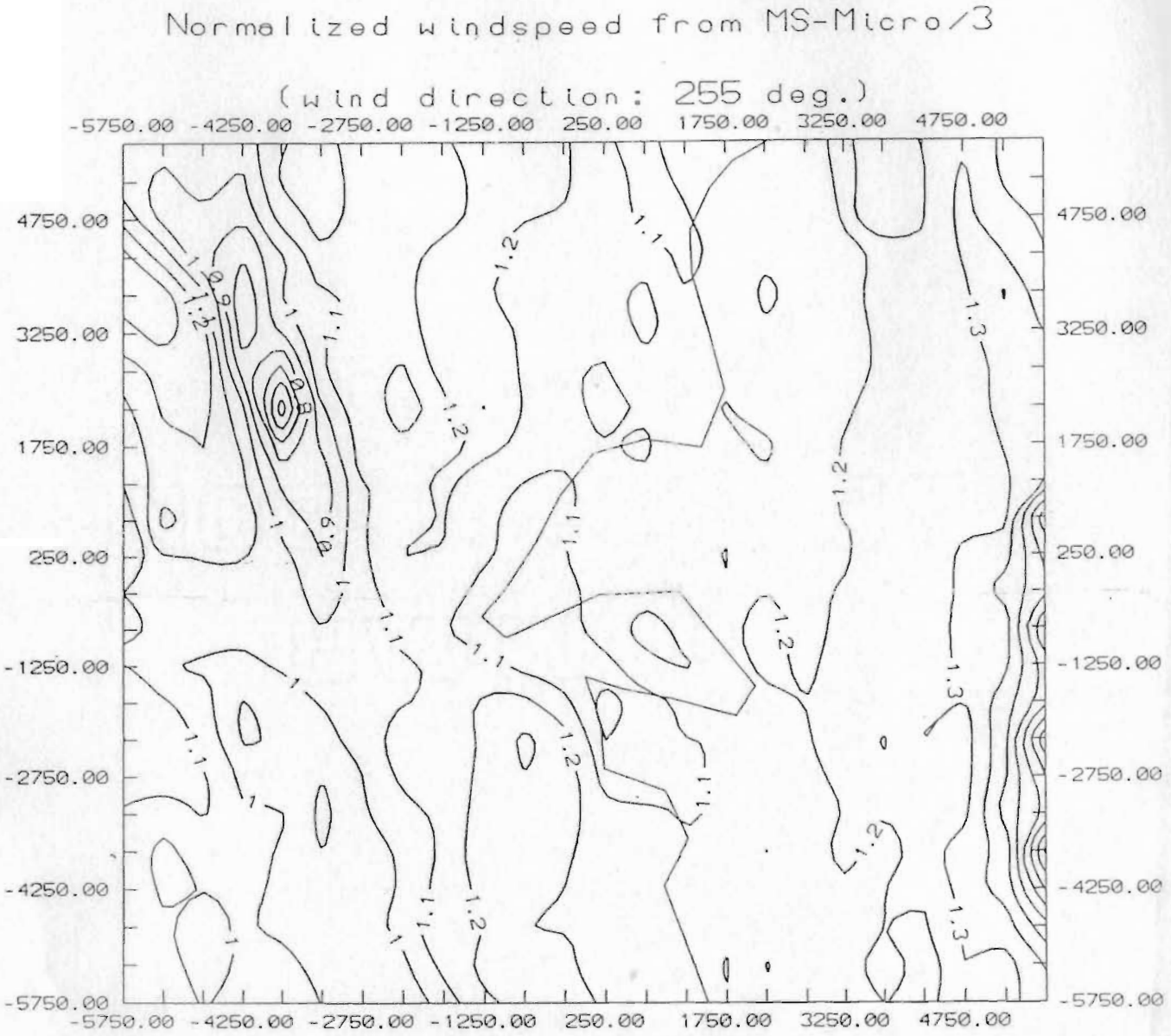


**Figure D.1. Normalized windspeed field at 255 deg. incident direction, 11 August, 1991.**

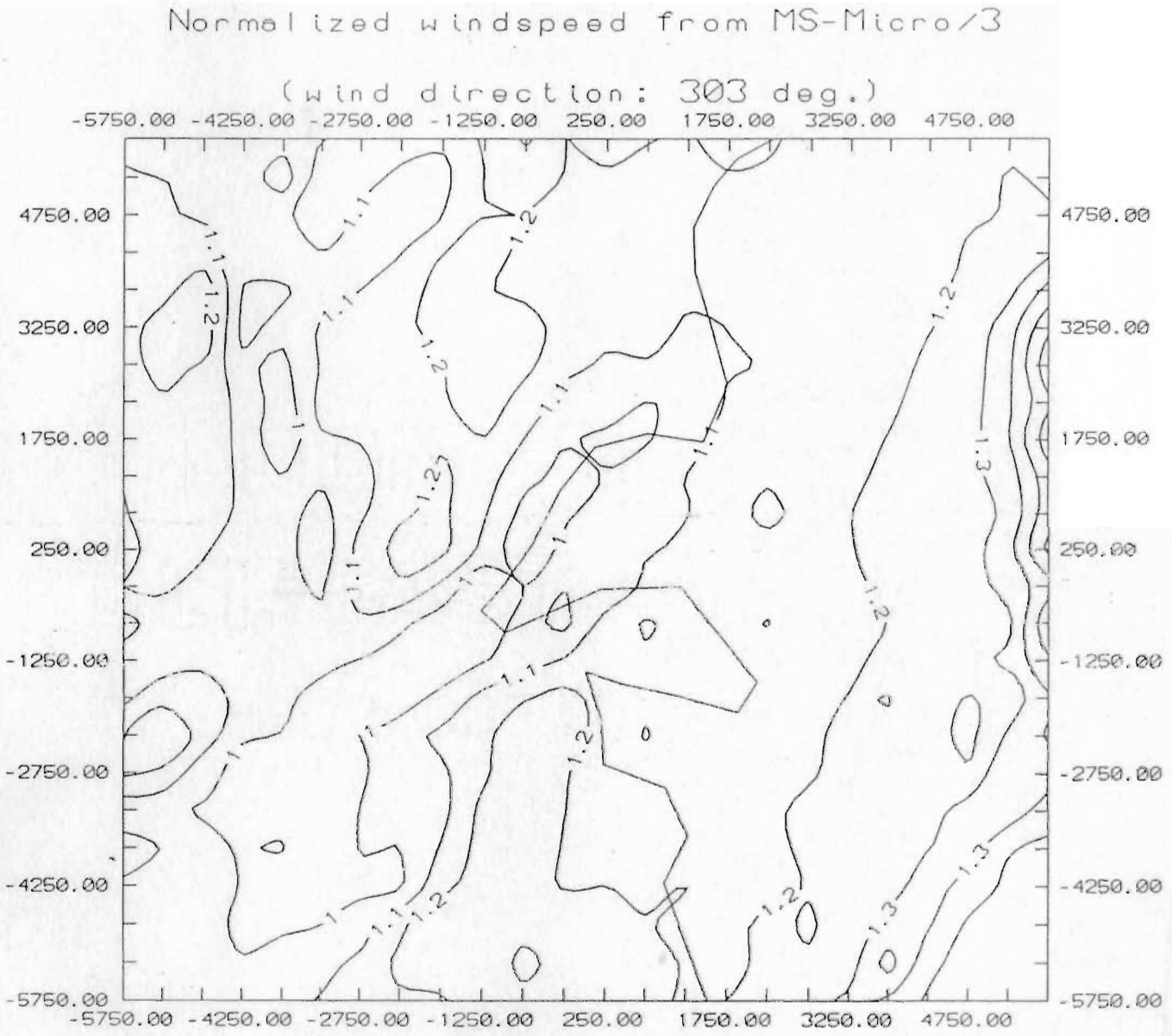


**Figure D.2. Normalized windspeed field at 308 deg. incident direction, 11 August, 1991.**

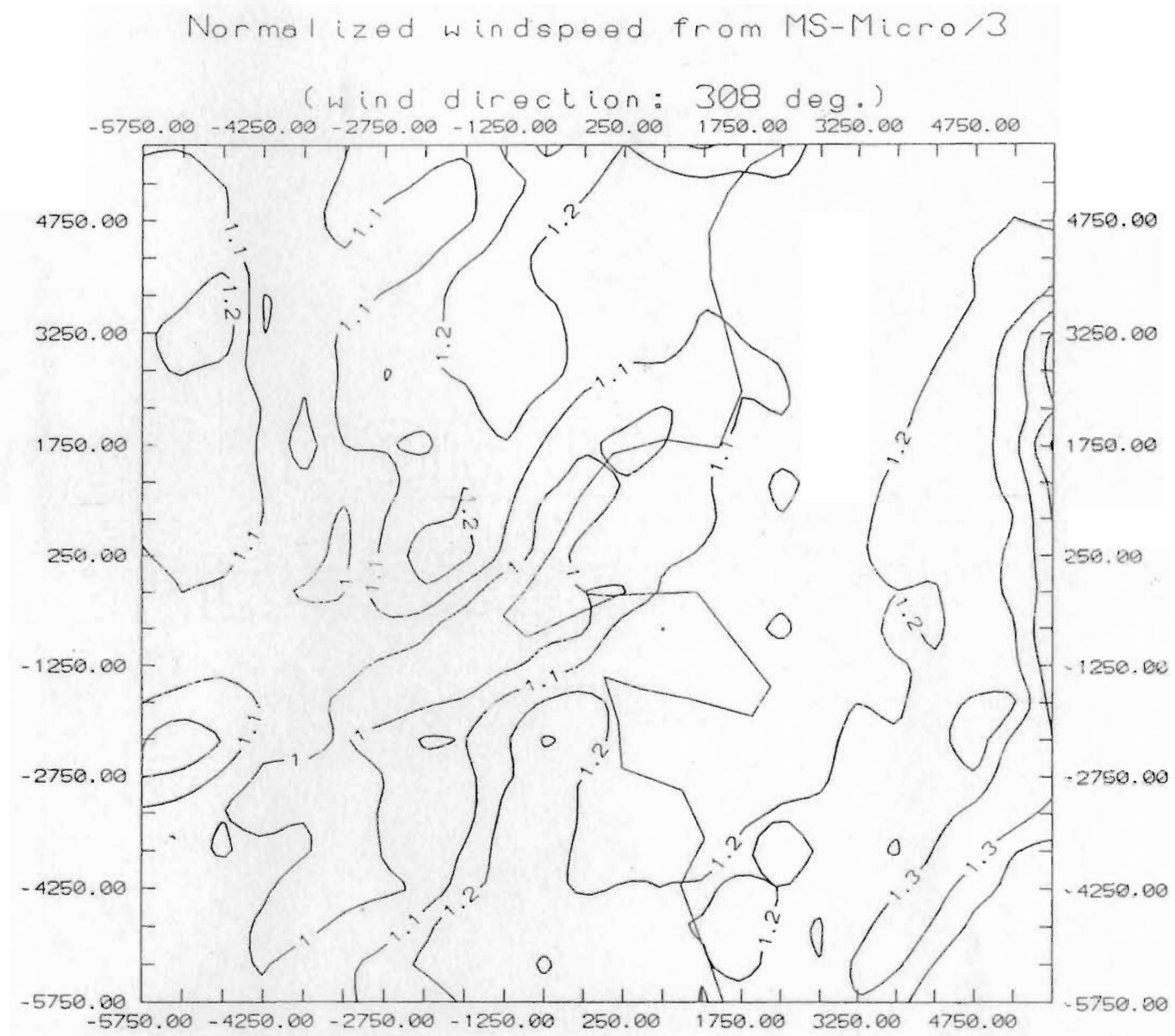


**Figure D.3. Normalized windspeed field at 303 deg. incident direction, 11 August, 1991.**

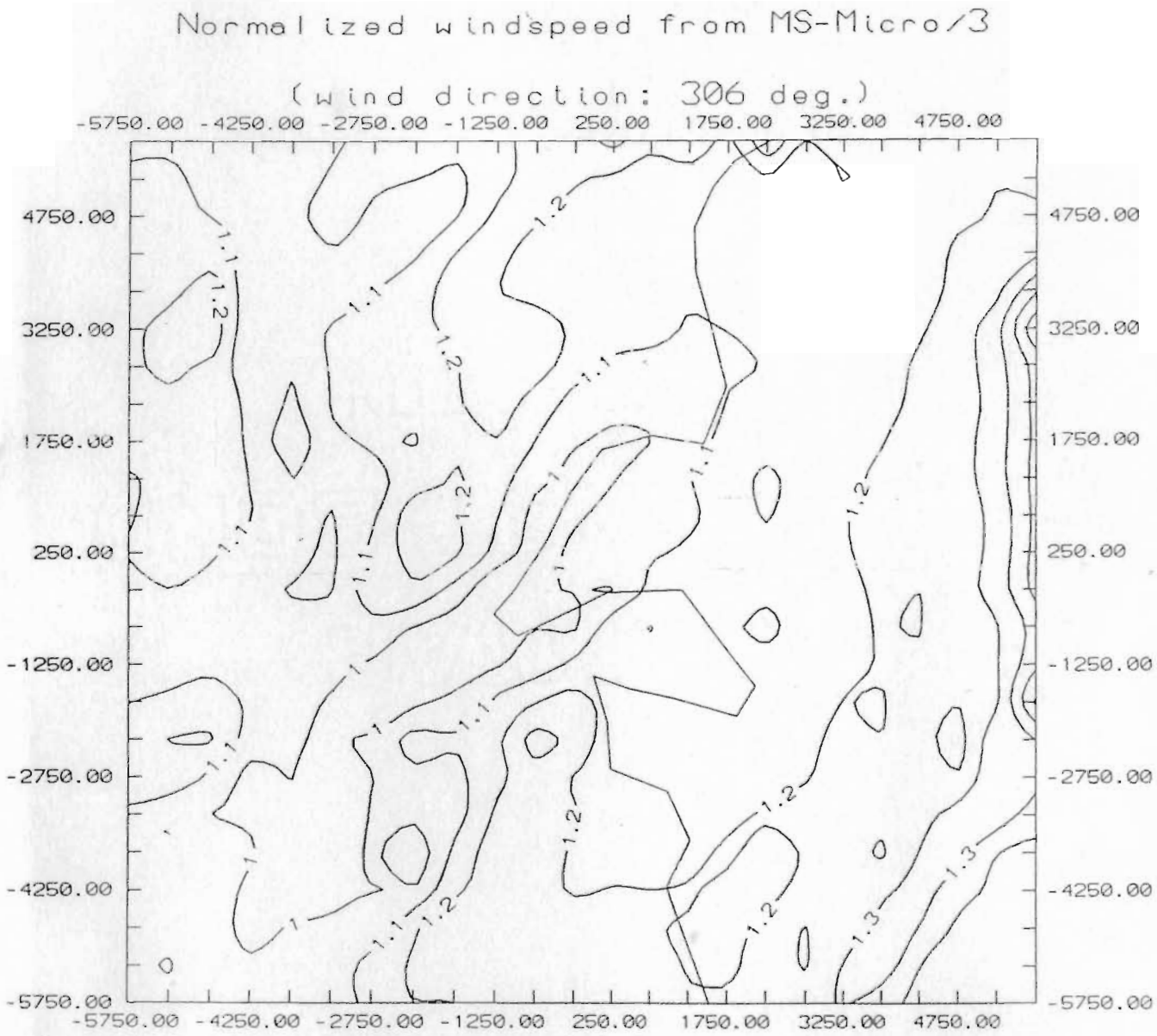


**Figure D.4. Normalized windspeed field at 306 deg. incident direction, 11 August, 1991.**

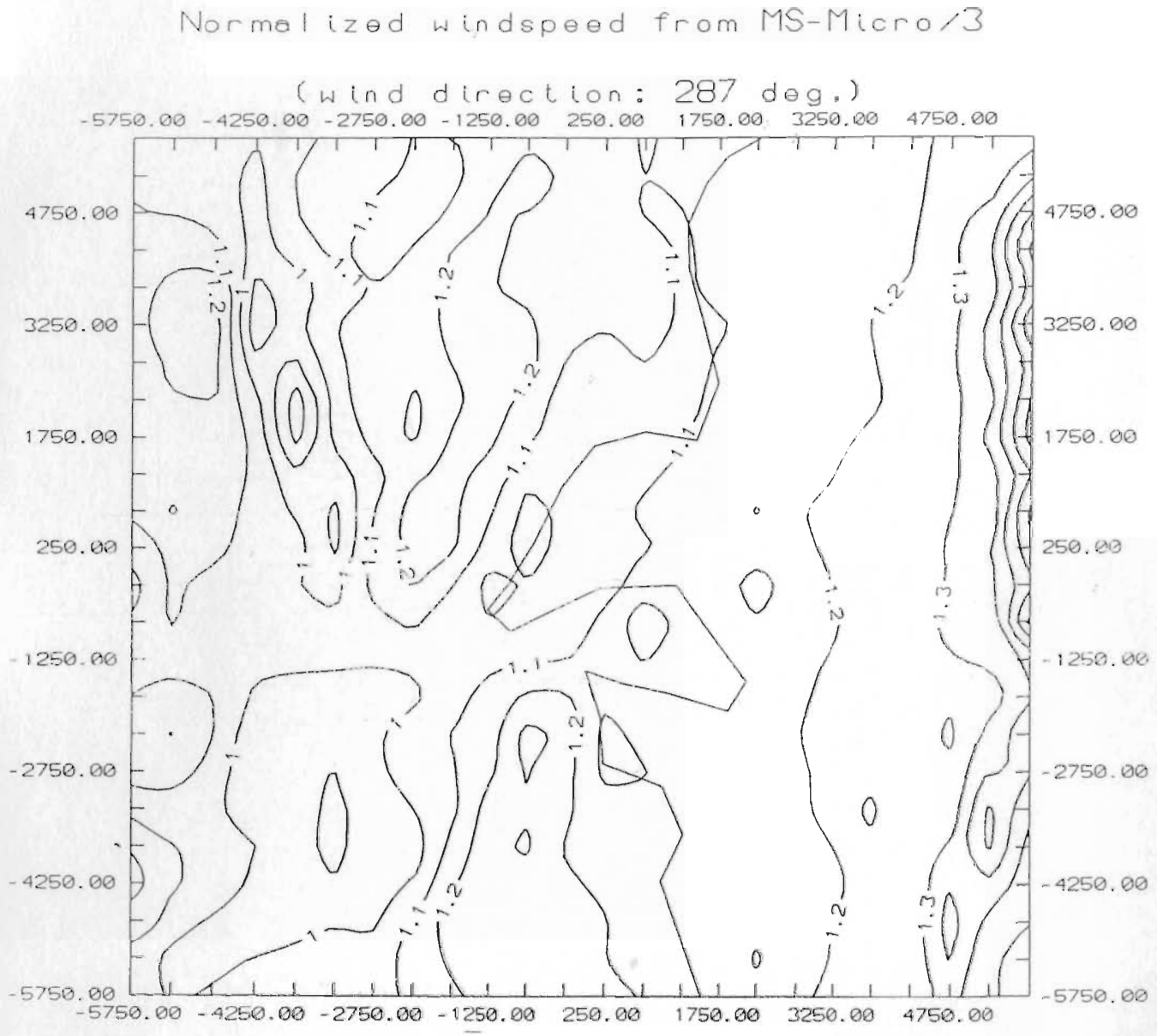


**Figure D.5. Normalized windspeed field at 287 deg. incident direction, 11 August, 1991.**